Photophysical Studies on the Dynamics of Guest Complexation with Cyclodextrins

by

Robert Scott Murphy
B.Sc., University of Prince Edward Island, 1995

A Dissertation Submitted in Partial Fulfillment of the
Requirements for the Degree of

DOCTOR OF PHILOSOPHY

in the Department of Chemistry

We accept this dissertation as conforming
to the required standard

© Robert Scott Murphy, 2000
University of Victoria

The author has granted a non-exclusive licence allowing the National Library of Canada to reproduce, loan, distribute or sell copies of this thesis in microform, paper or electronic formats.

The author retains ownership of the copyright in this thesis. Neither the thesis nor substantial extracts from it may be printed or otherwise reproduced without the author's permission.

L'auteur a accordé une licence non exclusive permettant à la Bibliothèque nationale du Canada de reproduire, prêter, distribuer ou vendre des copies de cette thèse sous la forme de microfiche/film, de reproduction sur papier ou sur format électronique.

L'auteur conserve la propriété du droit d'auteur qui protège cette thèse. Ni la thèse ni des extraits substantiels de celle-ci ne doivent être imprimés ou autrement reproduits sans son autorisation.

0-612-47292-2

Canada

Supervisor: Dr. C. Bohne

Abstract

The main objective of this research is to investigate aspects responsible for the dynamics of guest molecules complexed with cyclodextrins (CDs). We have shown with the use of a variety of photophysical techniques that the complexation dynamics for guests with CDs are dependent on the structure of the guest molecule.

An assortment of photophysical methods that included steady-state fluorescence, UV-Vis absorption, and laser-induced optoacoustic (LIOAS) spectroscopies, in combination with time-resolved techniques such as single photon counting fluorescence and triplet-triplet absorption (T-T$_{ab}$) spectroscopies were employed to obtain a detailed understanding of the photophysics for fluorenones. From these photophysical investigations, we have demonstrated that several effects such as the nature and position of substituents, and the properties of the microenvironment are responsible for the photophysics observed for these aromatic ketones.

The complexation of fluorenone and xanthone with CDs was investigated to obtain more information on how the structure of the guest molecule can affect the complexation dynamics of these host-guest systems. Induced circular dichroism (ICD) and picosecond fluorescence spectroscopy were employed to detail the structural differences observed for the CD complexes of these two ketones. Equilibrium constants were observed to be larger for xanthone with β-CD than with fluorenone. This result suggested that a more favorable complex is formed for xanthone than for fluorenone. However, in the presence of α-CD, fluorenone formed 2:1 host-guest complexes that were not observed for xanthone. These photophysical studies with additional support from theoretical calculations provided useful tools for understanding the structural intricacies of CD host-guest systems. These types of studies will be invaluable to the understanding of dynamics within supramolecular systems.

To expand our knowledge on the structure-dynamics relationship that exists for CD complexes, we investigated the complexation dynamics of charged probes with CDs. Two styrene derivatives, *trans*-anethole (t-Ane) and 4-vinylanisole (4-VA), were chosen as precursors for the radical cations examined in these investigations. Quenching studies have demonstrated that the exit of the radical cations of t-Ane and 4-VA complexed with CD, even in the presence of alcohols, was faster than 20 ns. In addition, complexes with 2:1 host-guest stoichiometries were unsuccessful in reducing the dissociation rate constant of these charged species.

From these studies we have shown that a structure-dynamics relationship does exist for CD host-guest systems. With the use of a variety of photophysical techniques and theoretical calculations, we have been able to better evaluate how the photophysics of probe molecules can be explored in the study of host-guest complexation. Small changes in structure have important consequences on the binding efficiencies of these probes to CDs. This information will aid in the understanding of the structure-dynamics relationship that occurs in supramolecular systems.

Table of Contents

PRELIMINARY PAGES

List of Figures

List of Tables

List of Schemes

.

List of Abbreviations

A	acceptor molecule
Abs	absorbance
t-Ane	*trans*-anethole
ΔA	change in absorbance
ΔA_{max}	maximum transient absorbance
Å	Ångstrom $(1 \times 10^{-10}\ m)$
BCU	baseline compensation unit
c	speed of light $(2.998 \times 10^8\ m\ s^{-1})$
CD	cyclodextrin
CPC	counts per cycle
D	donor molecule
2,7DBF	2,7-dibromo-9-fluorenone
1,3DCF	1,3-dichloro-9-fluorenone
2,7DCF	2,7-dichloro-9-fluorenone
2,7DFF	2,7-difluoro-9-fluorenone
ε	molar absorptivity $(M^{-1}\ cm^{-1})$
e^-_{solv}	solvated electron
E	energy
E_T	triplet state energy
$E°$	potential at standard conditions (V)
EA	electron affinity
ΔE	change in energy

ΔE_{ST}	change in energy between a singlet and triplet electronic state
f_{abs}	fraction of absorbed light
F	fluorescence
F	Faraday constant $(9.648 \times 10^4 \text{ C mol}^{-1})$
F-2CA	9-fluorenone-2-carboxylic acid
F-4CA	9-fluorenone-4-carboxylic acid
$\Delta G°$	change in free energy at standard conditions
h	hours
h	Planck constant $(6.626 \times 10^{-34} \text{ J s})$
$h\nu$	energy of a photon
I	intensity
IC	internal conversion
ICD	induced circular dichroism
IRF	instrument response function
ISC	intersystem crossing
ΔI	change in intensity
IE	ionization energy
J	spectral overlap integral
k_{diff}	diffusion-controlled rate constant
k_{-diff}	rate constant for the dissociation of an encounter complex
k_D	deactivation rate constant
k_F	rate constant for fluorescence
$k_F°$	rate constant for natural fluorescence
k_h	observed rate constant for a probe in a supramolecular system
k_{ic}	rate constant for internal conversion
k_{isc}	rate constant for intersystem crossing

k_o	intrinsic decay rate constant
k_{obs}	observed rate constant
k_{p+}	entry rate constant
k_{p-}	exit rate constant
k_q, k_{qo}	quenching rate constant
$k_q(obs)$	observed quenching rate constant
$k_q(eff)$	observed quenching rate constant for a probe in a supramolecular system
K_{eq}	equilibrium constant
K_n	equilibrium constant (for a n:1 host:guest stoichiometry)
K_{SV}	Stern-Volmer constant
λ	wavelength (nm)
λ_{max}	maximum wavelength (nm)
l	pathlength (mm)
LFP	laser flash photolysis
LIOAS	laser-induced optoacoustic spectroscopy
min	minutes
MCP	microchannel plate
4MF	4-methoxy-9-fluorenone
n	nonbonding
n	refractive index
N_A	Avogadro constant (6.022×10^{23} mol^{-1})
1-NpOH	1-naphthyl-1-ethanol
2-NpOH	2-naphthyl-1-ethanol
2OHF	2-hydroxy-9-fluorenone

3OHF	3-hydroxy-9-fluorenone
4OHF	4-hydroxy-9-fluorenone
θ	molar ellipticity
P	phosphorescence
$[P]_T$	total probe concentration
PMT	photomultiplier tube
Q	quencher
ϕ_e	quantum yield for solvated electron formation
ϕ_F	fluorescence quantum yield
ϕ_F^Q	fluorescence quantum yield in the presence of quencher
ϕ_{ic}	internal conversion quantum yield
ϕ_{isc}	intersystem crossing quantum yield
ϕ_{RC}	quantum yield for radical cation formation
R	radius of the laser beam
R_{AD}	donor-acceptor separation distance
s	spin quantum number
S_0	singlet ground state
S_n	n^{th} singlet excited state
S	total spin quantum number
SPC	single photon counter
t	time
T_n	n^{th} triplet excited state
TBAI	tetrabutylammonium iodide

T-T$_{abs}$	triplet-triplet absorption
τ_a	acoustic transient time
τ_s	observed singlet excited state lifetime
τ_s^o	natural singlet excited state lifetime
τ_s^Q	observed singlet excited state lifetime in the presence of quencher
τ_T	observed triplet excited state lifetime
VR	vibrational relaxation
4-VA	4-vinylanisole
ν	frequency (s^{-1})
υ_a	speed of sound in a solvent

Acknowledgements

I would like to express my sincere gratitude to my supervisor Cornelia Bohne for her guidance and assistance throughout this research project. My experiences in her research group have been invaluable to the beginning of my research career and to my focus in life.

A special thanks must be given to Luis Netter for his support and friendship. In many ways he has been my co-supervisor.

I have made many friends and colleagues during my time at the University of Victoria. They include graduate students, undergraduate students, chemistry faculty and staff. I could not begin to list them and neither would I try as each deserves a special recognition in which my words can not describe.

Always first and never last, I would like to thank my family for their support and heartfelt thoughts.

Dedication

To Mom and Dad

1. INTRODUCTION

1.1 Photophysics

Photoinduced processes can be classified as either photophysical or photochemical in nature. A molecule undergoing photophysical processes will lead to a change in the quantum states of the molecule, but the molecule will not rearrange or fragment. In contrast, a photochemical process involves a change in the chemical nature of the photoexcited molecule with the formation of a new chemical species.

1.1.1 Electromagnetic Spectrum

The electromagnetic spectrum is composed of many different frequencies of electromagnetic radiation (Figure 1.1). Electromagnetic radiation can be envisaged in terms of an oscillating electric field, and an oscillating magnetic field that are perpendicular to each other, and to the direction of propagation. The energy of these waves is proportional to the frequency (v), or the number of cycles per second that these waves travel through in a certain point in space as shown in Equation 1.1, where h is Planck's constant, equal to 6.626×10^{-34} J s. Electromagnetic radiation can also be described in terms of the wavelength (λ), or peak to peak distance of the electromagnetic wave. The wavelength

Equation 1.1

$$E = hv$$

of an electromagnetic wave is inversely proportional to the frequency of the electromagnetic wave as shown in Equation 1.2, where c is the speed of light.

Equation 1.2

$$v = \frac{c}{\lambda}$$

Frequency (s⁻¹)   **Wavelength (m)**

Frequency	Region	Wavelength
3×10^6	Radio waves	10^1
3×10^8		10^0
3×10^{10}	Microwave	10^{-2}
3×10^{12}	Infra-Red (IR)	10^{-4}
3×10^{14}	Visible	10^{-6}
3×10^{16}	Ultra-Violet (UV)	10^{-8}
3×10^{18}	X-ray	10^{-10}
3×10^{20}	Gamma-ray	10^{-12}

780 nm
Red
Orange
Yellow
Green
Blue
Indigo
Violet
390 nm
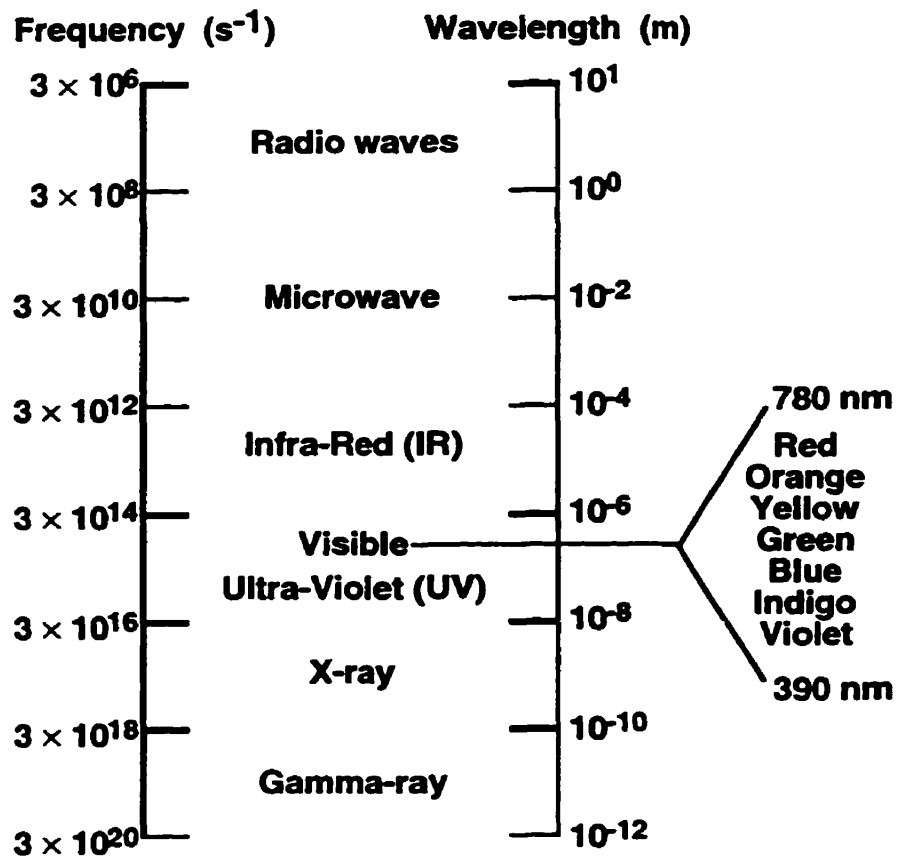
Figure 1.1   The electromagnetic spectrum (Adapted from reference 1).

The regions of energy most often employed when investigating the photochemistry and photophysics of organic molecules are in the visible (Vis) and ultraviolet (UV) regions of the electromagnetic spectrum. These regions of electromagnetic radiation are often called the regions of light energy.[1] Quantum mechanically, light is described in terms of discrete

packets of energy known as photons. This photon energy is called quanta, and the energy absorbed or emitted by a molecule is quantized or restricted to a series of discrete values.

1.1.2 Light Absorption

A photon can only be absorbed by a molecule if the energy of the photon corresponds to the difference in energy between two stationary states (i.e. electronic or vibrational) of the molecule. The photon energy or quanta required for this absorption is given by Equation 1.3 that describes the difference in energy between the two stationary states. When UV-Vis light is employed the electronic states of the molecule are involved in

Equation 1.3

$$\Delta E = h\nu$$

the absorption. This equation is commonly referred to as the Bohr frequency condition. Therefore, the energy between two electronic states of a molecule can be expressed in terms of a particular frequency of light. However, it is more common to express these energies in molar quantities. Therefore, to determine the energy carried by 1 mol of photons (i.e., an Avogadro number of photons, called an Einstein) of a specific frequency or wavelength of light, Equation 1.2 and Equation 1.3 are combined and Avogadro's number, N_A, is included to give Equation 1.4. Using this expression, the energy, in kJ mol^{-1}, required to excite an electron from one electronic state to another can be calculated for a particular wavelength of light.

Equation 1.4

$$\Delta E = N_A \frac{hc}{\lambda}$$

1.1.3 Electronic States

The absorption of UV-Vis light by organic molecules causes an electron from an electronic state of lower energy to be excited to a previously unoccupied electronic state of higher energy. These electronic states can be described in two common ways. The first involves a description of the electronic state in terms of its spin multiplicity. Each electron in a molecule has a spin angular momentum with a spin quantum number $s = 1/2$. An electron moving in an electric field gives rise to a magnetic moment, which in the presence of a magnetic field may take up one of two orientations. The magnetic moment can be aligned with the magnetic field or opposed to it, which gives rise to two different energy states of the electron that are designated by an up or down arrow, respectively. If no magnetic field is present there will be no difference in the electron spin energy levels, but the individual moments will still dictate how the electrons will interact with one another and with the nucleus. The spin of an electron can also be viewed in the more classical description of the atomic structure in which the electron is viewed as a small charged particle that orbits the nucleus of an atom and spins on its own axis.

To differentiate between different electronic states possible for molecules, the total spin angular momentum possessed by the molecule is represented by the total spin quantum number S. This value is calculated as the vector sum of all the different spin contributions from each electron. For example two electrons of the same spin can either be opposed or parallel. If the spins are opposed then the total spin quantum number is zero. If the spins are parallel then the total spin quantum number is one. The spin multiplicity is given by $(2S + 1)$, and describes the number of expected electronic states in the presence of a magnetic field. Therefore, a molecule with all the electrons spin-paired have a total spin quantum number of zero, and a spin multiplicity of one. These electronic states are referred to as singlets. A ground state singlet is abbreviated S_0, and a first excited singlet state is abbreviated S_1. If the opposite case arises, where two electrons are parallel the spin

multiplicity becomes three and these electronic states are referred to as triplets. This system of labeling electronic states is known as the enumerative system.[1]

Another way of characterizing an electronic state of a molecule is to specify the orbitals in which the excited electron leaves from and the new orbital it enters. Various schemes and notations have been used to describe these transitions. The Kasha system describes only the nature of the orbitals involved in the electronic transition.[2] Symbols for the ground state notation are σ, n, and π. Respectively, they refer to the sigma, nonbonding, and pi orbitals of a molecule. In the excited state the notation is shown as σ^* and π^*. In organic photochemistry, the n and π orbitals are most commonly involved in transitions initiated by light in the UV-Vis region of the electromagnetic spectrum. For example, in ketones where nonbonding electrons are readily available n,π^* transitions are common. Whereas, in aromatic systems where there are no available nonbonding electrons π,π^* transitions are common.

1.1.4 Spin Forbidden Transitions

When discussing electronic transitions involved in photochemical and photophysical processes it is useful to understand a few of the spin selection rules. In particular, in a transition where there is a preservation of the spin multiplicity or a conservation of spin the process is referred to as a spin allowed transition. This type of process is commonly characterized by large molar absorptivities. However, when there is a change in the spin multiplicity and disregard to the conservation of spin the process is referred to as a spin forbidden process. A spin forbidden process is not excluded as a possibility, but it often describes a considerably weaker process that is characterized by small molar absorptivities. One important consequence of spin forbidden processes is the transition from a singlet excited state to a triplet excited state (i.e., intersystem crossing) by way of spin-orbit coupling.

1.1.5 Spin-orbit coupling

The dominant mechanism used to describe the intersystem crossing process of organic molecules is spin-orbit coupling.[3] This mechanism is responsible for the "flip" of the spin of an electron and the change in the spin multiplicity of a molecule. One analogy to describe spin-orbit coupling is to envisage the motion of an electron about a nucleus in terms of classical Bohr-like orbits. In this model two kinds of motion are important. They are the movement or orbit of the electron about the nucleus, and the spin of the electron about its own axis. Since a moving charged particle generates a magnetic field, both the orbital and spin motion of the electron generate magnetic fields. The magnetic torque generated from the interaction of these two fields will cause the spin of the electron to "flip" and it is expected that this will occur when the electron is in the region of its orbit close to the nucleus because the motion of the electron and the magnetic moment should be greatest as the negatively charged electron approaches the positively charged nucleus. However, the magnetic torque generated is insufficient to cause the spin flip since the total angular momentum of the system must be conserved. This can only be achieved if there is a compensating change in the orbital angular moment. This change in the orbital angular momentum is satisfied by the "jump" of the electron from one orbital to another (i.e. as between two π orbitals). Thus, it is the coupling of the change in spin and the change in the orbital angular momentum that allows an electron to "flip" its spin in most organic molecules.

1.1.6 Spin Correlation

The energy of the triplet excited states of organic molecules is usually lower than their corresponding singlet excited states. This observation is a consequence of spin correlation and a result of the electron-electron repulsion experienced between electrons.

Triplet excited states have lower energies because the electron-electron repulsion experienced between the two electrons with spins parallel to one another is less than the repulsion experienced between two electrons with opposing spins. This is a consequence of the Hund's rule of maximum multiplicity that states that the repulsion between two electrons occupying different orbitals is minimized if their spins are opposed because their motion is correlated.

1.2 Deactivation of Excited States

Electronically excited states typically have short lifetimes. Many different processes are responsible for the dissipation of the energy gained by these excited state molecules. This section will discuss the various pathways and the molecularity involved in the deactivation of excited states.

1.2.1 Unimolecular Deactivation Processes

Energy absorbed by a molecule can be released through many unimolecular processes that can be referred to as either a radiative or nonradiative process. As will be discussed, this energy can also be transferred to other molecules through bimolecular processes.

1.2.1.1 The Jablonski Diagram

Electronically excited states of organic molecules may return to their ground states via photophysical or photochemical pathways. Photophysical pathways are unimolecular processes that are responsible for the dissipation of the excess energy gained by an excited state molecule. The following energy level diagram conveniently summarizes the different

possible types of transitions that are available to an excited state molecule undergoing

photophysical deactivation. This diagram is known as a Jablonski diagram.[1]
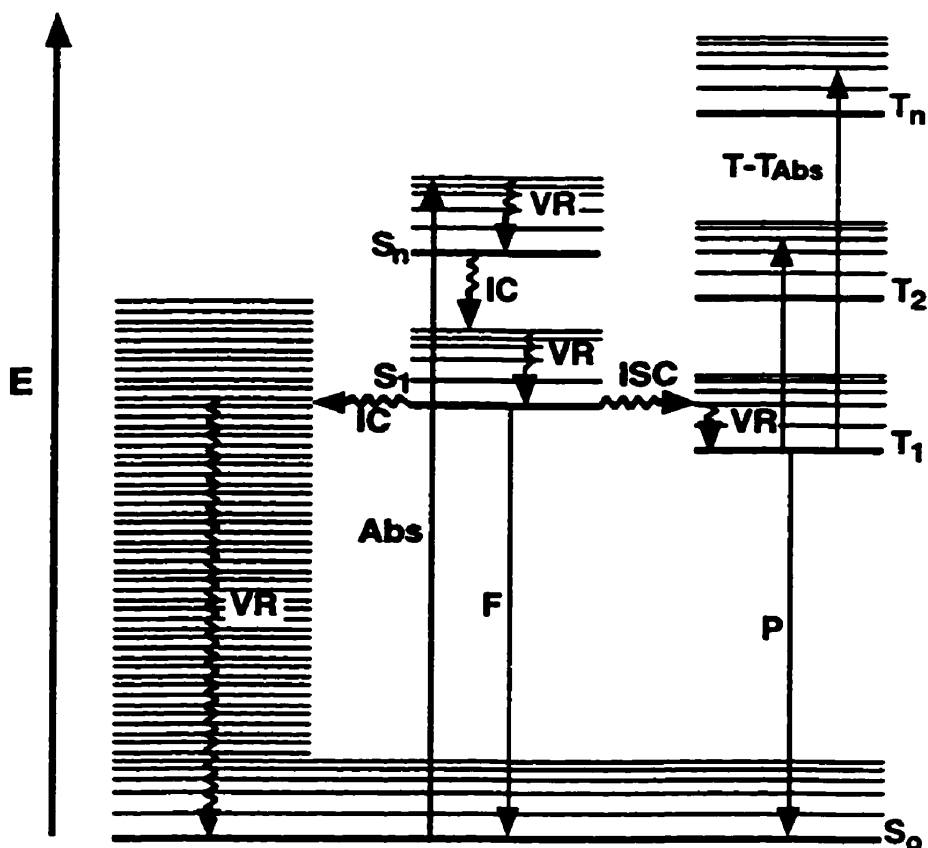
Figure 1.2 Jablonski diagram. Absorption (Abs) and emission processes are indicated by straight arrows (F = fluorescence, P = phosphorescence, T-T$_{Abs}$ = triplet-triplet absorption), and radiationless processes are indicated by wavy arrows (IC = internal conversion, ISC = intersystem crossing, VR = vibrational relaxation).

1.2.1.2 Kinetics

If a population of excited state molecules, [M*], decays through a single radiative process, the decay of this population will return to its initial state as a function of time due to the spontaneous emission of radiation (Scheme 1.1). The energy of the spontaneous

Scheme 1.1

$$M^* \longrightarrow M + h\nu'$$

emission given as *hv'* is lower in energy than the photon initially absorbed by the ground state molecule M. For an individual molecule the probability of emission is time-independent, and the total intensity of the emission depends on the number of molecules in the excited state. However, for the spontaneous emission of a large number of molecules in the excited state the rate of decay follows first order kinetics (Equation 1.5), where k_F^o is

Equation 1.5

$$-\frac{d}{dt}[M^*] = k_F^o[M^*]$$

Equation 1.6

$$[M^*] = [M^*]_o e^{-k_F^o t}$$

the rate constant for the first order natural fluorescence process. Integration of Equation 1.5 yields Equation 1.6, which is the first-order rate law where $[M^*]_0$ and $[M^*]$ are the concentrations of the electronically excited molecules immediately following excitation ($t=0$) and at a later time t, respectively. The average statistical time that the molecule spends

in the excited state is called the natural singlet lifetime, $\tau_s^{\,\circ}$.[1] This is given by inverse of the rate constant for the natural fluorescence process (Equation 1.7). The natural singlet lifetime can be determined using Equation 1.6, where at time $t = \tau_s^{\,\circ}$, the concentration of excited state molecules falls to $1/e$ of it initial value and as a result $\tau_s^{\,\circ}$ is sometimes referred to as the $1/e$ lifetime.

Equation 1.7

$$\tau_s^{\,\circ} = \frac{1}{k_F^{\,\circ}}$$

Experimentally, $k_F^{\,\circ}$ is not determined as additional radiative or nonradiative processes contribute to the decay of the excited state concentration. Therefore, the natural fluorescence rate constant $k_F^{\,\circ}$ becomes a measured fluorescence rate constant k_F. For example, fluorescence from the S_1 state of M is in direct competition with internal conversion to give vibrationally excited S_0 and with intersystem crossing to give a T_1 state. The rate for this decay is then given by Equation 1.8, where k_{isc} is the rate constant for

Equation 1.8

$$-\frac{d}{dt}[M^*] = k_F^{\,\circ}[M^*] + k_{isc}[M^*] + k_{ic}[M^*]$$

intersystem crossing , and k_{ic} is the rate constant for internal conversion. The decay of $[M^*]$ still follows first-order kinetics, but now the observed rate constant for the fluorescence is the sum of rate constants for all the possible deactivation pathways (Equation 1.9). With the additional deactivation pathways, a decrease in the measured

Equation 1.9

$$[M^*] = [M^*]_o e^{-(k_f + k_{ic} + k_{isc})t} = [M^*]_o e^{-k_r t}$$

lifetime will also be observed compared to the natural singlet lifetime. In addition, with

fewer excited molecules to emit radiation the intensity of the fluorescence will also decrease

as compared to the situation, where there is no competition between the photophysical

processes.

1.2.1.3 Quantum Yields

A convenient way of describing the efficiency of photophysical and photochemical

processes that occur for a molecule is to determine quantum yield, ϕ, for the respective

process. The quantum yield ϕ_j of a process j is defined as the number n_A of molecules A

undergoing that process divided by the number n_Q of light quanta absorbed (Equation

1.10). However, quantum yields are more commonly used to compare the efficiency

Equation 1.10

$$\phi_j = \frac{n_A}{n_Q}$$

of one process over all the processes responsible for the deactivation of the excited state

molecules. These quantum yields can be written in either terms of rate constants, or

lifetimes. For example, the quantum yield for fluorescence ϕ_F in terms of rate constants

would be given as the rate constant for the natural fluorescence, k_F^o, divided by the rate

constants for all the other deactivation pathways $\sum_j k_j$ including that of the natural

fluorescence rate constant (Equation 1.11). As shown the quantum yield of fluorescence

can also be calculated from the product of the rate constant of fluorescence and the observed singlet lifetime, τ_s. Written in terms of lifetimes, the fluorescence quantum yield can also be shown as a ratio of the observed singlet lifetime to that of the natural singlet lifetime.

Equation 1.11

$$\phi_F = \frac{k_F^o}{k_F^o + \sum k_j} = k_F^o \tau_s = \frac{\tau_s}{\tau_s^o}$$

1.2.1.4 Nonradiative Deactivation

Nonradiative processes of excited state molecules involves the release of heat as they return to lower electronic levels. The three most common types of nonradiative transitions are vibrational relaxation, internal conversion and intersystem crossing. Vibrational relaxation occurs within a set of vibrational levels in one electronic state. In solution, vibrational relaxation to the vibrational ground state, or zeroth vibrational level can be reached in times as short as 10^{-11} s. This vibrational energy is converted to heat through collisions with solvent molecules. From the zeroth vibrational level of a molecule in an excited electronic state the molecule can undergo further nonradiative or radiative processes. If the molecule returns thermally from a singlet excited state to the ground singlet state, the process is referred to as internal conversion since the multiplicity of the states involved in the transition are the same. In contrast, if the radiationless deactivation occurs between states of different multiplicity then this process is termed intersystem crossing. The selection rules for transitions between electronic states of different multiplicity that involve spin inversion by the spin-orbit coupling mechanism are known as El-Sayed's rules.[4] These rules explain that spin-orbit coupling between electronic states with different electronic configurations are more efficient since the change in the spin of the

electron is compensated by the change in its orbital angular momentum upon entering a different orbital. In contrast, spin-orbit coupling between electronic states with the same electronic configurations are very inefficient since the change in spin is not compensated by a change in the orbital angular momentum. In both internal conversion and intersystem crossing, a transition occurs between the lowest vibrational level of an excited electronic state, and an isoenergetic, but higher vibrational level of a different electronic state. Then through vibrational relaxation the excited state molecule will cascade down to the lowest vibrational level of this new electronic state. These nonradiative transitions are represented by wavy lines in the Jablonski diagram. Vibrational relaxation is represented with vertical wavy lines as they move from higher to lower vibrational levels, whereas internal conversion and intersystem crossing are represented by horizontal wavy arrows because these processes occur between isoenergetic vibrational levels of different electronic states.

1.2.1.5 Radiative Deactivation

Radiative processes involve the emission of photons when an excited state molecule returns to its ground state. Two types of radiative transitions frequently encountered in photophysical studies are fluorescence and phosphorescence. The most common of the two radiative transitions is fluorescence. Fluorescence is the emission of photons between electronic states with the same multiplicity. Fluorescence is a spin allowed transition. Since all closed-shell molecules have singlet ground states, fluorescence is commonly observed from the first excited singlet state, S_1. The other emissive process that is frequently used to characterize the triplet excited states of organic molecules is phosphorescence. Phosphorescence is the emission of photons between electronic states with different multiplicities. This is a spin forbidden transition. As shown in Figure 1.2, these processes are drawn as straight vertical arrows. They are viewed in this way since the electronic motion within a molecule occurs at a higher frequency than the nuclear

motion of the molecule. This is the basis of the Frank-Condon principle.[1] Electronic

motion has a typical frequency of ca. 3×10^{15} s^{-1} that is much faster than the frequency of

vibrational motion at ca. 3×10^{13} s^{-1}. As a result, the frequencies of light used for

electronic excitation are too high to allow for any change in the nuclear motion of the

molecule during the absorption of light. Thus, the nuclear coordinates of the molecule

before excitation are virtually the same during excitation. However, after excitation the

nuclear coordinates do change and for this reason, it is the greatest overlap of the

vibrational levels within the ground and excited electronic states that are responsible for the

largest transition moments.

1.2.2 Bimolecular Deactivation Processes

In addition to unimolecular processes, there are bimolecular deactivation processes

that involve the transfer of energy, or electrons from one molecule to another. Any external

deactivation process is called a quenching process.

1.2.2.1 Quenching of Excited States

Fluorescence quenching is a general type of quenching that can occur by a variety

of different mechanisms. Photophysical quenching processes that do not lead to new

chemical species can in general be represented in Scheme 1.2, where M' is the ground

Scheme 1.2

$$M^* \ + \ Q \ \longrightarrow \ M'$$

state, or another excited state of M. If the quencher Q is the same molecule as M then this

quenching process is referred to as self-quenching or concentration quenching. Most

intermolecular deactivation processes are based on collisions between an excited state molecule M* and a quencher Q. Two other quenching mechanisms that involve the formation of complexes with their own photophysical features are exciplexes (MQ*) and excimers (MM*). These complexes represent a new chemical species with a well defined geometrical structure. The deactivation of these excited state complexes can occur through a variety of mechanisms such as fluorescence and phosphorescence, by decay into M + Q* that corresponds to an energy transfer (Section 1.2.2.2), by electron transfer (Section 1.2.2.3) to give M^+ and Q^-, or M^- and Q^+, by internal conversion, or by intersystem crossing. All of these deactivation processes lead to the quenching of the excited state M* and are referred to as quenching processes.

1.2.2.2 Energy Transfer

Electronic energy transfer reactions are an important class of bimolecular deactivation process available to excited state molecules. Energy transfer can be subdivided into two main categories. It can occur through both radiative and nonradiative mechanisms. Of the latter type, a further subdivision can be made to give the Coulombic or electron-exchange mechanisms for nonradiative energy transfer. A basic reaction used to describe energy transfer is Scheme 1.3 where "D" represents a donor molecule and "A" represents an acceptor molecule.

Scheme 1.3

$$D^* + A \longrightarrow D + A^*$$

Radiative energy transfer is also called the trivial mechanism. This mechanism is referred to as "trivial" because the donor and acceptor molecules are a part of a two-step

process, whereby there is no direct interaction between the two molecules (Scheme 1.4).

In radiative energy transfer, the emission of a photon from an excited donor molecule is

followed by the absorption of the emitted photon by the acceptor molecule. The efficiency

of the radiative energy transfer depends on a high emission quantum yield of the donor in a

region of the spectrum where the light absorbing ability or molar absorptivity of the

Scheme 1.4

$$D^* \longrightarrow D \; + \; h\nu$$

$$h\nu \; + \; A \longrightarrow A^*$$
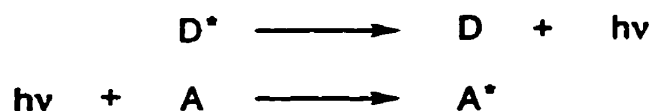
acceptor is high. This criterion is often quantified in terms of the spectral overlap integral,

J, which is the integrated overlap of the experimental absorption and emission curves. This

can be described mathematically by Equation 1.12 where I_D is the emitted light intensity of

the donor, and ε_A is the molar absorptivity of the acceptor

Equation 1.12

$$J = \int_0^\infty I_D \varepsilon_A dv$$

all as a function of frequency. In addition, the efficiency of radiative energy transfer is also

dependent on the concentration of acceptor molecules.

As mentioned, energy transfer can take place by two distinct nonradiative pathways

known as the Coulombic and electron-exchange mechanisms.[1] The former is also

proportional to the spectral overlap between the donor and acceptor molecules, but unlike

radiative energy transfer, the nonradiative energy transfer process requires the presence of a

specific interaction between the donor and the acceptor.

In general, the mechanisms for nonradiative energy transfer are dependent on the distance between the donor and acceptor molecules. Energy transfer according to the Coulombic mechanism, which is also referred to as the Förster mechanism, is based on long-range dipole-dipole interactions between the donor and acceptor molecules. These interactions cause perturbations of the electronic structures of the donor and acceptor molecules that are transmitted by the electromagnetic fields of the D* and A molecules. In this energy transfer process, the change in dipole moment from D* returning to its ground state induces a change in the dipole moment of A, giving rise to the quenching mechanism. The distance required for these dipole-dipole interactions can range from 20 to 100 Å.[5] The interaction energy for the Coulombic mechanism is proportional to R^{-6}_{AD}, where R_{AD} is the donor-acceptor separation. In contrast, the electron-exchange mechanism for energy transfer, which is also known as the Dexter mechanism, is a short-range process that occurs at much shorter distances (6 to 20 Å) than the Coulombic mechanism.[5] The efficiency of the electron-exchange mechanism decreases exponentially with the R_{AD}. This mechanism requires much shorter "encounter" distances between the donor and acceptor since some orbital overlap is required. In both the Coulombic and electron-exchange mechanisms it is necessary that the total spin for the reaction is conserved. This conservation of spin is governed by the Wigner-Witmer spin-conversion rules.[6] In some cases, the involvement of both mechanisms can be present. For example, when the distance between the donor and acceptor is ca. 100 Å from one another the Coulombic mechanism dominates. However, as the distance between the donor and acceptor molecules decreases the contribution to the energy transfer process by the Coulombic mechanism diminishes. At the same time, the contribution to the energy transfer process by the electron-exchange mechanism increases, and to a point where it eventually dominates, and the Coulombic mechanism is nonexistent.

According to the Wigner-Witmer spin-conversion rules, both singlet-singlet and triplet-triplet energy transfer are spin allowed processes (Scheme 1.5). The naming of

Scheme 1.5

$$^1D^* \ + \ ^1A \ \longrightarrow \ ^1D \ + \ ^1A^*$$

$$^3D^* \ + \ ^1A \ \longrightarrow \ ^1D \ + \ ^3A^*$$
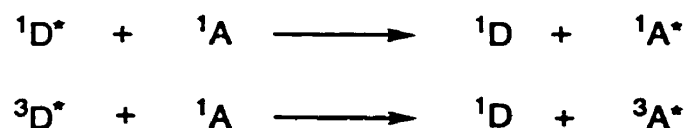
these reactions is classified according to the initial spin multiplicity of D* and the final spin multiplicity of A*. The Coulombic mechanism is predominately associated with singlet-singlet energy transfers since the emission efficiency for triplets is usually low. Since the Förster mechanism depends on the spectral overlap of the donor and acceptor molecules, triplet-triplet energy transfer does not usually occur via this mechanism. Triplet-triplet energy transfer by way of the electron-exchange mechanism is a very important type of energy transfer. In triplet-triplet energy transfer, an excited donor molecule in its triplet state transfers its energy to an acceptor molecule with a lower excited state energy. In most cases, this process is referred to as the quenching of the donor by the acceptor molecule, where the acceptor molecule is called the quencher. However, in situations where the acceptor molecule is of interest the process is referred to as photosensitization. Another example of a process that involves energy transfer by the electron-exchange mechanism is triplet-triplet annihilation. This process is common only if a large concentration of triplet excited states is available (Scheme 1.6).

Scheme 1.6

$$^3M^* \ + \ ^3M^* \ \longrightarrow \ ^1M^* \ + \ M$$

1.2.2.3 Electron Transfer

Electron transfer is another example of a bimolecular deactivation process. It can be described in two different ways (Scheme 1.7). Reaction (1) of Scheme 1.7 involves the transfer of an electron from D^* to a suitable acceptor molecule (A) with a lower reduction potential. Excited state molecules are better electron donors than their ground state since the ionization energy (IE) required to remove an electron from an excited state molecule is lower relative to the IE for the ground state molecule. In addition, excited state molecules

Scheme 1.7

$$D^* + A \longrightarrow D^{+\bullet} + A^{-\bullet} \quad (1)$$

$$D^+ + A \longrightarrow D + A^+ \quad (2)$$

$$D^- + A \longrightarrow D + A^- \quad (3)$$
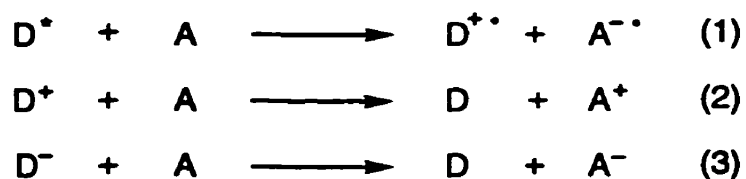
are also better electron acceptors since the electron affinity (EA) of an excited state molecule is higher relative to the EA for a ground state molecule.

Reactions (2) and (3) describe electron transfer processes between ground state molecules. Reaction (2) involves a hole transfer where a molecule that has lost an electron effectively transfers its vacancy to the acceptor molecule. This process can also be viewed as an electron transfer from A to D^+. Reaction (3) demonstrates the typical electron transfer, where a negatively charged donor molecule transfers an electron to an acceptor molecule with a lower reduction potential. In the same way that we can view energy transfer as a two-step mechanism we can also view electron transfer as a two-step process (Scheme 1.8). This mechanism involves the photoionization of a donor molecule by either

Scheme 1.8

$$D \xrightarrow{\quad h\nu \quad} D^+ \;+\; e^-_{solv}$$
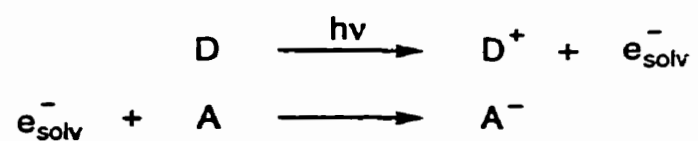
$$e^-_{solv} \;+\; A \longrightarrow A^-$$

one or more photons (hv) to yield a solvated electron (e^-_{solv}) in solution. This solvated electron can then be trapped by a suitable acceptor molecule.

Energy and electron transfer processes are similar in many ways. To illustrate further how interrelated electron and energy transfer are, one can envisage electron transfer as the combination of electron and hole transfer (Figure 1.3).
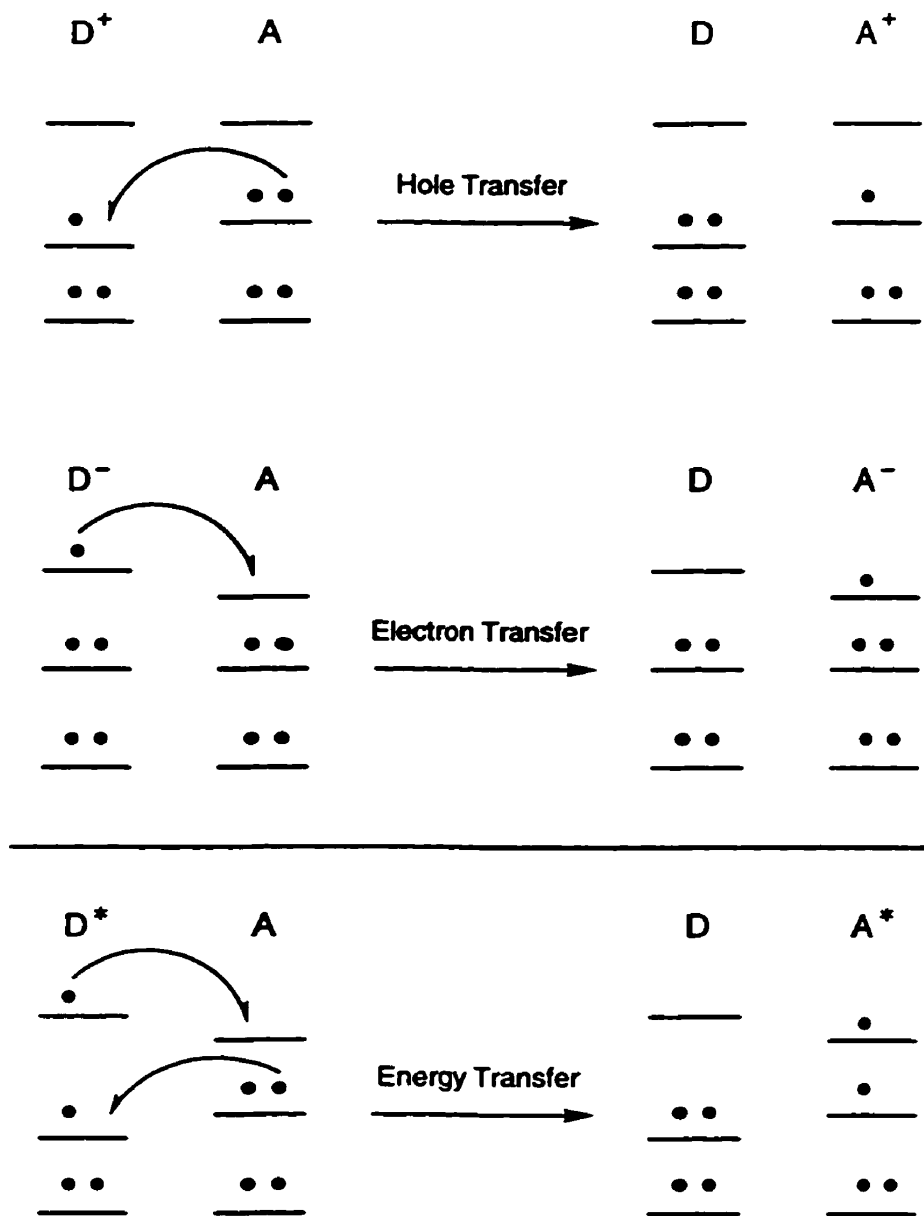
Figure 1.3 A schematic representation showing energy transfer as the combination of hole and electron transfer.

1.2.2.4 Kinetics

From preceding sections, it is now clear that in the absence of photochemical reactions an excited state molecule M* can be deactivated through a number of different pathways, namely by emission, radiationless decay, or quenching (Scheme 1.9). In this

Scheme 1.9
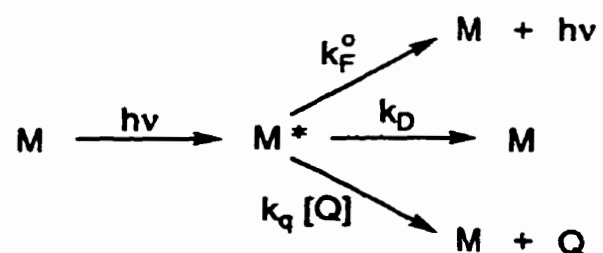
section, we will detail the kinetics of the bimolecular deactivation process, quenching. From Scheme 1.9 the quantum yield of fluorescence can be written as Equation 1.13. In the absence of quencher Equation 1.13 becomes Equation 1.14. Hence the ratio $\dfrac{\phi_F}{\phi_F^Q}$ of the

Equation 1.13

$$\phi_F^Q = \frac{k_F^o}{k_F^o + k_D + k_q[Q]}$$

Equation 1.14

$$\phi_F = \frac{k_F^o}{k_F^o + k_D}$$

quantum yield of fluorescence in the absence of quencher to that in the presence of quencher is given by Equation 1.15, where K_{SV} is the Stern-Volmer constant, which is a product of the excited state lifetime of M* in the absence of quencher (τ_s) and the quenching

Equation 1.15

$$\frac{\phi_F}{\phi_F^Q} = \frac{k_F^o + k_D + k_q[Q]}{k_F^o + k_D} = 1 + \frac{k_q[Q]}{k_F^o + k_D} = 1 + K_{SV}[Q] = 1 + k_q\tau_s[Q]$$

rate constant (k_q). Equation 1.15 is known as the Stern-Volmer equation.[7] If $\frac{\phi_F}{\phi_F^Q}$ is plotted against the quencher concentration [Q] a straight line with a slope of $k_q\tau_s$ will result. Therefore, if τ_s is known, then the quenching rate constant k_q can be obtained. The Stern-Volmer equation can also be transformed in terms of lifetimes to give Equation 1.16.

Equation 1.16

$$\frac{\tau_s}{\tau_s^Q} = 1 + k_q\tau_s[Q]$$

For many bimolecular systems the quenching rate constants are close to the diffusion-controlled rate constant (k_{diff}). This suggests that quenching is so efficient that the rate-determining step becomes the actual diffusion of the molecules to form an encounter complex (Scheme 1.10). Under steady-state conditions we obtain

Scheme 1.10

$$M^* + Q \underset{k_{-diff}}{\overset{k_{diff}}{\rightleftharpoons}} (M^* \cdots Q) \xrightarrow{k_q} M + Q$$
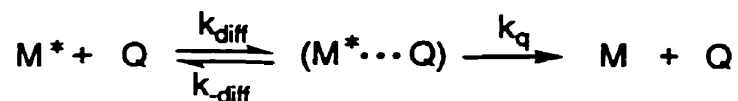
Equation 1.17. If we solve for the rate of formation of the product M and apply the steady-state conditions while substituting in Equation 1.17, we obtain Equation 1.18. Equation 1.19 describes the observed quenching rate constant.

Equation 1.17

$$k_{diff}[M^*][Q] = [M^* \bullet \bullet \bullet Q](k_q + k_{-diff})$$

Equation 1.18

$$k_q[M^* \bullet \bullet \bullet Q] = \frac{k_q k_{diff}}{k_q + k_{-diff}}[M^*][Q] = k_q(obs)[M^*][Q]$$

Equation 1.19

$$k_q(obs) = \frac{k_q k_{diff}}{k_q + k_{-diff}}$$

If $k_q \gg k_{-diff}$, then $k_q(obs) \approx k_{diff}$. The observed quenching rate constant is equal to the diffusion rate constant, and will be dependent on solvent viscosity. If $k_q \ll k_{-diff}$, then $k_q(obs) \approx k_q k_{diff} / k_{-diff} = k_q K$, where K is the equilibrium constant for the formation of the complex. In the latter case, the observed rate constant will be independent of solvent viscosity. Finally, if k_q and k_{-diff} are of the same order of magnitude, then $k_q(obs)$ will be less than k_{diff}. Therefore, by observing the kinetics of bimolecular quenching reactions under different experimental conditions (i.e., viscosity), information on the formation of encounter complexes can be obtained.

1.3 Probe Molecules

1.3.1 Fluorenone and Xanthone

The photochemical reactivity of aromatic ketones is determined by the configuration of the lowest excited electronic state. For example, excited triplet ketones with n,π^* configurations are much more reactive than triplet states with π,π^* configurations in hydrogen abstraction reactions.[5] Some aromatic ketones have excited states with different
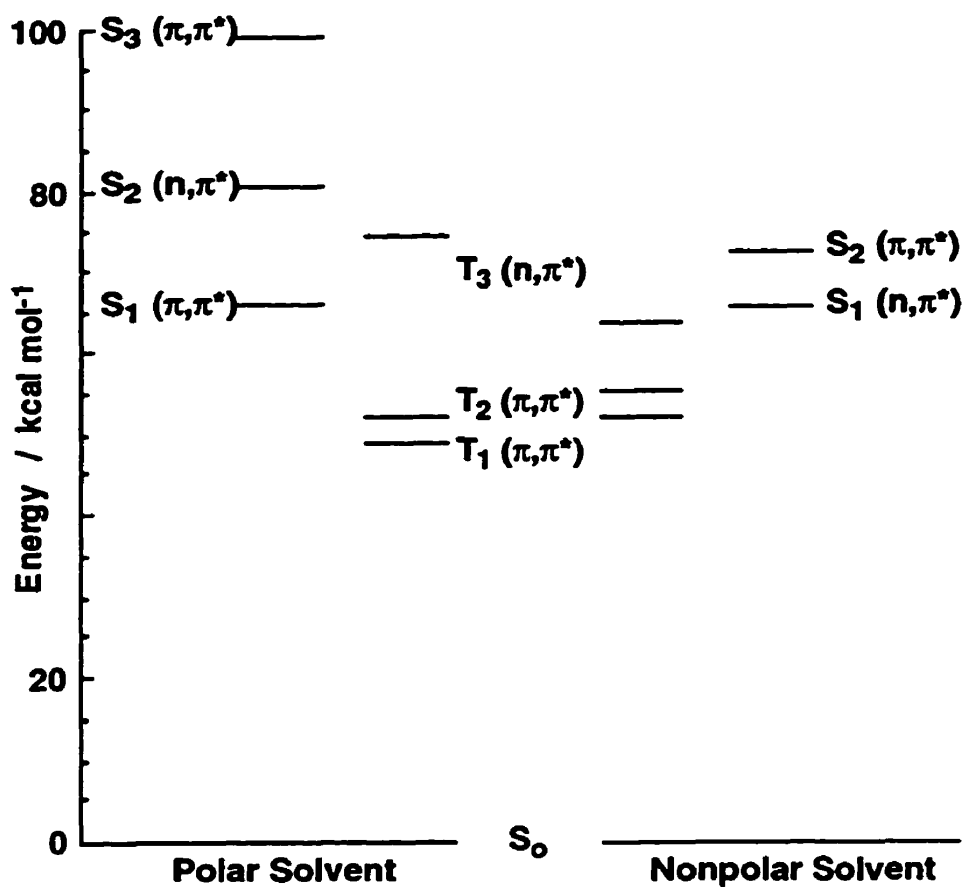
Figure 1.4 Energy level diagram for fluorenone in polar and nonpolar solvents (Adapted from reference 19).

configurations that are very close in energy. Such ketones frequently exhibit complex photophysics and photochemistry. Fluorenone is a particularly interesting aromatic ketone that has afforded such complexity. As a consequence of fluorenone having excited states with different configurations that are close in energy, the addition of electron-donating or electron-withdrawing substituents and the polarity of the solvent have an effect on the configuration of the lowest excited singlet and triplet states (Figure 1.4). Hence, this dependence strongly affects the photophysics and reactivity of fluorenone.

The complexity associated with the photophysics of fluorenone has been the topic of many investigations. [8-24] This complexity arises from the relative energy of the lowest singlet excited electronic state (S_1) with that of the upper triplet electronic state (T_3) of fluorenone. The T_3 state of fluorenone has a n,π^* electronic configuration that is stabilized by nonpolar solvents and electron-withdrawing substituents. Therefore, the magnitude of the T_3 state stabilization with respect to the S_1 governs much of the photophysics observed for fluorenone. For example, in nonpolar solvents the energy difference between these states in fluorenone is relatively small and efficient intersystem crossing is observed, whereas in polar solvents, the energy of the T_3 state is raised relative to the S_1 state, and the energy gap increases causing the efficiency of the intersystem crossing process to decrease.

This influence of solvent polarity on the configuration and energy of the S_1 state and on its relative position to the T_3 state has been established using steady-state and time-resolved fluorescence studies[19,22], and laser flash photolysis.[8] The effect of temperature on the photophysics of fluorenone has also been investigated.[9,10] In nonpolar solvents, the fluorescence quantum yield was low, the fluorescence lifetime was short, the intersystem crossing quantum yield and rate constant were high, and a temperature dependence was observed for the latter rate constant. In polar solvents, the fluorescence quantum yields and lifetimes increased. The intersystem crossing quantum yields were much smaller than in nonpolar solvents, and no temperature dependence on the intersystem crossing rate constant was observed. In addition, internal conversion was a significant

deactivation pathway for the singlet excited state in polar solvents. As mentioned, this behavior is primarily due to significant changes in the singlet-triplet energy gap (ΔE_{ST}) in solvents with different polarities. In nonpolar solvents, it is believed that the T_3 state has an energy comparable to that for the S_1 state, and is involved in the intersystem crossing process. In contrast, in polar solvents the energy of the T_3 state is increased relative to S_1 and the T_3 state is not involved in the crossing to the triplet surface.

Quite recently studies on the role that hydrogen-bonding solvents have on the photophysics of fluorenone have been reinvestigated.[11,12,16-18,21-25] It has been suggested that solvents capable of hydrogen bonding increase the internal conversion by effectively quenching the fluorescence, and inhibiting triplet formation. The photophysics of fluorenone has also been suggested to be affected by the formation of intramolecular hydrogen bonding for 1-aminofluorenone.[21,26] However, recent investigations have shown that this may not be the case because the distance between the carbonyl and amino groups is too large. The authors suggested that the radiationless deactivation was induced through an intermolecular hydrogen bond between the hydroxyl hydrogen of ethanol and the carbonyl oxygen of the aminofluorenones.[23]

A variety of fluorenone derivatives substituted at the 2-position and their photochemistry and photophysics have also been investigated.[10,12] In nonpolar solvents, triplet state formation was the dominant process from the singlet excited state when an electron-withdrawing group was attached to the fluorenone moiety, whereas an electron-donating substituent promoted internal conversion. In the same way that substituents affect the ΔE_{ST}, the polarity of the solvent employed also affects the ΔE_{ST}. It was reported that the addition of an electron-donating group at the 2-position decreases the relative energy of the S_1 to the T_3 increasing the S_1-T_3 energy gap, and lowering the efficiency of intersystem crossing for these compounds. In the same study, the nitro derivative was investigated, and displayed unique characteristics from the other derivatives in that both of its lowest

singlet and triplet states had n,π* electronic configurations. As a result, intersystem

crossing was suggested to occur through an intermediate triplet state with a π,π*, which is

favored according to El-Sayed's rules for spin-orbit coupling. This was suggested as the

reason for the high triplet yields for this compound. The quenching of fluorenones

substituted in the 2-position by alcohols was also correlated with the change in their dipole

moment upon excitation. It was observed that by introducing an electron-donating group

into the fluorenone backbone, the electron density on the carbonyl oxygen was increased,

and the hydrogen-bonding-accepting power of the singlet excited state was enhanced. As a

consequence, the quenching of the singlet excited state was more efficient. In contrast, the

introduction of electron-withdrawing substituents had the opposite effect. These

substituents reduced the electron density on the carbonyl oxygen and as a result decreased

the strength of the hydrogen bonds with the alcohols. This then led to a reduction in the

quenching rate constant of the excited state by the solvent. The importance of charge-

transfer character in excited states have also been pointed out to explain the changes in the

absorption spectra and fluorescence behavior of nitro-, perester-, and

aminofluorenones.[23,27]

Xanthone is an aromatic ketone, like fluorenone, that has excited electronic states

that are dependent on solvent polarity and temperature.[28] This dependence arises from the

low-lying singlet and triplet electronic levels that are close in energy and have either n,π*,

or π,π* electronic configurations. As a result, the triplet lifetimes of xanthone are very

dependent on solvent polarity. It has been reported that the triplet lifetime of xanthone in

cyclohexane is 22 ns; however, upon moving to a more polar solvent mixture of 1:1

water:acetonitrile the triplet lifetime increases by ca. 9 fold to 17.2 μs.[28] In addition, the

triplet-triplet absorption maximum of xanthone is very sensitive to solvent polarity with

shifts to shorter wavelengths of over 70 nm observed on going from carbon tetrachloride

$(\Delta A_{max} = 655$ nm) to water $(\Delta A_{max} = 580$ nm).[28,29]

The sensitivity afforded by xanthone to its environment makes this probe a very good candidate for the study of supramolecular systems that are often composed of microenvironments that have different polarities than the bulk aqueous phase. Xanthone has been employed to study complexation dynamics with supramolecular systems such as CDs by means of the direct spectroscopic method, for which no other triplet excited state probes are yet available.[29-32] The direct spectroscopic methodology requires two criteria. A property of the probe must be sensitive to its microenvironment, and a driving force for relocation has to be created upon excitation. The excited triplet state of xanthone fulfills both of these requirements. As mentioned, both the triplet state lifetimes and triplet-triplet absorption spectra of xanthone are dependent on solvent polarity.[28,29] The π,π^* nature of the lowest triplet excited state of xanthone is responsible for a higher dipole moment in its excited state when compared to the ground state. Upon excitation, π,π^* transitions lead to an increase in the dipole moment with respect to the ground state, whereas for n,π^* transitions the reverse occurs. In the case of xanthone, the driving force for relocation is believed to be the large change in dipole moment experienced upon excitation to its excited triplet state. It is these properties of xanthone that enable one to directly observe from the triplet-triplet absorption measurements the relocation of the complexed triplet state of xanthone from the less polar environment provided by a CD cavity to the polar aqueous phase. As a result, a detailed understanding of the complexation dynamics of xanthone with CDs and other supramolecular systems can be achieved.

1.3.2 Styrenes and Styrene Radical Cations

We chose to study the complexation dynamics of styrene radical cations to obtain an estimate of the residence time of charged organic molecules within CD cavities. This choice is based on the observation that the formation of radical cations of styrenes can be easily achieved in a two photon process (Scheme 1.11). In addition, the reactivity of these

radical cations had been reported previously.[33-38] Upon laser excitation of these styrenes, the first photon leads to the formation of an excited state, and the second photon leads to photoionization and formation of radical cations and solvated electrons. The reactivity of these radical cations can be studied by following their transient absorption.

Scheme 1.11
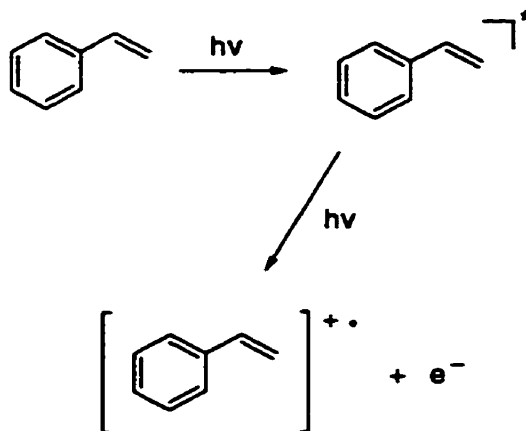
1.4 Cyclodextrins (CDs)

1.4.1 Properties of Cyclodextrins

A cyclodextrin (CD) is a cyclic oligosaccharide composed of D-glucopyranose units linked by $\alpha(1,4)$ bonds. The family of CDs is mainly composed of three well-known industrially produced cyclic oligomers that are referred to as the α-, β-, and γ-CDs. They are composed of six, seven, and eight D-glucopyranose units, respectively. These three CDs are white, crystalline, non-hygroscopic substances that take on a truncated-cone or torus-like structure.[39,40] One rim of the CD cavity is lined (for n glucose units) with n primary hydroxy groups, and the other rim is lined with $2n$ secondary hydroxy groups.
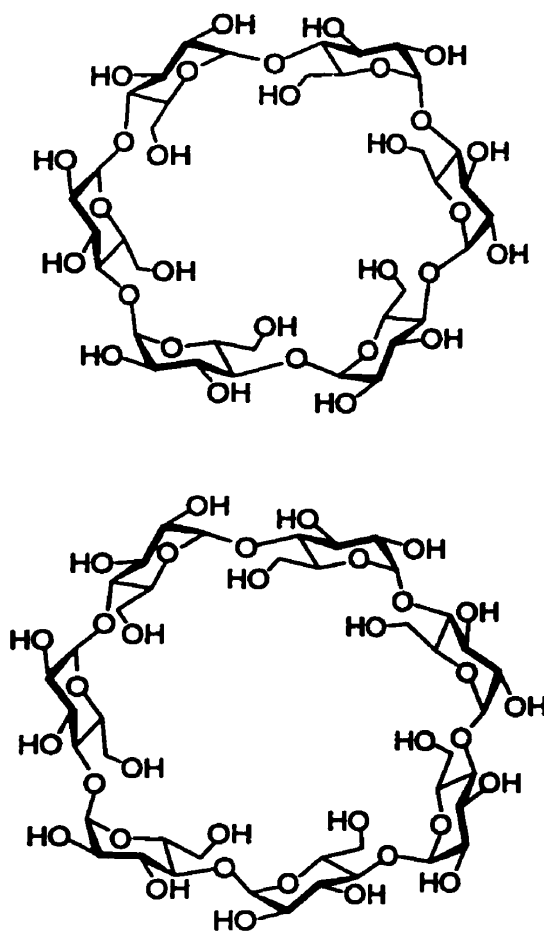
Figure 1.5 The structures of α- (top) and β-CD (bottom).

The two CDs of interest in this study were the α-, and β-CDs (Figure 1.5). Both CDs are soluble in water with α-CD (14.5g/100 mL) having a greater solubility than β-CD (1.85 g/100 mL), primarily because the structure β-CD is such that a rather rigid hydrogen bonded structure is formed between the secondary hydroxyl groups of the adjacent glucopyranose units. In α-CD, the hydrogen bonding network is incomplete because one of the glucopyranose units is in a distorted position. The cavity diameters at both ends of the CDs vary in size, whereas the height of the torus in both cases is unchanged (7.9 ± 0.1 Å) (Figure 1.6). The cavity diameters vary slightly from the end containing the primary hyroxyl groups to that of the secondary hydroxyl groups with distances of 4.7 to 5.3 Å and

6.0 to 6.5 Å for α- and β-CD, respectively. Consequently, the volume of the cavities is different with *ca.* 174 and 262 Å³ for α- and β-CD, respectively.
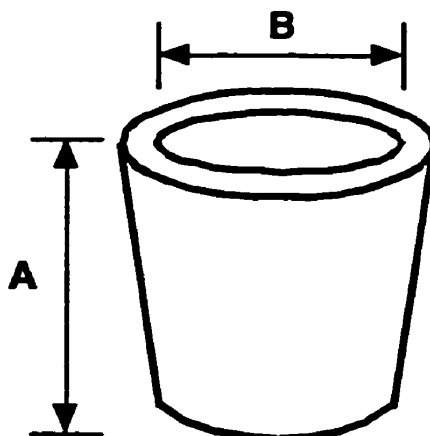
Figure 1.6 A cartoon pictorial of a CD detailing the axes for the height of the torus (A) and the cavity diameter (B).

1.4.2 Cyclodextrin Complexes

Supramolecular chemistry has evolved into a discipline of chemistry that investigates the intermolecular interactions between species, where covalent bonds are not established. The majority of these interactions have been of the host-guest type. CDs have been the most widely used molecules investigated as hosts for their potential application in such areas as catalysis, chromatography, drug delivery systems, and as biomimics for enzyme-substrate binding.[39,40] CDs are seminatural products that are easily produced from starch by a relatively simple enzymatic reaction. They are produced in the thousands of tons per year using environmentally friendly technologies, and the cost of their production has dropped over the decades making them more acceptable for most industrial processes. In addition, their toxic effects are limited so that CDs can be consumed by humans as ingredients in drugs, foods, and cosmetics.

In the past century, the evolution of CD technology has advanced through three main stages of development. Initially, the study of CDs was limited to understanding their structure. In the second stage of CD technology, the chemical and inclusion properties of these molecules were heavily investigated. It was not until the 1970's when CDs were deemed non-toxic, that the industrial production and widespread application of these systems became popular.

The momentum behind the investigations into CDs has been their ability to form inclusion complexes with many different types of guest molecules. In aqueous solution, the slightly nonpolar cyclodextrin cavity is filled with water molecules that are energetically not favored because of the polar-nonpolar interactions. As a result, these cavities are readily favorable to exchanges with less polar guest molecules. Upon complexation, these less polar guests are protected from the aqueous phase and at the same time the formally complexed water molecules of the CD cavity are released into the bulk aqueous phase. These conditions describe what is known as the hydrophobic effect. In addition, van der Waals forces and hydrogen bonding are also responsible for the binding of guests with CDs.[41,42]

The most frequently observed CD complexes have a 1:1 host-guest stoichiometry. However, complexes with 2:1, 1:2, 2:2 and higher order host-guest stoichiometries have been observed.[42-44] The main consequences of host-guest complexes involving a poorly soluble guest with CDs in aqueous solution are that the concentration of the guest molecule in solution increases significantly, and the spectral properties (i.e., UV-Vis absorption, fluorescence and circular dichroism) of the guest molecule changes upon inclusion with CD. Consequently, CDs have been widely used in many industrial applications that include drug delivery in the pharmaceutical industry, as stabilizers in the food industry, solubilizers in the cosmetic industry, and in chromatography for their chiral and polarity properties

Investigations into the probe dynamics involved with the complexation of guests with supramolecular systems such as CDs will continue to develop a more comprehensive understanding of the association and dissociation mechanisms. Most often complexation studies are limited to the determination of equilibrium constants in the ground state. To date, there have been far less examples of detailed investigations into the dynamics of guest molecules[45] within supramolecular systems than compared to the compilation of data that has focused on the determination of ground state equilibrium constants.[43]

Some of the initial studies on the dynamics of the host-guest systems involving CDs were carried out with α-CD and a series of naphthylazobenzenes using temperature-jump relaxation methods.[46] The equilibrium constants determined for these guest molecules showed little variation with the structure of the guest molecules with values ranging from 270 to 1010 M^{-1}. However, upon close inspection of the dynamic processes involved, it was observed that the association rate constants varied from 2.8 $M^{-1}s^{-1}$ to 5.2 × $10^7 M^{-1}s^{-1}$ and the dissociation rate constants ranged from 0.01 s^{-1} to 1.3 × $10^5 M^{-1}s^{-1}$. The differences in the dynamic processes were explained in terms of the desolvation of the guest molecules from the aqueous phase upon complexation with the CD cavity and resolvation upon returning to the aqueous environment. The insensitivity observed from the equilibrium constants was attributed to the similarity in the association and dissociation rate constants involved with the desolvation processes. This emphasizes the point that the determination of equilibrium constants is not sufficient for detailing dynamic events occurring within these host-guest systems.

Ultrasonic relaxation techniques have also been used to determine the entry and exit rate constants associated with the complexation of various inorganic ions with β-CD.[47] It was shown that the perchlorate anion (ClO_4^-) and periodate anion (IO_4^-) had an association rate constant that was ca. 30 times larger than a variety of other inorganic anions that included iodide, thiocyanate, bromide, chloride and nitrate. These larger association rate

constants were interpreted as a result of the larger radii possessed by the perchlorate and periodate ions and how this affected the solvation processes of the anions.

Bromonaphthoyl derivatives were used to study the effect of alkyl chain length on the complexation with CDs.[48] Complexation was observed with both β- and γ-CDs but not with α-CD. This suggested that the cavity afforded by α-CD was too small for the bromonaphthoyl moieties, yet appropriate for the larger CDs. The association and dissociation rate constants for these complexes were determined from quenching studies involving Co^{3+}. In the case of β-CD, the entry rate constants for the bromonaphthoyl derivatives were observed to be slightly higher for the probes with the shortest alkyl chains. This dependence was determined to be even smaller for the exit rate constants. In the case of γ-CD, the entry rate constants were very similar, but there was a significant dependence on alkyl chain length with the exit rate constants. A increase in the dissociation rate constant of a factor of ca. 3.5 on going from the bromonaphthoyl derivative with the alkyl derivative containing ten carbons to the derivative that contained only one carbon was observed. In addition, for the long chain derivative a biexponential decay was observed in the presence of quencher. This was assigned to two complexes with different structures, where one structure is better protected from quenchers in the aqueous phase. This dependence was again interpreted on the basis of the size of the guest molecule and the role of desolvation required for complexation, as shown for the naphthylazobenzenes discussed earlier. These studies were also performed using nitrite ions as the quencher. These studies yielded identical exit rate constants within experimental error. This demonstrates that the exit rate constants are independent of the quencher employed.

The complexation dynamics of xanthone with CDs was studied employing various methods. As discussed earlier (Section 1.3.1), xanthone is an aromatic ketone, like fluorenone, that has excited states that are dependent on solvent polarity. As a result, xanthone has been employed to study complexation dynamics with CDs by means of the direct spectroscopic method, for which no other triplet excited state probes are yet

available.[29-32] The direct spectroscopic methodology requires two criteria. A property of the probe must be sensitive to its microenvironment, and a driving force for relocation has to be created upon excitation. The excited triplet state of xanthone fulfills both of these requirements. The triplet-triplet absorption maximum of xanthone is very sensitive to solvent polarity with shifts to shorter wavelengths of over 70 nm observed on going from carbon tetrachloride ($\Delta A_{max} = 655$ nm) to water ($\Delta A_{max} = 580$ nm).[28,29] It is these properties of the triplet excited state of xanthone that enables one to directly monitor its relocation from the CD cavity to the aqueous phase.

The complexation dynamics of triplet xanthone were investigated for β-, Hp-β- and γ-CDs.[29,30,49] The association rate constants were much higher for β-CD than for γ-CD, suggesting that the latter CD was too large to accommodate triplet xanthone. The Hp-β-CD has several ether groups in the place of the hydroxyl groups. This CD was observed to have lower association rate constants for triplet xanthone than with β-CD. This decrease was assigned to the larger cavity size created by the ether appendages. In contrast, the dissociation rate constants were independent of the CD employed.[30,49] From these exit and entry rate constants the equilibrium constants for triplet xanthone were determined and compared with those of the ground state equilibrium constants. Those for the excited state were significantly smaller than those determined by fluorescence quenching experiments in the ground state. This provides one of the few examples, where the equilibrium constants for excited and ground states can vary by orders of magnitude. In addition, it stresses the point that any extrapolation of excited state dynamics using parameters obtained from the ground state should be avoided.[30,45,49] Quenching studies have also been employed to determine the exit and entry rate constants for triplet xanthone with CDs.[29,30,49] These were performed using high concentrations of cupric ions. The rate constants obtained from these studies were comparable, except for the higher exit rate constants observed for γ-CD

that was attributed to the capability of the quencher to access the probe within the CD cavity.

In recent studies, it has been shown that the exit rate constant of triplet xanthone from β- and γ-CD significantly decreases in the presence of alcohols by at least a factor of five over that in the absence of the alcohols.[31] It was suggested that these co-solvents could be solvating preferentially the entrances of the CD cavities. As a result of this preferential solvation, a barrier for the exit of the excited triplet state of xanthone from the CDs to the aqueous phase could be created. Thus, a decrease in the dissociation rate constants would be observed.

To this point much of the discussion has focused on host-guest complexes formed between a variety of guests and different sizes of CDs. To this end, much of the reasoning for differences in the exit and entry rate constants has been interpreted from size arguments and desolvation processes. Size restrictions on the part of the guest, or host has been shown to greatly favor or disfavor the association and dissociation events. However, little has been studied on how the structure of these host-guest complexes affects the dynamic events associated with complexation. Until recently, the majority of the complexation dynamics have been studied for 1:1 host-guest complexes with CDs. In a recent study, quenching studies were used to determine exit and entry rate constants for a 2:2 host-guest complex.[50] The complexation of 1- and 2-naphthyl-1-ethanols (1- and 2-NpOH) with β-CD were studied with a variety of spectroscopic techniques. Equilibrium constants for the 1:1 complexes of both probes with β-CD were determined using fluorescence and ^{1}H NMR. From the fluorescence studies, an excimer emission for the complex of 2-NpOH at higher concentrations with β-CD was observed. This emission was assigned to the formation of a 2:2 host-guest complex. From quenching studies, employing Mn^{2+} as a quencher, the exit and entry rate constants were determined for the NpOHs with β-CD. The association rate constants for the 1:1 host-guest complexes of 1- and 2-NpOH with β-CD were the same within experimental error, whereas the dissociation rate constant was

smaller by a factor of *ca.* 2.5 for the 2-NpOH. It was suggested that this difference could be explained in terms of the structure of the complex.[50] For example, if 2-NpOH is more deeply included in the β-CD cavity than 1-NpOH, then this difference in the structure of the CD complex could be the determining factor behind the decrease in the exit rate constant observed for 2-NpOH when compared with 1-NpOH.

In the quenching of the 2:2 complexes formed with 2-NpOH and β-CD, much less efficient quenching by Mn^{2+} was observed for triplet state of 2-NpOH observed in water, or for the 1:1 CD complex. This protection was assigned to the encapsulation of the probes by two CD molecules. In such a case, for the quencher to access the probe it would have to enter the CD cavity from the narrower entrance as opposed to the 1:1 complexes where the probe is exposed to the aqueous phase and the quencher only has to interact with the rim of the CD in order to interact with the triplet state of 2-NpOH. It was also suggested that efficient quenching of the 2:2 complex may first depend on the dissociation of the CD dimer enclosing the two NpOHs.[50] CDs have been used as host systems for many studies involving ground state host-guest complexation; however, there is still much more to learn about the complexation dynamics associated with these host-guest systems in the excited state.

1.4.2.1 Equilibrium Constants and the Benesi-Hildebrand Treatment

The equilibrium constants (K_{eq}) for CD complexes can be recovered from the analysis of the change in the absorption, fluorescence, or ICD intensities with increasing CD concentrations. The observed intensity change (ΔI) is given by Equation 1.20, where $[P]_T$ is the total probe concentration and Δ_x is related to the differences in the molar absorptivities, the emission quantum yields, or the molar ellipticities of the free and complexed probe in the case of the absorption, fluorescence, or ICD experiments,

Equation 1.20

$$\Delta I = \frac{[P]_T \, \Delta_x \, K_{eq} \, [CD]^n}{1 + K_{eq} \, [CD]^n}$$

respectively. In Equation 1.20, a n:1 (n=1, or 2) CD:probe stoichiometry, where for n=2 no 1:1 complex is formed, is assumed.[51] In addition, the CD concentration can be assumed to be constant because it is present in an excess over the probe concentration.

A linear relationship, frequently referred to as the Benesi-Hildebrand plot,[52] is obtained for the double-reciprocal plot of Equation 1.20:

Equation 1.21

$$\frac{1}{\Delta I} = \frac{1}{[P]_T \Delta_x} + \frac{1}{[P]_T \Delta_x K_{eq}[CD]^n}$$

The K_{eq} values were obtained from the non-linear fit of the experimental data to Equation 1.20 since this plot properly weights the experimental data. However, Equation 1.21 is very useful to check if the assumed stoichiometry is valid. If deviations from linearity for a plot of $1/\Delta I$ against $1/[CD]^n$ are observed this indicates that the assumed stoichiometry (n) is incorrect.

Alternatively, when a complex with 2:1 CD:probe stoichiometry is observed, the 1:1 complex can also be present at moderate CD concentrations (Scheme 1.12). The ΔI

Scheme 1.12

$$P + CD \underset{}{\overset{K_1}{\rightleftharpoons}} PCD$$

$$PCD + CD \underset{}{\overset{K_2}{\rightleftharpoons}} PCD_2$$
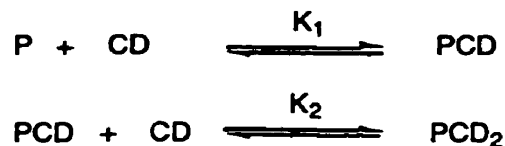
value is a function of the differences in molar absorptivities, fluorescence quantum yields, or molar ellipticities for the probe in solution and when incorporated into the 1:1 ($\Delta_x(1)$) and 2:1 ($\Delta_x(2)$) CD complexes.

Equation 1.22

$$\Delta I = \frac{[P]_T K_1 \Delta_x(1)[CD] + [P]_T K_1 K_2 \Delta_x(2)[CD]^2}{1 + K_1[CD] + K_1 K_2[CD]^2}$$

Equation 1.22 is reduced to Equation 1.23 when $\Delta_x(1)$ is equal to zero, which is the case when the fluorescence quantum yields are the same for the probe in water and incorporated in a 1:1 complex:

Equation 1.23

$$\Delta I = \frac{[P]_T K_1 K_2 \Delta_x(2)[CD]^2}{1 + K_1[CD] + K_1 K_2[CD]^2}$$

1.4.2.2 Quenching Studies

The mobility of an excited state molecule between a homogeneous phase and that of a supramolecular system can be investigated using an indirect method known as the quenching methodology (Figure 1.7).[45] Using this methodology the association and dissociation rate constants for the excited probe molecule can be determined. In homogeneous solution the kinetics of an excited state molecule follows Equation 1.24

Equation 1.24

$$k_{obs} = k_o + k_q[Q]$$
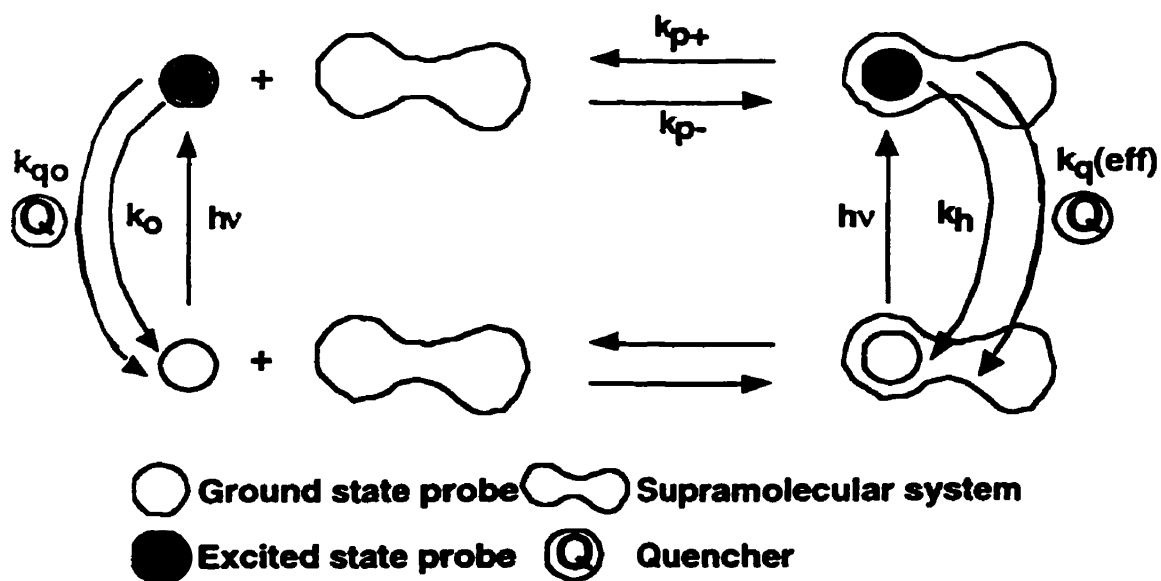
Figure 1.7 Kinetic scheme representing the excited state quenching of a probe molecule in the presence of a supramolecular system.

where k_{obs} is the observed rate constant, k_o is the first-order rate constant for the decay of the excited probe in the absence of quencher, k_q is the second-order quenching rate constant, and [Q] is the quencher concentration. From linear plots of k_{obs} against the concentration of quencher, k_q can be recovered from the slope of the dependence and the y-intercept will be k_o. Generally, in the presence of a host molecule, the plot is no longer linear but levels off with increasing quencher concentrations. The leveling off occurs if the efficiency of the quencher is reduced because the complexed probe is protected by the host molecule and the entry and exit dynamics of the guest with the host is of the same order of magnitude as k_{obs}. At high quencher concentrations, the decay of the excited state in the aqueous phase will be very fast and the exit from the host molecule will be rate determining.[45] The fitting of these curved plots is complex and a variety of other variables are introduced in Equation 1.25. The expression used to fit this data is shown in Equation 1.25, where k_{p+} and k_{p-} are the association and dissociation rate constants, respectively.

Equation 1.25

$$k_{obs} = k_h + k_{p-} + k_q(eff)[Q] - \frac{k_{p-}k_{p+}[H]}{k_{p+}[H] + k_o + k_{qo}[Q]}$$

The rate constants k_o and k_q are for the decay of the excited state probe in the absence and presence of the host molecule, respectively. These values can be determined from independent experiments in the absence of quencher molecules. The rate constants that describe the quenching of the excited state molecule by the quencher in the absence and presence of the host molecule are k_{qo} and $k_q(eff)$, respectively.

1.4.2.3 Induced Circular Dichroism

A compound is considered to be optically active if it shows the phenomenon of circular dichroism. Circular dichroism arises when a molecule absorbs with different molar absorptivities, ε_L and ε_R, for left- and right-handed circularly polarized light, respectively (Equation 1.26). For linearly polarized light the direction of the electric vector is constant

Equation 1.26

$$\Delta\varepsilon = (\varepsilon_L - \varepsilon_R)$$

about an axis in which the photon propagates, whereas the magnitude of this electric vector changes periodically. For circularly polarized light, the magnitude of the electric vector is constant, whereas the direction of propagation is constantly changing. When viewed perpendicular to the direction of propagation, the electric vector moves on a circular path, clockwise for right-handed circularly polarized light and counterclockwise for left-handed circularly polarized light. Using the same viewpoint, the electric vector of linearly polarized light oscillates in a plane, whereas for circularly polarized light the electric vector

forms a helix of constant pitch. The helix is right-handed if the light polarization is right-handed and left-handed if the light polarization is left-handed. Linearly polarized light can also be viewed as a superposition of right-handed and left-handed circularly polarized light of identical frequency and identical amplitude.

Circular dichroism is measured using a circular dichroism spectrophotometer that modulates a monochromatic beam of light between left-handed and right-handed circular polarization. A difference between ϵ_L and ϵ_R at a particular wavelength of light produces an intensity that can be amplified and displayed. Circular dichroism spectra are often not plotted as a difference in molar absorptivities, $\Delta\epsilon$, but as a molecular ellipticity, $[\theta]$ (Equation 1.27).

Equation 1.27

$$[\theta] = 3300 \, \Delta\epsilon$$

Although the guest molecules investigated here are achiral, in the chiral environment of a CD a guest molecule may exhibit induced circular dichroism (ICD). ICD spectroscopy has been useful in deducing the structure of CD complexes. ICD is based on the Kirkwood-Tinoco theory of polarizabilities that was developed for truncated cone-shaped hosts like CDs.[53-57] Generally, the rule states that if the transition dipole moment of the guest chromophore is aligned parallel to the axis of the CD cavity then the sign of the ICD signal will be positive, whereas if the axis of the guest chromophore is aligned perpendicular to the cavity axis then the sign of the ICD signal will be negative. This rule only applies if the chromophore resides within the cavity. If the chromophore is located outside the cavity then the signs of the ICD signals are reversed. Ideally, the theory is also able to predict the magnitude of the ICD signals, but it has been recently reported that due to the inherent structural flexibility and deviations from radial symmetry in CDs both the

shape and intensity of these ICD signals are affected.[58] As a result, differences from theoretical predictions should be expected and interpretations of the ICD spectra and the associated structures of the CD complexes should be performed with caution.

1.5 Research Proposal

The dynamics of host-guest systems involving CDs has been explored recently.[29-31,42,43,45-50,59,60] Our group has dedicated much of its research efforts to attaining a better understanding of the dynamics involved in CD complexes.[30,31,49,50] Xanthone was employed to study the complexation dynamics for a variety of different CDs[30,31,49] because xanthone has key photophysical properties that make it very useful in the study of host-guest dynamics. It was shown that the equilibrium constants for triplet xanthone with CDs, calculated from the exit and entry rate constants, are very different from the equilibrium constants for the ground state. Values for the equilibrium constants of triplet xanthone with CDs are ca. 20, 100 and > 50 times smaller than the equilibrium constants for the ground state xanthone with β-, Hp-β- and γ-CD, respectively.[30,49] In addition, the exit rate constants of triplet xanthone from β-, and γ-CD were decreased significantly in the presence of alcohols.[31] It was suggested that in the presence of alcohols these co-solvents could be solvating preferentially the entrances of the CD cavities. As a result of this preferential solvation, a barrier for the exit of the excited triplet state of xanthone from the CDs to the aqueous phase could be created.

In a similar study, the complexation dynamics of 1- and 2-naphthyl-1-ethanols (1- and 2-NpOH) with β-CD were studied.[50] Quenching studies established that the exit rate constants for 1:1 complexes with β-CD were smaller for 2-NpOH than 1-NpOH, suggesting that the shape of the molecule is important in determining the complexation

dynamics. In addition, dissociation of a guest from a 2:2 complex (β-CD:2-NpOH) was shown to be slower than the dissociation from the 1:1 complex.

The objective of this research is to investigate, in more detail, the aspects responsible for the dynamics of guest molecules in CD complexes. We initially began our study with the development of new probes similar to xanthone that could also be used to study mobility on CD systems by way of the direct spectroscopic methodology. We chose fluorenone since the photophysics of this aromatic ketone was known to be similar to that for xanthone. An earlier report has shown that the triplet quantum yield of fluorenone was low in the presence of hydroxylic solvents.[25] Although this effect on the triplet quantum yield of fluorenone limits the ability of fluorenone as a probe for the study of mobility in aqueous CD solutions, it was hypothesized that substituted fluorenones may have higher triplet quantum yields in hydroxylic solvents than the parent fluorenone. For example, a series of halogenated fluorenones were investigated to determine whether or not a heavy-atom effect can enhance the intersystem crossing quantum yields of the fluorenone derivatives over that of the parent fluorenone. As a result, a detailed photophysical characterization for several fluorenone derivatives was performed to achieve a better understanding on the role of solvent and substituents on several photophysical parameters, namely the intersystem crossing quantum yields.

The second objective was to obtain more information on the structure of host-guest complexes, so as to understand how structural parameters can affect the complexation dynamics. We studied the complexation of both xanthone and fluorenone to CDs. From the experimental point of view, we measured the induced circular dichroism spectra for the complexes. In addition, we developed a picosecond fluorescence system to obtain additional information on the complexation environment of the probes. These studies were supported by theoretical calculations done by Dr. B. Mayer (University of Vienna, Vienna, Austria) and Dr. G. Marconi (Istituto FRAE-CNR, Bolonga, Italy).[61]

Previous studies on the dynamics of guest complexation with CDs used organic triplet molecules as probes. To expand our understanding on the structure-dynamics relationship for CD complexation, we studied the complexation dynamics of charged guests. Complexation and quenching studies were performed with two styrene derivatives that are known to form radical cations upon two photon excitation.

A variety of photophysical techniques were employed to investigate the complexation dynamics of guest molecules with CDs. From these investigations, we have been able to better evaluate how the photophysics of probe molecules can be explored in the study of host-guest complexation. With this information, we will gain further insight into structure-dynamics relationship that exists for these host-guest systems.

2. EXPERIMENTAL

2.1 Reagents

9-Fluorenone (Aldrich®, 98%), 9-fluorenone-2-carboxylic acid (F-2CA, Aldrich®, 98%), 9-fluorenone-4-carboxylic acid (F-4CA, Aldrich®, 97%), 2-hydroxy-9-fluorenone (2OHF, Aldrich®), 2,7-dibromo-9-fluorenone (2,7DBF, Aldrich®, 96%), 2,7-dichloro-9-fluorenone (2,7DCF, Aldrich®, 90%), and ortho-hydroxybenzophenone (Aldrich®, 99%) were purified by recrystallization from ethanol/water mixtures. Xanthone (Aldrich®, 97%) was recrystallized from ethanol. Sodium azide (Aldrich®, 99%) was recrystallized from water. trans-Anethole (t-Ane, Aldrich®, 99%) and 4-vinylanisole (4-VA, Aldrich®, 97%) were distilled using a short-path distillation apparatus. 1,3-Dichloro-9-fluorenone (1,3DCF, ABC library, Aldrich®), 2,7-difluoro-9-fluorenone (2,7DFF, ABC library, Aldrich®), 3-hydroxy-9-fluorenone (3OHF, ABC library, Aldrich®), 4-hydroxy-9-fluorenone (4OHF, Aldrich®, 98%), 4-methoxy-9-fluorenone (4MF, ABC library, Aldrich®), sodium cyanide (Aldrich® ReagentPlus™, 99.99%), tetrabutylammonium iodide (Sigma-Aldrich®, Flukabrand, Ion-Pair Reagent), and potassium ferrocyanide(II) trihydrate (Aldrich®, 99%) were used as received. α-Cyclodextrin (α-CD, Lot F 8035) and β-cyclodextrin (β-CD, Lots C6 034-13 and F 6080-191) were a generous gift from Cerestar USA, Inc. and were used without further purification. The water employed was deionized (Sybron-Barnstead). Acetonitrile (ACP chemicals, spectrograde), toluene (ACP chemicals, spectrograde), methanol (ACP, spectrograde), 1-pentanol (Aldrich®, 99+%), (±)-2-butanol (Aldrich®, 99%) and 1-butanol (Anachemia, 99.4%) were used as received.

2.2 Instrumentation

2.2.1 UV-Vis Absorption

Cary 1, or Cary 5 spectrophotometers were employed to measure ultraviolet and visible (UV-Vis) absorption spectra at room temperature. A baseline correction of air against air was always performed at the beginning of the day and each run was instrument zeroed at a wavelength where there was no absorbance for the samples. The scan rate and bandwidth were 200 nm/min and 2 nm, respectively. All samples were measured in 10 mm × 10 mm quartz, long, or short stem absorbance, or fluorescence cells, or 7 mm × 7 mm Suprasil laser cells.

2.2.2 Fluorescence

2.2.2.1 Steady-State Fluorescence

Steady-state fluorescence spectra were obtained with a Perkin Elmer MPF-66, or a PTI QM-2 spectrofluorimeters at (20.0 ± 0.5) °C. The emission and excitation bandwidths were set between 2 and 10 nm on both instruments in order to maximize the emission intensities for the different probes. All samples were measured in 10 mm × 10 mm quartz, long, or short stem fluorescence cells.

2.2.2.2 Time-Resolved Fluorescence

2.2.2.2.1 Single Photon Counting

A PTI LS-1 nanosecond single photon counter (SPC) was employed to measure fluorescence lifetimes at (20.0 ± 0.5) °C. The instrument response function was obtained with a suspension containing finely ground silica at the excitation wavelength employed for the lifetime measurements of the various samples. The count accumulation was kept below 2% of the excitation rate, and 10,000 counts were accumulated at the channel of highest intensity. Decays were analyzed using the PTI software and the goodness of fit was judged by the value of the χ^2, and by visual inspection of the weighted residuals and the autocorrelation function. A χ^2 approaching unity indicates that no systematic deviation between the experimental data and the fit exists. All the fluorenone samples were excited at 285 nm and the emission and excitation slits were set such that the bandwidths were between 20 and 30 nm. All samples were measured in 10 mm × 10 mm square Suprasil fluorescence cells and were purged with nitrogen for at least 15 min to remove any oxygen present in solution.

2.2.2.2.2 Streak Camera Detection

A picosecond fluorescence system was used to measure the fluorescence lifetimes of fluorenone and xanthone and CD complexes of these probes (Figure 2.1). Excitation pulses (≤ 0.2 ps) are generated from a Ti:sapphire laser ((2), Coherent Mira 900-F) that is pumped by an argon ion laser ((1), Coherent Innova 400, 13W). The repetition rate of the pulse train is set with a pulse picker ((3), Coherent 9200) to values that are lower than the time frame being monitored by the streak camera. A small portion (< 4%) of the IR beam that leaves the Ti:sapphire laser and passes through the pulse picker is split by a
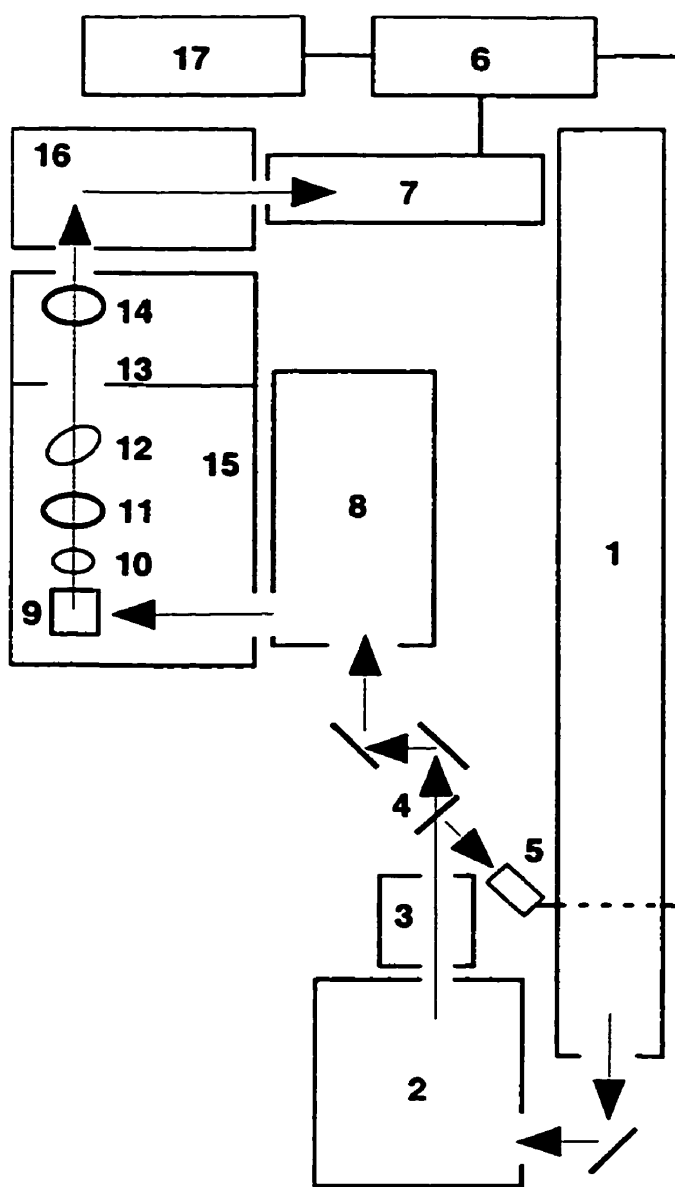
Figure 2.1 Picosecond fluorescence system.

beam splitter (4) and sent into a photodiode ((5), Thorlabs Inc. 201/579-7227). The pulse

detected by the photodiode is used to trigger the streak scope ((6), Hamamatsu Streak

Scope C4334), which in turn collects information from the steak camera detector (7). The

remaining part of the beam is passed through a tripler ((8), CSK SuperTripler 8315) in order to obtain the UV excitation light that is directed into the sample chamber (15).

The sample was placed in a 10 mm × 10 mm square, long stem, quartz fluorescence cell with a flat transparent bottom. The excitation beam was redirected through the sample holder (9) with a prism so that the exciting light passes through the bottom face of the cell. This arrangement helps to minimize reflections from the laser light passing through the fluorescence cell. When fast lifetimes (≤ 200 ps) were measured, an iris (10) was placed in front of the fluorescence cell ca. 12 mm from the front face of the cell at a 90° to the excitation source and is closed to a diameter of ca. 5 mm. This procedure was used to limit the area of the fluorescence cell from which the fluorescence was collected. When measuring short lifetimes, if the iris is not used then a broadening of the instrument response function and the sample signal will be observed because the light emitted from the bottom of the cell will be detected ca. 100 ps earlier than light emitted from the top of the cell (ca. 3 cm). As an additional precaution to reduce reflections of laser light, the remaining sides of the prism and fluorescence cell that were not involved in the pathlengths of the laser light, or fluorescence emission were covered in black electrical tape.

The light emitted from the sample holder was collimated with a first lens (11) and then focused onto the slit of the polychromator by a second lens (14). The amount of light reaching the detector was attenuated by inserting neutral density filters (12) between the two collection lenses. All the optical components between the sample holder and the polychromator were tilted slightly off axis so as to prevent reflections. The entire sample chamber was enclosed in a metal box lined with black felt and a cardboard cutout (13) was placed between the two lenses in order to diminish the collection of stray light.

The light collected from the sample holder was dispersed by a polychromator ((16), Chromex 250IS) before entering the streak camera so that a range of wavelengths can be monitored at the same time. The streak camera is triggered by the streak camera controller. The data collected by the streak camera is transferred through the controller to a Hamamatsu

frame grabber in a Power Macintosh 7100/80 computer ((17), 32 MB Ram, 500 MB HD). Communication between the Macintosh and the streak camera controller was achieved through a GPIB interface.

The timing in the picosecond fluorescence experiments is established from two sequential laser pulses (Figure 2.2). The first laser pulse (P1) triggers the photodiode. This photodiode signal is delayed passively through an appropriate length of 50 Ω coaxial (A to B) for repetition rates ranging from 1.449 to 4.717 MHz. Following this delay, the streak camera controller is triggered (B) and then encounters its own intrinsic delay (B to C) before it signals the sweep voltage generator of the streak scope to sweep the voltage (C). If the delay cables are chosen accurately for the delay of the photodiode signal to the streak camera controller then the second pulse (P2) will fall within the detection window (C to D) and the fluorescence signal is measured. For lower repetition rates a delay generator
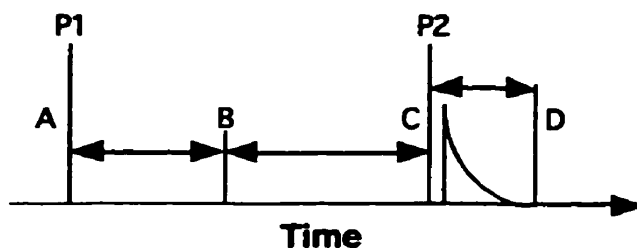
Figure 2.2 Timing diagram for the picosecond fluorescence system.

can be used to set the appropriate delays. Data acquisitions in the binary or photon counting modes (see below for the modes of collection) were always measured at the highest gain (16) of the streak camera. For each emission decay of the sample, an instrument response function (IRF) profile was collected by dispersing the laser light on a sandblasted aluminum plate that was inserted into the laser beam at the same position as the sample cell, or by using laser light scattered by the solvent used in the preparation of the sample. For short collection times, a better deconvolution was obtained when the IRF was

measured with the cell containing solvent because both the IRF and sample traces are collected for emission that has the same spatial distribution.

Data was acquired using the Hamamatsu Photolumi 2.45f program. The total collection time ranges from 1 ns to 10 ms and was set so that the decay of interest was measured for at least five lifetimes. The fluorescence maximum was centered in the spectral range set on the polychromator (90-100 nm range for the two 150 nm/groove gratings blazed at 300 nm and 500 nm, or a 140-150 nm range for the 100 nm/groove grating blazed at 450 nm). The slit of the polychromator was kept constant for the sample and IRF measurements. Calibration of the polychromator was performed periodically using the Hamamatsu software and a mercury lamp. Samples were typically excited with the tripled IR laser beam, but stray doubled laser light was also present in the tripler output. The decay kinetics can not be measured in the region where the doubled laser emission is detectable.

Data can be collected in the binarization, or photon counting modes. In the binarization mode, the intensity of the light collected above a set threshold is measured for each pixel. The collection time for this mode is faster than the photon counting mode but the intensity for each photon collected in the binarization mode is blurred over many pixels. As a result the best χ^2 values are larger than unity and is directly related to each particular streak camera. The best χ^2 value for our streak camera in the binarization mode was six. In photon counting mode the photon may also be blurred over many pixels but only the pixel with the highest intensity is assigned a value of unity. The collection time for the photon counting mode is slower, however χ^2 values of unity can be obtained. The discrimination between pixels is all carried out by the computer software written by Hamamatsu. In addition to the different collection modes, a correction for the sensitivity of the streak camera is carried out. The detection sensitivity is not constant over the whole area of the detector's microchannel plate (MCP). This MCP is used to amplify the photoelectrons that pass through the streakscope. This correction is known as "shading"

(set in the Hamamatsu program) and must be applied when the binarization mode is employed. The shading correction files have to be acquired for each set of experimental conditions that includes the slit width and wavelength range. Such a correction is not necessary in the photon counting mode.

To ensure that no photon pile up occurs (i.e. detection of more than one photon per measurement) the number of counts per cycle (CPC) has to be calculated at the emission maximum. A number of sequential pulses are acquired by the streak camera (frames per cycle, always set at 30) before the data is transferred to the frame grabber. Equation 2.1 and Equation 2.2 are the definitions for the CPC for the binarization and photon counting modes, respectively. These are related to the procedure Hamamatsu employs to collect data.

Equation 2.1

$$CPC\ (Bin)\ =\ \frac{Intensity\ recorded}{number\ of\ \lambda\ channels\ *\ frame\ per\ cycle\ *\ number\ of\ cycles}$$

Equation 2.2

$$CPC\ (pc)\ =\ \frac{Intensity\ recorded}{number\ of\ \lambda\ channels\ *\ number\ of\ cycles}$$

The time increment between two pixels on the target of the streak camera is not a constant value, since it depends on the rate of the voltage ramp applied to the streak camera. Each streak camera has its own calibration for each time range. The data analysis package from Hamamatsu interpolates the intensity data so that a constant time increment is used by the fitting routine. In our experience this interpolation procedure leads to deviations from first-order fits for standard molecules that have a monoexponential decay (e.g., anthracene in cyclohexane). For this reason an alternate data analysis procedure was developed. Data

analysis is achieved with a commercial PTI (Photon Technology International) fitting

software used on a PC computer that was adapted by PTI to fit decays with non-constant

time increments. The PTI software can be employed to perform fits to single decays, or for

global analysis. A Labview 4.0 (National Instruments) program (Dr. L. Netter)

transforms the Hamamatsu raw data file into a file that can be read by the PTI fitting

software. In this program the data and IRF files are displayed on the screen and the

wavelength range that will be integrated for each decay profile is defined.

2.2.3 Induced Circular Dichroism

Induced circular dichroism (ICD) spectra were recorded with a Jasco-720

spectropolarimeter. The scan rate, bandwidth, and integration time set for each spectrum

was 10 nm/min, 2 nm, and 8 s, respectively. A 10 mm cylindrical quartz circular

dichroism cell was used and all measurements were recorded at room temperature. An

average of two, or three spectra was obtained for samples with small signals. A baseline

was collected by recording the circular dichroism spectrum for aqueous solutions of achiral

probes at the same parameters as the other CD solutions. These achiral probes do not have

any circular dichroism signals but were important to record because the photomultiplier

voltage for the baseline run in the region where these molecules absorb will be similar to

that for the samples containing the probes and CD. In addition, an aqueous solution of the

highest CD concentration used was also recorded to correct for the CD signals observed for

the chiral CDs. Corrections of the spectra for these CD:probe complexes were carried out

with three different treatments. First the baseline spectrum was subtracted from the

spectrum of the CD:probe complex. Then an additional subtraction of the spectrum for the

aqueous CD solution was applied. If the CD concentration of the complex of interest was

smaller than the stock CD solution then the appropriate ratio of concentrations was applied.

It was assumed that the CD signal was proportional to and had a linear relationship with

concentration. Finally the spectrum was normalized to zero in a region where there was no CD signal present. This was carried out by averaging five ellipticity values in the specific region and then either adding, or subtracting this value to the entire data set.

2.2.4 Laser Flash Photolysis

2.2.4.1 Transmission Measurements

The setup for transmission measurements using the laser flash photolysis system is shown in Figure 2.3. The two excitation sources used for this system are a Lumonics Excimer laser model EX-510 operated with a Xe/HCl gas mixture ((1), 308 nm, ≤ 40 mJ/pulse), or a Spectra Physics Quanta-Ray GCR-12 Nd:YAG laser ((2), 266 nm, ≤ 40 mJ/pulse; 355 nm, ≤ 70 mJ/pulse). In the case of the Excimer laser, the laser pulse energies can be attenuated to less than 20 mJ/pulse through the use of neutral density filters ((3), 63, 40, 25, and 10% transmission of neutral density filters). For the YAG laser the flash lamp energy (i.e., intensity) can be attenuated with an external dial. The YAG laser beam is directly aligned onto the sample holder (i.e. (8) and (9) are removed) with occasional use of a 350 nm band-pass filter that is placed in front of the sample holder and is used to diminish interference from other laser light (i.e., 532 nm) that can not be separated entirely. In contrast, the Excimer laser beam is passed through a lens (4) and then reoriented using a mirror (5) and focused with the use of a spherical lens (7). A prism (8) is used to alter the direction of the laser beam so that it strikes the sample holder (10) at a 90° angle relative to the monitoring beam, after being further focused by an additional spherical lens (9) behind but not into the sample holder.

A 150 W xenon lamp ((11), Oriel housing model 66057, PTI power supply model LPS-220) is used as the light source for the monitoring beam. The pulser ((12), custom
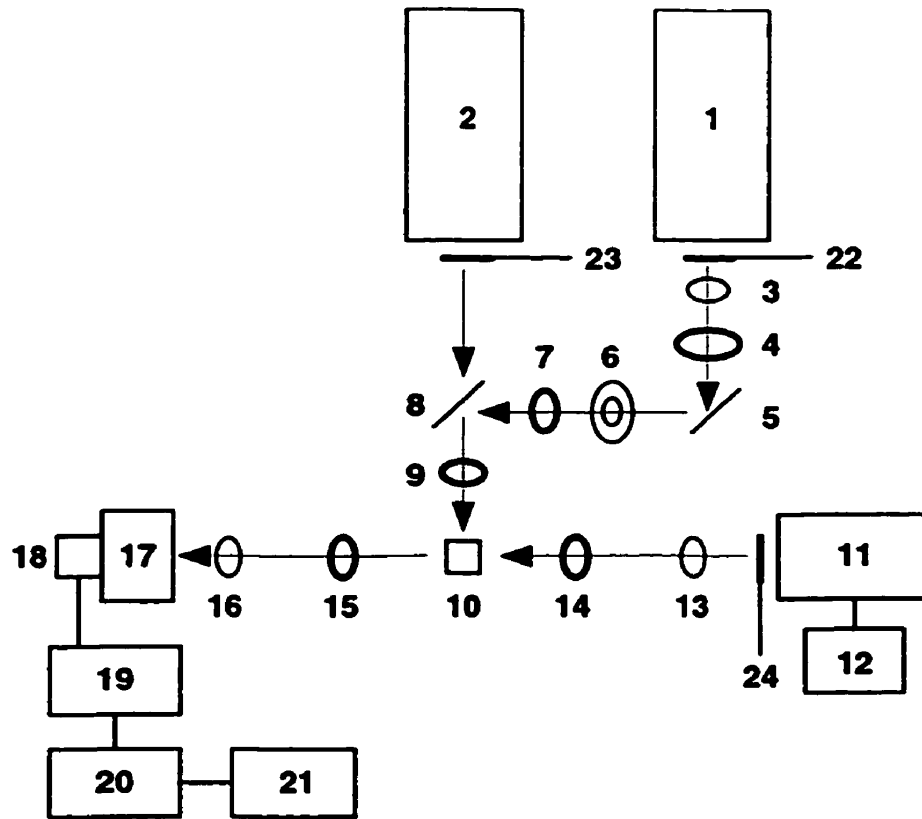
Figure 2.3 The laser flash photolysis system set up for transmission measurements.

built, University of Victoria) is used to create, upon triggering, a high intensity output of the xenon lamp for a period of 4 ms. The monitoring beam passes through a cut-off filter ((13), no filter, 320, 375, 435, or 590 nm) to reduce the degradation of the sample that may take place due to the constant irradiation of the sample during data accumulation. The beam is then focused with a lens (14) so that the focal point lies behind the sample. The beam then passes through a pinhole on the front face of the sample holder. After passing through the sample, the monitoring beam proceeds through a focusing lens (15) to collimate the beam into the detection system, not before passing through another cut-off filter (16) to ensure that overtones of the wavelength being monitored and scattered laser light are not observed by the detection system. The detection system employed is a

photomultiplier ((18), PMT, Hamamatsu R446, five dynodes) coupled with a

monochromator ((17), CVI Digikrom 240) which together leads to the detection of light

intensities at fixed wavelengths. The high voltage for the PMT tube is set by a custom-built

programmable power supply that is interfaced to the computer. Signals from the PMT are

then sent into a baseline compensation unit ((19), BCU) that incorporates a sample and

hold amplifier with digital memory based on a published circuit.[62] Figure 2.4 shows

details on how the BCU is used to obtain a kinetic trace. In the diagram, a Xe lamp profile

(above) is shown with the corresponding output measured by the scope (below). The

BCU continuously offsets the lamp signal. The lamp is pulsed at A. On receiving a trigger

pulse (B) and before the laser pulse hits the sample (C), the BCU holds constant the value

of the background intensity of the Xe lamp (V_o) detected by the PMT, measured as a dc

output proportional to its magnitude. At this point (B), the BCU stops compensating the

signal and subtracts the held dc value from the new voltage (bottom trace). This light
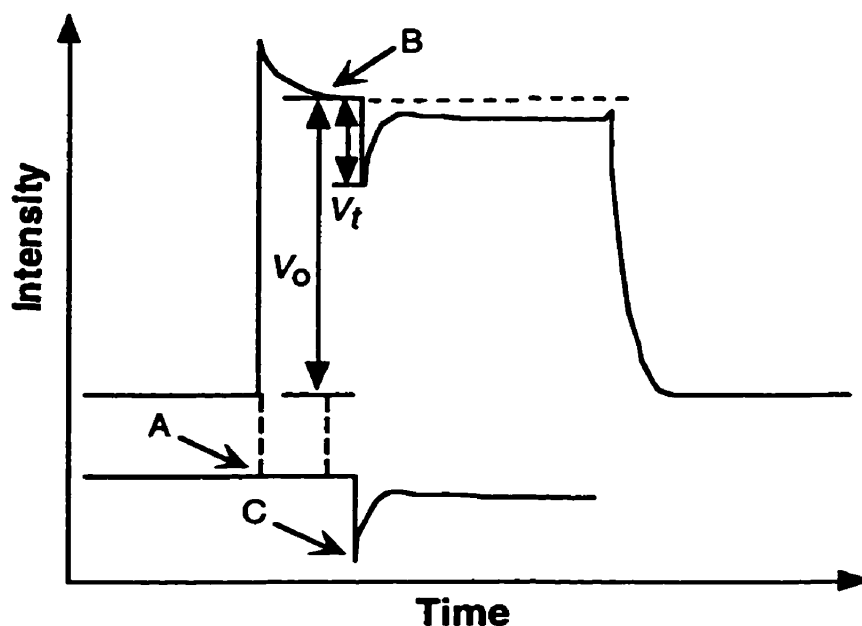
Figure 2.4 A schematic representation of a Xe lamp profile during the acquisition of a
kinetic trace (above) and the resulting output from the BCU (below).

intensity (i.e., the transient signal) is then measured with a digital oscilloscope ((20),

Tektronix TDS 520) that is interfaced to a Macintosh IIci computer (21).
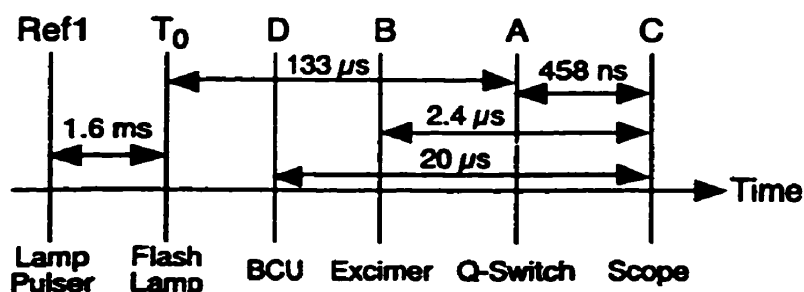
Figure 2.5 The timing diagram for transmission measurements using the laser flash photolysis system.

The timing for the lamp pulsing, the laser pulsing, the baseline compensation unit, and the oscilloscope were set by a custom-built pulse generator (millisecond delays) that acts as the master clock and drives a Stanford Research System delay generator model DG535 (nanosecond delays). The timing was set so that the "flat" portion of the 4 ms lamp pulse was used. The timing sequence begins with the triggering of the lamp pulser, that was triggered by a pulse received from the master clock (Figure 2.5). The reference point (Ref1) in this sequence of events was the pulsing of the lamp. A delay of 1.6 ms was introduced after the pulsing of the lamp before the flash lamp of the YAG and the external trigger for the delay generator were triggered by the master clock. The triggering of the flash lamp and delay generator were defined as time zero (T_0). The Q-switch of the YAG was triggered 133 μs after T_0, which corresponds to delay A of the delay generator (A = T_0 + 133 μs). Delay C was used to trigger the oscilloscope 458 ns after the Q-switch of the YAG was triggered (C = A + 458 ns). Delay D was responsible for the triggering of the BCU. The BCU was triggered 20 μs prior to the triggering of the scope and hence before the Q-switch of the YAG was triggered (D = C - 20 μs). The YAG laser pulses at a repetition rate of 1 Hz. Both the shutters in front of the YAG laser (23), in front of the lamp (24) and the Excimer (6 and 22) were opened prior to the triggering of the lamp

pulser. The triggering of the Excimer laser was also controlled from the master clock and delay generator in the same manner as for the YAG. The only difference being that an additional delay, delay B, was introduced for the triggering of the Excimer. Delay B was set 2.385 μs prior to delay C (B = C - 2.385 μs). Data collection occurred at a rate of 0.3 Hz because some time was required to allow for the capacitors of the lamp pulser to recharge. When a transient was monitored over a time scale ≥ 20 μs, a baseline shift due to the profile of the lamp pulse was observed. To correct for this shift, a baseline correction shot was measured immediately following the signal shot. This correction shot was acquired in the absence of the laser pulse that was obtained by lowering the shutters (6, or 23). The correction shot was then subtracted from the signal shot before the calculation of ΔA and after the data was transferred to the computer.

Software written on the Labview 4.1 platform (National Instruments, Dr. L. Netter) subtracts correction shots, controls the experimental settings (i.e. opening and closing shutters and setting filter wheels), transforms voltage data tracked from the oscilloscope into absorbance values, averages sets of measurements and saves the data into computer files.

Absorbance values (ΔA) are equal to the negative logarithm of the ratio of light intensities being detected on the PMT in the absence and presence of transients. This relationship (Equation 2.3) assumes a linear response of the signal measured at the PMT

Equation 2.3

$$\Delta A = -\log\left\{1 - \left(\frac{(V_t)_{corrected}}{(V_0)}\right)\right\}$$

with the light intensity irradiating the detector. The response of PMTs is not linear. For this reason only small changes in light intensity are measured that corresponds to ΔA values ≤ 0.2. As a result, an algorithm was incorporated into the program to acquire the data at a

constant target value for V_0 of 250 mV. At wavelengths where the Xe lamp has a high light

intensity output, the high voltage on the PMT is initially kept at 800 V, and the slit on the

monochromator is adjusted to an experimentally determined calibration curve. Toward

either ends of the lamp spectrum the maximum slit width of 2000 μm is used, and the

voltage is increased to a value also determined by calibration. During the data acquisition

the high voltage on the PMT (v) is constantly being adjusted when the experimental V_0

value is off by more than 10% from the target V_0. From calibration data it was determined

that relationship between the high voltage on the PMT and the target voltage was to the

power of six (i.e., $V_0 \propto v^6$; (Equation 2.4)). If the maximum voltage on the PMT is used

and the target V_0 is not reached, then the program will increase the monochromator slit.

Equation 2.4

$$\upsilon_{new} = \left[\left(\frac{V_{0,\,target}}{V_{0,\,exp}}\right)(\upsilon_{old})^6\right]^{\frac{1}{6}}$$

The kinetic analysis of the decay curves was fit with a program written in C (Dr.

A.D. Kirk, Department of Chemistry, University of Victoria) based on Levenberg-

Marquardt algorithms and interfaced into Labview. Alternatively, Kaleidagraph (Synergy

Software version 3.08d) was used to fit the data.

2.2.4.2 Photoacoustic Measurements

The setup for the photoacoustic measurements, or laser-induced optoacoustic

spectroscopy (LIOAS) is shown in Figure 2.6. As described above the YAG laser (1) at

355 nm is used as the excitation source and is directed with a small prism (2) towards the
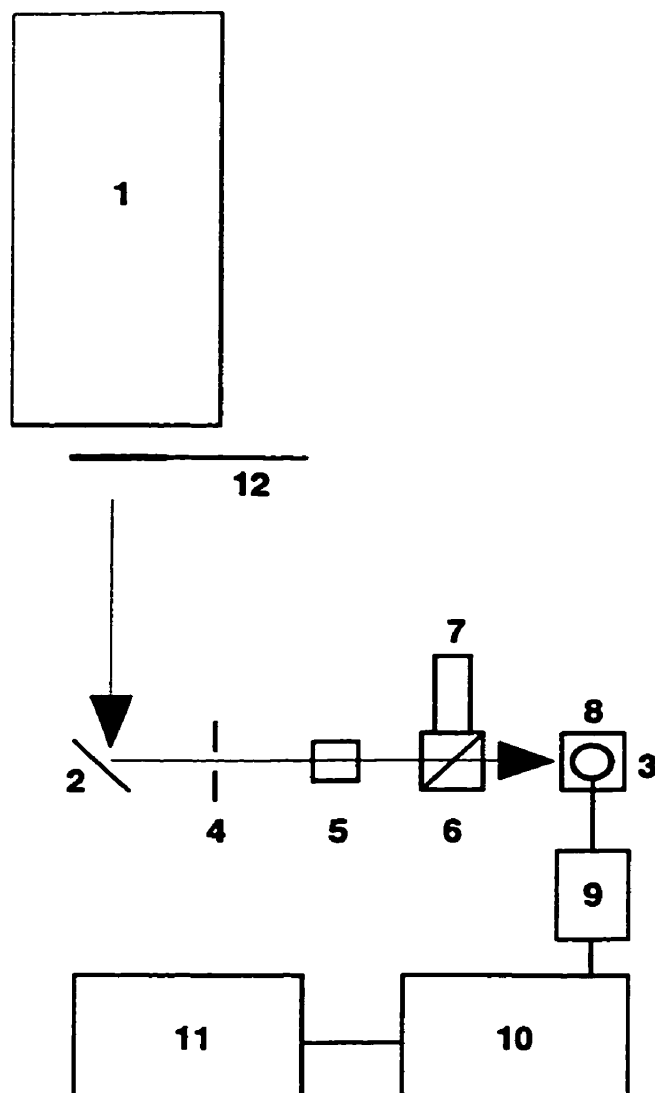
Figure 2.6 The laser flash photolysis system set up for photoacoustic measurements.

sample holder (3). Before reaching the sample holder the laser pulse passes through a 0.8 mm pinhole (4) and then through a potassium dichromate solution (5) that is used to attenuate the laser energy. Before the laser pulse reaches the sample cell a small portion of the laser pulse is split off with a beam splitter (6) into a photodiode (7) that is used to measure the relative energy of the laser. The sample cell is a 10 mm × 10 mm long stem

quartz absorbance, or fluorescence cell that was placed on top of a piezoelectric transducer ((8), Panametrics, model V-104-RB transducer, 2.25 MHz). Vacuum grease was used to improve the transmission of the heat wave generated in the cell to the transducer. The transducer/cell pair was placed in a home-built sample holder and was not moved during the experiment so as to not change the shape of the measured waveform. The signal of the transducer was amplified ((9), Panametrics model 5670) and then recorded and averaged with a digital oscilloscope ((10), Tektronix TDS 520). The signal from the photodiode was averaged in a second channel of the oscilloscope that was all interfaced to a Macintosh IIci computer (11). Software, written on the Labview 4.0 platform (National Instruments), was employed to synchronize the different components of the equipment and to analyze the data.

2.3 Methods: Sample Preparation and Procedures

2.3.1 UV-Vis Absorption

2.3.1.1.1 Fluorenone

The samples for the absorption measurements of fluorenone complexed to α- and β-CD in water were prepared as follows. Saturated aqueous fluorenone solutions were prepared by stirring fluorenone in deionized water for at least 48 h. The solution was then filtered using Millipore filters (0.45 μm). The CD stock solutions containing 10 mM β-CD, or 30 mM α-CD were prepared by dissolving the appropriate amount of CD in the saturated aqueous fluorenone solution. These solutions were stirred for at least 4 h. The CD solutions at lower concentrations were prepared by diluting the CD stock solution of highest concentration with the saturated aqueous fluorenone solution in 10 mL vials. Dilutions were performed with an Eppendorf pipettor. After dilution the vials were capped

and sealed with Parafilm. These solutions were then inverted and allowed to shake (one cycle/sec, home built shaker) for at least 10 h. All absorption experiments were performed with the same 10 mm × 10 mm quartz absorbance cell. Samples containing the highest concentration of the respective CDs were also prepared in the absence of the fluorenone and their absorption spectra were recorded. This data was used to correct for a small absorption in the CD stocks that was suggested to be due to the presence of impurities in the CD stocks. These corrections were achieved by subtracting the absorption spectrum for the respective CD from the spectrum of the samples containing fluorenone at the highest CD concentration. For samples that contained lower CD concentrations, a ratio of the lower CD concentration to the highest CD concentration was calculated and multiplied by the absorption spectrum of CD at its highest concentration. The resulting spectrum was then used to correct for the samples containing fluorenone in the presence of the lower concentrations of CD in the same manner as described above.

2.3.1.1.2 Styrenes

The samples for the absorption measurements of t-Ane and 4-VA complexed to both α- and β-CD were prepared using the following procedure. Methanolic stock solutions (ca. 2.3 mM for 4-VA and 2.0 mM for t-Ane) were prepared and were stirred for at least 1h. Then aqueous stock solutions (ca. 4.6 μM for 4-VA and 3.6 μM for t-Ane) of

the styrenes were prepared from the methanolic styrene stock solutions. The solutions were stirred for at least 5 h to ensure the solubilization of the styrenes. The final methanol volume was less than 0.3 % (v/v). The CD solutions containing α- and β-CD were prepared in the same manner as described above for fluorenone. In addition, the same corrections for CD absorbance were employed (Section 2.3.1.1.1).

2.3.2 Fluorescence

2.3.2.1 Steady-State Fluorescence

2.3.2.1.1 Fluorenones

In the determination of the steady-state fluorescence quantum yields (ϕ_f) for fluorenone and derivatives the following procedure was used. The ϕ_f for fluorenone in acetonitrile was determined using quinine sulfate in $1N$ H_2SO_4 as a standard.[63] In turn, the quantum yield for fluorenone in acetonitrile was employed as a secondary standard to measure the quantum yields for the fluorenone derivatives. This procedure was necessary due to the low emission quantum yields of the fluorenones. In this respect it was more accurate to compare the emission of compounds that have similar quantum yields. In acetonitrile, F-2CA, F-4CA, 3OHF and 2OHF were excited at 375 nm; 2,7DBF, and 2,7DCF were excited at 325 nm, 4OHF, and 4MF were excited at 418 nm, and 1,3DCF, and 2,7DFF were excited at 347 and 400 nm, respectively. All of the fluorenone derivatives in toluene were excited at 360 nm. The absorbances of the solutions containing the standard, or the sample were adjusted to $ca.$ 0.050 ±0.001. Oxygen was removed from the samples by bubbling nitrogen for at least 15 min through the solution containing the samples and a different cell containing solvent. The absorbance was checked again and solvent purged with nitrogen was added with a gas-tight syringe if solvent evaporation had occurred. A fluorescence spectrum was obtained for this original sample. Two more spectra were then collected after diluting the original sample by a factor of two and four with the deaerated solvent.

Solvent Raman emission was observed for some fluorenones with low fluorescence quantum yields. For these compounds, a correction was performed to quantify the total area of the fluorescence spectra ($A_{T, dilute}$) without any contribution from the Raman

emission. A concentrated sample of the fluorenone derivative was prepared and its

emission spectrum was recorded, since in this spectrum the Raman emission was

negligible. From this spectrum a ratio of the fluorescence area where the contribution from

the Raman emission does not appear ($A_{nR, conc}$) to the total fluorescence area ($A_{T, conc}$) was

calculated. Using this ratio and the fluorescence area from the less concentrated sample

($A_{nR, dilute}$), the total fluorescence for the compound was determined (Equation 2.5) without

interference from the Raman emission.

Equation 2.5

$$A_{T, dilute} = \left(A_{nR, dilute} \right) \left(\frac{A_{T, conc}}{A_{nR, dilute}} \right)$$

For the fluorescence experiments requiring solutions of fluorenone complexed to α-

and β-CD in water, the following procedure was used. Saturated aqueous fluorenone

solutions were prepared by stirring fluorenone in deionized water for at least 48 h. The

solution was then filtered using Millipore filters (0.45 µm). The CD stock solutions

containing 10 mM β-CD, or 30 mM α-CD were prepared by dissolving the appropriate

amount of CD in the saturated aqueous fluorenone solution. These solutions were stirred

for at least 4 h. The CD solutions at lower concentrations were prepared by diluting the CD

stock solution of highest concentration with the saturated aqueous fluorenone solution in 10

mL vials. Dilutions were performed with an Eppendorf pipettor. After dilution the vials

were capped and sealed with Parafilm. These solutions were then inverted and allowed to

shake (one cycle/sec, home built shaker) for at least 10 h. All fluorescence experiments

were performed with the same 10 mm × 10 mm quartz fluorescence cell. Samples

containing the highest concentration of the respective CDs were also prepared in the

absence of the fluorenone and their fluorescence spectra were recorded. This data was

used to correct for impurities in the CD stocks that gave a small amount of fluorescence

intensity. These corrections were achieved by subtracting the fluorescence spectrum for the respective CD from the spectrum of the samples containing fluorenone at the highest CD concentration. For samples that contained lower CD concentrations, a ratio of the lowest CD concentration to the highest CD concentration was calculated and multiplied by the fluorescence spectrum of CD at its highest concentration. The resulting spectrum was then used to correct for the samples containing fluorenone in the presence of the lower concentrations of CD in the same manner as described above. Since fluorenone was excited at 300 nm where CD shows a small absorbance, this absorbance leads to an inner filter effect that causes the fluorenone fluorescence intensity to be artificially lowered. Depending on the contribution of CD absorbance at the excitation wavelength, this additional correction[64] was employed.

2.3.2.1.2 Styrenes

The samples used for the fluorescence measurements of t-Ane and 4-VA complexed to both α- and β-CD were prepared using the following procedure. Methanolic stock solutions (ca. 2.3 mM for 4-VA and 2.0 mM for t-Ane) were prepared and were stirred for at least 1h. Then aqueous stock solutions (ca. 4.6 μM for 4-VA and 3.6 μM for t-Ane) of the styrenes were prepared from the methanolic styrene stock solutions. The solutions were stirred for at least 5 h to ensure the solubilization of the styrenes. The final methanol volume was less than 0.3 % (v/v). The CD solutions containing α- and β-CD were prepared in the same manner as described above for fluorenone. In addition, the same corrections for CD fluorescence and the inner filter effect were employed (Section 2.3.2.1.1).

2.3.2.2 Time-Resolved Fluorescence

2.3.2.2.1 Single Photon Counting

2.3.2.2.1.1 Fluorenones

For fluorenone samples measured using the PTI LS-1 nanosecond single photon counter (SPC), solutions were prepared in either acetonitrile, or toluene so as to obtain an absorbance of *ca.* 0.25 (l = 10 mm) at the excitation wavelength (285 nm). All SPC samples were prepared in Suprasil fluorescence cells and purged with nitrogen for at least 15 min to remove oxygen present in solution.

2.3.2.2.2 Streak Camera Detection

2.3.2.2.2.1 Fluorenone and Xanthone

For time-resolved fluorescence measurements using the picosecond system, solutions of both fluorenone and xanthone complexed to α- and β-CD were prepared in the following manner. Saturated aqueous ketone solutions were prepared by stirring ketones in deionized water for at least 48 h. The solutions were then filtered using Millipore filters (0.45 μm). The CD stock solutions containing 10 mM β-CD, or 30 mM α-CD were prepared by dissolving the appropriate amount of CD in the saturated aqueous ketone solutions. These solutions were stirred for at least 4 h. The CD solutions at lower concentrations were prepared by diluting the CD stock solution of highest concentration with the saturated aqueous ketone solutions in 10 mL vials. Dilutions were performed with an Eppendorf pipettor. After dilution the vials were capped and sealed with Parafilm. These solutions were then inverted and allowed to shake (one cycle/sec, home built shaker)

for at least 10 h. All fluorescence experiments were performed with 10 mm × 10 mm quartz fluorescence cells and all samples were purged with nitrogen for at least 20 min to remove oxygen present the solutions.

2.3.3 Induced Circular Dichroism

2.3.3.1.1 Fluorenone and Xanthone

For induced circular dichroism (ICD) measurements, solutions of both fluorenone and xanthone complexed to α- and β-CD were prepared in the same manner as described for the picosecond fluorescence experiments for the ketones (Section 2.3.2.2.2.1). All ICD experiments were performed in a matched set of 10 mm cylindrical quartz cells. Samples containing the highest concentration of the respective CD were also prepared in the absence of the ketones and their circular dichroism spectra were recorded because CDs are chiral. These spectra were then subtracted from the respective spectra containing the aqueous ketones in the presence of the highest concentration of either CD. For samples that contained lower CD concentrations, a ratio of the lowest CD concentration to the highest CD concentration was calculated and multiplied by the circular dichroism spectrum of CD at its highest concentration. The resulting spectrum was then used to correct for the samples containing the ketones in the presence of the lower concentrations of CD in the same manner as described above. As described earlier (Section 2.2.3), in ICD measurements an additional baseline spectrum was recorded for the aqueous solutions of ketones. Although these achiral ketones do not have any circular dichroism signals, it was important to measure the baseline with the ketones present because the photomultiplier voltage in the region where these molecules absorb will be similar to that for the samples containing the ketones in the presence of CDs.

2.3.3.1.2 Styrenes

The samples for ICD measurements of styrenes complexed to α- and β-CD were prepared in the following manner. Higher styrene concentrations were required for these studies than for fluorescence and ground state absorption studies. Saturated aqueous styrene solutions were prepared by adding 2 to 3 drops of distilled styrene to *ca.* 250 mL of deionized water and were stirred for at least 10 h. The saturated aqueous styrene solution was retrieved from the bottom of the flask, since neat styrene that did not dissolve remained on the surface of the stock solution. The CD solutions containing α-, or β-CD were prepared in the same manner as described above for the ketones. In addition, the same corrections for CD circular dichroism were performed.

An additional baseline spectrum was recorded for the aqueous solutions of styrenes in a similar manner as described for fluorenone and xanthone (Section 2.3.3.1.1).

2.3.4 Laser Flash Photolysis

2.3.4.1 Transmission Measurements

2.3.4.1.1 Fluorenones

Fluorenone samples were prepared in the following manner for transient absorption measurements acquired with the laser flash photolysis (LFP) system. The fluorenones were dissolved in either acetonitrile, or toluene to achieve an absorbance of *ca.* 0.25 (l = 7 mm) at the excitation wavelength employed. All LFP samples were measured in 7 mm × 7 mm Suprasil cells and were purged with nitrogen for at least 20 min so as to remove oxygen from the solution. Transient absorption spectra for the fluorenones were acquired using a 7 mm × 7 mm Suprasil flow cell.

2.3.4.1.2 Styrenes

The samples for transient absorption measurements using the LFP system of styrenes complexed to α- and β-CD were prepared in the following manner. Saturated aqueous styrene solutions were prepared by adding 2 to 3 drops of distilled styrene to *ca.* 250 mL of deionized water and stirring for at least 10 h. The saturated aqueous styrene solution was retrieved from the bottom of the flask, since neat styrene that did not dissolve was observed on the surface of the stock solution. When necessary these solutions were diluted with deionized water to obtain an absorbance of *ca.* 0.25 (l = 7 mm) ([4-VA] ≈ 60 μM and [t-Ane] ≈ 50 μM) at the excitation wavelength employed. The CD stock solutions containing 10 mM β-CD, or 30 mM α-CD were prepared by dissolving the appropriate amount of CD in the aqueous styrene solutions. These solutions were stirred for at least 4 h. The CD solutions at lower concentrations were prepared by diluting the CD stock solution of highest concentration with the saturated styrene solutions in 10 mL vials. Dilutions were performed with an Eppendorf pipettor. After dilution the vials were capped and sealed with Parafilm. These solutions were then inverted and allowed to shake (one cycle/sec, home built shaker) for at least 10 h. For studies performed in the presence of alcohols as co-solvents (1% v/v), the alcohols were added to the stock solutions containing the styrenes in the presence of the highest concentration of CD. Samples at the lower CD concentrations were prepared from these stock solutions in the same manner described above.

In the quantum yield experiments, absorbances of the styrene samples in the presence and absence of CD were matched. Dilutions of the prepared stocks with either of the aqueous styrene, or CD stock solutions were made in the 7 mm × 7 mm Suprasil cells until absorbances were matched to within *ca.* 5%. These styrene samples were not purged with nitrogen because the radical cations generated upon laser excitation are not quenched

by oxygen.[34] Transient absorption spectra were acquired using a 7 mm × 7 mm Suprasil flow cell to ensure that each laser shot irradiated a fresh sample of styrene solution.

In the quenching experiments, Eppendorf pipettors were used to dispense 2 mL aliquots of the styrene samples into the 7 mm × 7 mm Suprasil cells for precise determinations of quencher concentrations. Quencher solutions (TBAI, NaN_3, or NaCN) were prepared in deionized water at high concentrations ([TBAI] $\leq$ 0.02 M, [NaN_3] $\leq$ 0.1 M and [NaCN] $\leq$ 1.15 M). In addition, all samples were purged with nitrous oxide (N_2O) for at least 20 min to avoid interference from the absorption due to solvated electrons.

2.3.4.2 Photoacoustic Measurements

2.3.4.2.1.1 Fluorenones

When photoacoustic measurements were acquired with the LFP system, stock solutions of both the unknown fluorenone sample and standard (ortho-hydroxybenzophenone) were prepared with matched absorbances between 0.100 and 0.150 in a 10 mm × 10 mm long stem quartz absorbance, or fluorescence cell. The cell was then placed into a brass assembly and not removed until the end of the experiment. Any changes in the alignment of the cell with respect to the laser beam led to changes in the waveform of the photoacoustic signal. Such changes indicated that the contact between the cell and the piezoelectric transducer had changed, which meant that the acoustic signals measured for the unknown and the standard were no longer relative. If such a change occurred the results were discarded. Washing of the cell was performed with the cell in place using a peristaltic pump. Alternate solutions (ca. 3 mL) of the standard and unknown were placed in the cell. For each experiment, data for three standard and two unknown samples were measured.

2.3.5 Data Analysis

2.3.5.1 Fluorescence Quantum Yields

The fluorescence quantum yields were calculated by employing Equation 2.6 that includes the dependence of the standard (s) and unknown (u) samples on the absorbance (A), solvent refractive index (n), the integrated areas for the emission spectra (I), and the known fluorescence quantum yield of the standard (ϕ_s).[63] The values for the three different concentrations were averaged for each experiment and the standard deviation was reported for the average of experiments performed on different days.

Equation 2.6

$$\phi_F = \phi_S \frac{A_s I_u n_u^2}{A_u I_s n_s^2}$$

2.3.5.2 Photoacoustics

Photoacoustic techniques have their basis in calorimetry and follow energy balance equations. If the lifetime of an excited triplet state is longer than the response time of the transducer, the energy stored in the triplet state is not released during the measurement. This leads to a reduction in the signal's amplitude. The product of the intersystem crossing quantum yield (ϕ_{isc}) and the triplet energy (E_T) can be obtained from Equation 2.7, the energy balance equation, where N_A, h, v_e, and v_f are Avogadro's number, Planck's

Equation 2.7

$$N_A h v_e = \phi_F N_A h v_e + \alpha N_A h v_e + \phi_{isc} E_T$$

constant, the frequency for the excitation wavelength, and the average frequency for the

fluorescence, respectively. Since fluorescence was only a minor decay pathway, the

frequency corresponding to the wavelength with maximum intensity in the fluorescence

spectrum was employed. The parameter α corresponds to the ratio between the signal

intensity for the unknown sample and the signal intensity for a standard that releases the

absorbed energy as heat into solution. The standard employed was *ortho*-

hydroxybenzophenone.[65] The signal amplitude was measured between the first maximum

and minimum of the transducer signal. A linear relationship between the signal amplitude

and the laser energy was observed for the sample and the standard solutions. The signal

amplitude was measured at different laser energies to ensure that the above linearity was

encountered and to determine a more precise value for α. The parameter α was calculated

from the ratio of the slopes for the linear relationships.

After data collection, the absorbance of each sample was recorded, and the fraction

of light absorbed was calculated as shown in Equation 2.8. This was performed to ensure

that the dependence on the amount of light that irradiated the sample was taken into account

for the slopes obtained. The slope for the dependence of the signal with the relative laser

energy was divided by f_{abs}. The corrected slope values for the unknown and standard were

averaged and the value of α was calculated.

Equation 2.8

$f_{abs} = 1 - 10^{-A}$

3. FLUORENONE PHOTOPHYSICS - RESULTS AND DISCUSSION

3.1 Structure and Derivatives

Fluorenone is an aromatic ketone that is composed of two benzene groups fused to

a five-membered ring containing a carbonyl group (Figure 3.1). A total of ten fluorenone

derivatives (listed below) were studied to compare and contrast how the substituent, the

substitution patterns, and microenvironment affect the photophysics of the fluorenone.
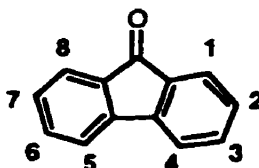
Figure 3.1 Fluorenone

2,7-dibromo-9-fluorenone   (2,7DBF)
1,3-dichloro-9-fluorenone   (1,3DCF)
2,7-dichloro-9-fluorenone   (2,7DCF)
2,7-difluoro-9-fluorenone   (2,7DFF)
9-fluorenone-2-carboxylic   acid   (F-2CA)
9-fluorenone-4-carboxylic   acid   (F-4CA)
2-hydroxy-9-fluorenone   (2OHF)
3-hydroxy-9-fluorenone   (3OHF)
4-hydroxy-9-fluorenone   (4OHF)
4-methoxy-9-fluorenone   (4MF)

A series of halogenated fluorenones at the two and seven positions were studied, so as to

determine how heavy atoms affect the photophysics of fluorenone. A comparison based on

substitution pattern was also investigated for the chlorinated derivative. The hydroxy and

carboxylic acid derivatives were studied to compare how the position of the substituent on

the aromatic ring affects the photophysics of fluorenone. These latter molecules also have

the ability to form hydrogen bonds with protic solvents. A 4-methoxy substituted

derivative was also investigated to detail the effect an electron-donating substituent has on

the photophysics of the parent fluorenone molecule. An electron-donating substituent is one which can donate electron density into the π orbitals of the aromatic molecule through resonance. In contrast, an electron-withdrawing molecule is one which withdraws electron density from the π-system through resonance.

3.2 Fluorescence Spectra and Quantum Yields

The fluorescence spectra of fluorenone and its derivatives were very broad. This broadening is representative of overlapping vibrational transitions and solvent reorganization. The fluorescence emission maxima for the fluorenone derivatives in acetonitrile and toluene (Figure 3.2 and Figure 3.3) were observed between 460 and 560 nm. The emission maxima of the fluorescence spectra were sensitive to the polarity of the solvent, the nature of the substituents, and the substitution pattern on the fluorenone.
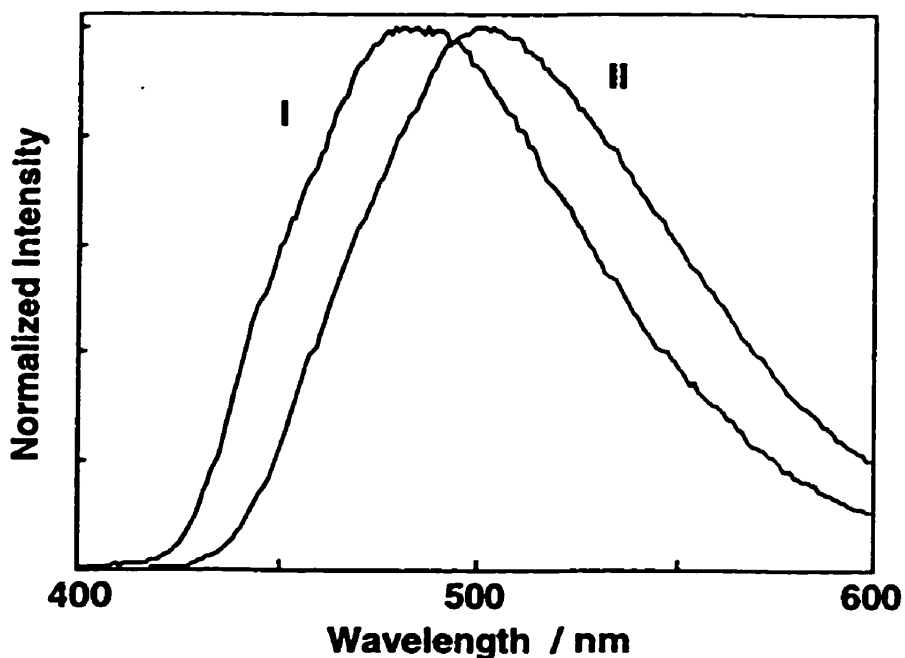
Figure 3.2 Normalized fluorescence spectra for fluorenone in toluene (I) and acetonitrile (II).
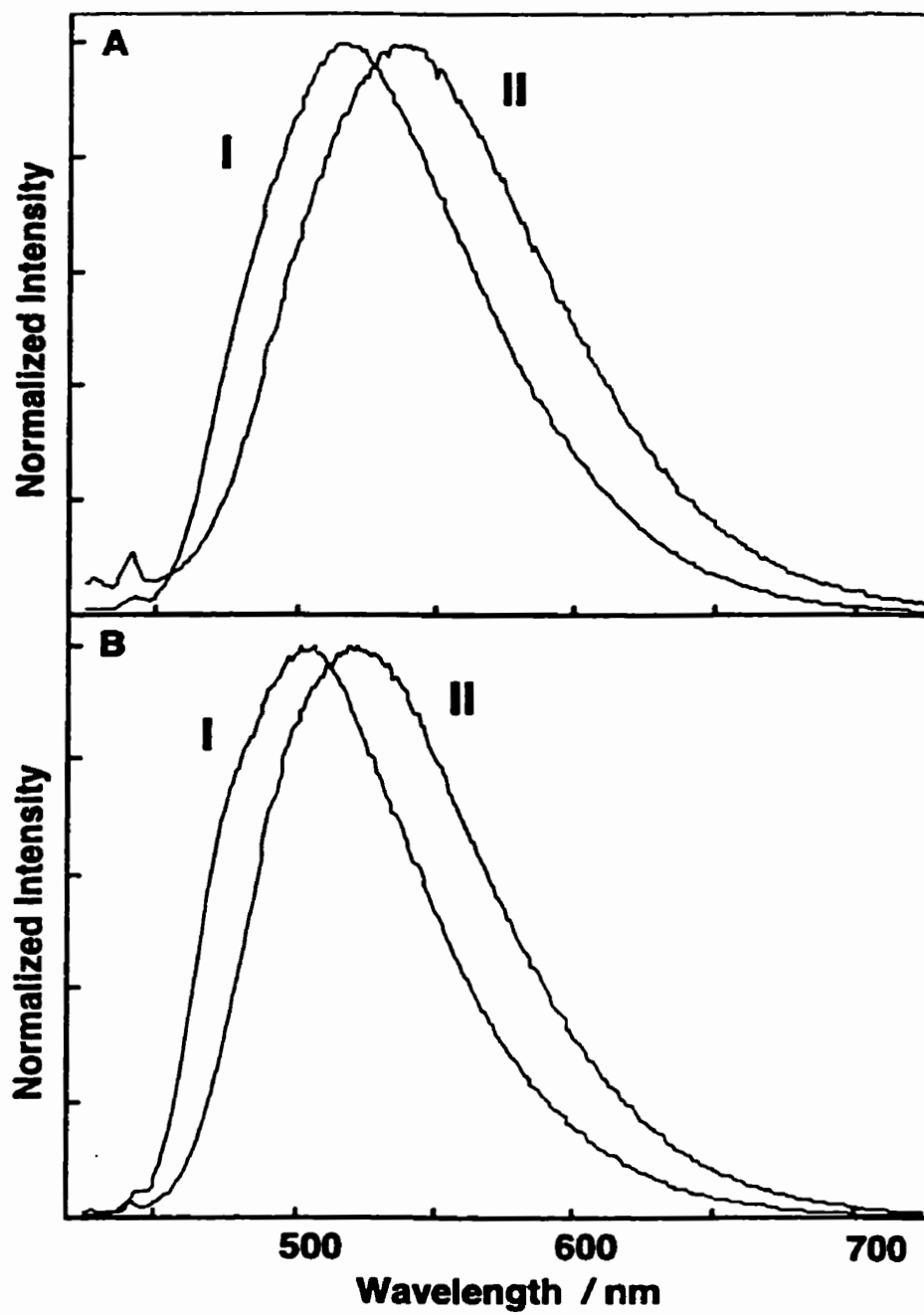
Figure 3.3 Normalized fluorescence spectra for 2,7DFF (A) and 2,7DBF (B) in toluene (I) and acetonitrile (II).

A table of values containing the fluorescence maxima, and quantum yields for the fluorenones in acetonitrile and toluene is shown below (Table 3.1). Acetonitrile and toluene were used since they represent solvents of high and low polarity, respectively. The dielectric constant for acetonitrile is *ca.* 36 and toluene is *ca.* 2. For three of the fluorenone derivatives: F-4CA, F-2CA and 1,3DCF, there was a shift in the fluorescence maxima to shorter wavelengths in both acetonitrile and toluene when compared to the unsubstituted fluorenone. All the other derivatives show fluorescence maxima that were observed at

Table 3.1 Fluorescence quantum yields and emission maxima of fluorenone derivatives in acetonitrile and toluene.[a]

Compounds	Acetonitrile		Toluene	
	λ_{max} / nm	ϕ_F / 10^{-2}	λ_{max} / nm	ϕ_F / 10^{-2}
FL	510	2.7 ± 0.2 (3)	490	0.98 ± 0.06 (3)
2,7DFF	545	0.36 ± 0.06 (2)	525	1.6 ± 0.1 (3)
2,7DCF	530	2.4 ± 0.2 (6)	510	6.0 ± 0.5 (3)
1,3DCF	495	<0.26 (3)	460	0.020 ± 0.008 (3)
2,7DBF	530	0.9 ± 0.1 (5)	510	0.96 ± 0.05 (3)
2OHF	535	0.22 ± 0.05 (3)	535	1.0 ± 0.1 (3)
3OHF	510	3.2 ± 0.4 (3)	500	<1.2 (3)
4OHF	530	2.8 ± 0.2 (3)	500	4.9 ± 0.3 (3)
4MF	530	2.9 ± 0.2 (3)	510	6.7 ± 0.5 (3)
F-2CA	490	3.2 ± 0.2 (3)	470	0.87 ± 0.02 (3)
F-4CA	500	1.4 ± 0.1 (3)	485	< 0.28 (3)

(a) All measurements are an average of at least two determinations. For experiments performed twice, the errors were calculated as average deviations, while other errors correspond to standard deviations. The numbers in parenthesis correspond to the number of independent experiments performed. Errors for λ_{max} are ± 5 nm.

longer wavelengths than the parent fluorenone. The fluorescence quantum yield of

fluorenone in acetonitrile was determined using Equation 2.6 (Section 2.3.5.1), and

quinine sulfate in 1 N H_2SO_4 as a standard.[66] The quantum yield was determined to be

0.027 ± 0.002, and was found to be within experimental error to previously reported

values that ranged between 0.029 and 0.034.[8,19,22] All the other quantum yields were

determined using fluorenone in acetonitrile as a secondary standard. This procedure led to

more precise values since the integrated areas of the emission intensity for the derivatives

were of comparable magnitude to that of fluorenone. The fluorescence quantum yield of

fluorenone in toluene was the same as determined previously (0.0097).[9] Upper limits were

given for the fluorescence quantum yields of the fluorenones, where biexponential decays

were observed since the presence of an additional component with a long lifetime increases

the intensity of the steady-state spectrum.

3.3 Fluorescence Lifetimes

The fluorescence lifetimes for fluorenone and derivatives were determined from

single photon counting measurements (Table 3.2). Fluorenone in acetonitrile had a

monoexponential fluorescence decay (Figure 3.4). The previously reported fluorescence

lifetimes[8,9] of 18.7 and 21.5 ns were comparable to the lifetime of 16.5 ± 1.5 ns that we

obtained. The decay for fluorenone in toluene was also monoexponential with a lifetime of

3.6 ± 0.5 ns, and comparable to the 3.0 ± 0.2 ns reported previously.[9]

The fluorescence decays for 2OHF in acetonitrile, and both 1,3DCF and F-2CA in

toluene could not be measured by single photon counting. Either low fluorescence

quantum yields or low solubility made these measurements unattainable. In the case of

1,3DCF in acetonitrile (Figure 3.5) and F-4CA in toluene, a biexponential decay was

observed. The short-lived components with preexponentials ≥ 0.96 were the largest

contributors to the biexponential decays, whereas the contribution of the long-lived

Table 3.2   Fluorescence lifetimes of fluorenone derivatives in acetonitrile and toluene.[a]

Compounds	Acetonitrile τ_f/ ns	Toluene τ_f/ ns
FL	16.5 ± 1.5 (5)	3.6 ± 0.5 (4)
2,7DFF	4.4 ± 0.4 (2)	10.3 ± 0.3 (2)
2,7DCF	8.5 ± 1.2 (2)	13.9 ± 0.4 (2)
1,3DCF	1.1 ± 0.1 and 9.6 ± 0.1[b] (2)	c
2,7DBF	2.7 ± 0.1 (2)	1.7 ± 0.2 (3)
2OHF	c	4.3 ± 0.2 (2)
3OHF	13.5 ± 0.5 (2)	2.7 ± 0.5 and 7.5 ± 0.8[b] (3)
4OHF	7.0 ± 0.5 (2)	8.4 ± 0.6 (3)
4MF	6.0 ± 0.1 (2)	10.1 ± 0.3 (2)
F-2CA	9.1 ● 0.8 (2)	c
F-4CA	8.4 ± 0.1 (2)	< 1ns and 4.0 ± 0.3[b] (2)

(a) All measurements are an average of at least two determinations. For experiments performed twice, the errors were calculated as average deviations, while other errors correspond to standard deviations. The numbers in parenthesis correspond to the number of independent experiments performed. (b) Biexponential decays. (c) Compounds with low quantum yields, or not sufficiently soluble for reliable measurements to be obtained.

components to the decays were very small. The long-lived component in 1,3DCF was assigned to a unknown impurity in the compound. As the fluorescence quantum yield for 1,3DCF in acetonitrile is low, any fluorescence intensity observed from a trace impurity will be relatively more pronounced than for fluorenone compounds with higher fluorescence quantum yields. In the case of F-4CA in toluene the long-lived component was not attributed to an impurity but to the possible formation of dimers or aggregates of F-4CA since a monoexponential decay was observed for F-4CA in acetonitrile. It is possible that the formation of dimers, or aggregates of F-4CA are responsible for the
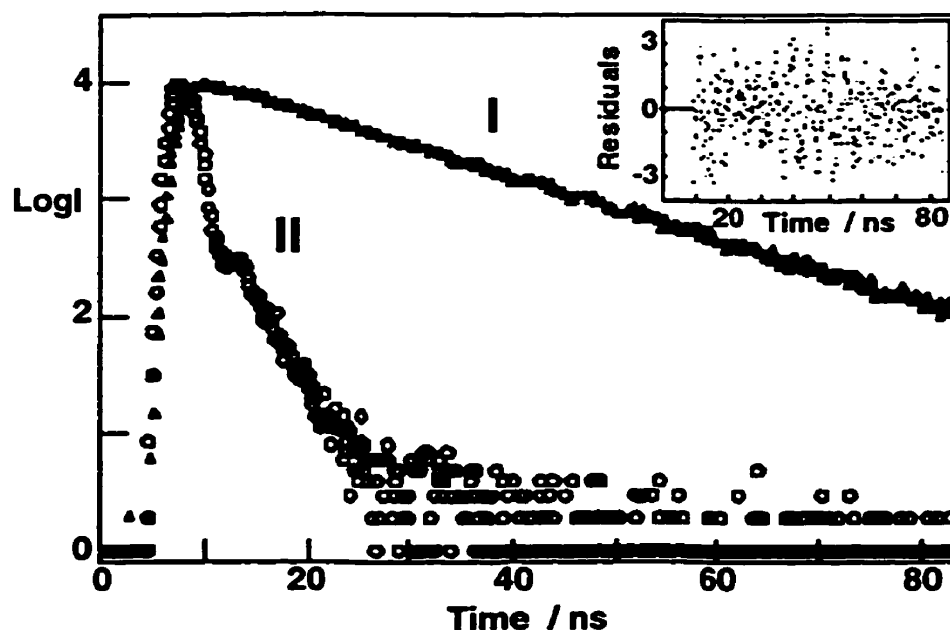
Figure 3.4 Single photon counting fluorescence decay of fluorenone in acetonitrile. The
residual for the fit is shown in the inset. Decay I is for the fluorenone
fluorescence and decay II is the instrument response function.

biexponential decay as these assemblies will have different photophysical parameters than

for the monomer. The formation of dimers or aggregates is conceivable considering the

higher sample concentrations (ca. two fold) required for single photon counting

measurements when compared to steady-state fluorescence measurements. Although the

contribution of the long-lived species is small with respect to the preexponential factors for

the fluorescence decay, it may still have a significant contribution to the total fluorescence

intensity. The fraction of the total fluorescence intensity observed for either species is

dependent of its fluorescence quantum yield, which is directly proportional to its

fluorescence lifetime. Therefore, it is not surprising that a component with a longer lifetime

will have a more significant contribution to the total emission intensity of the steady-state

spectrum than described by the preexponentials for the fluorescence decay. As a result, the
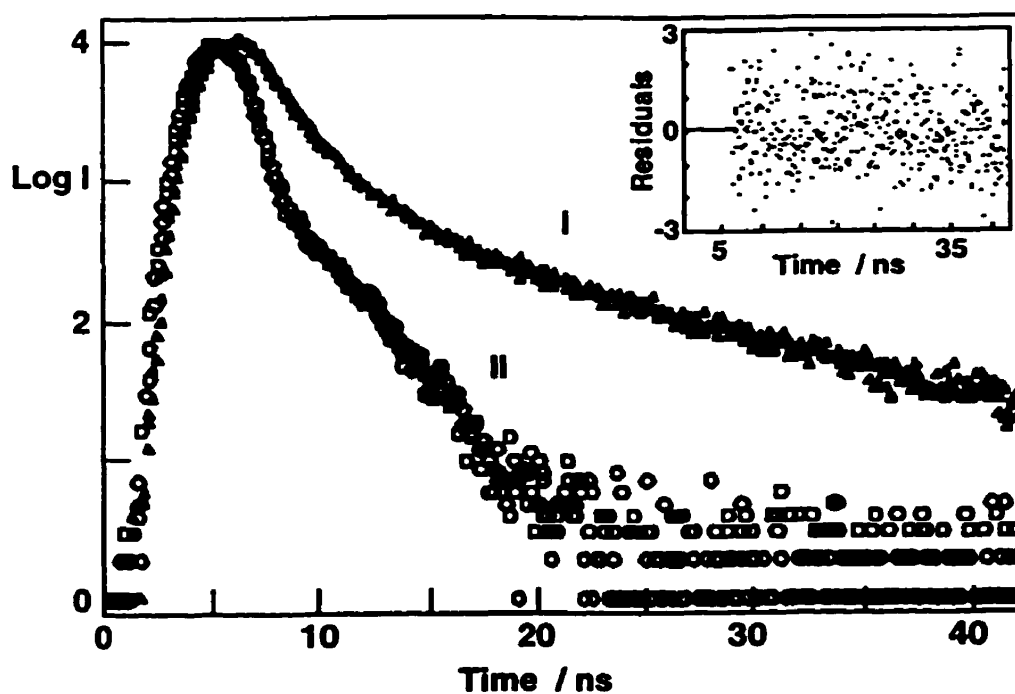
Figure 3.5 Single photon counting fluorescence decay of 1,3DCF in acetonitrile. The residual of the fit for two exponentials is shown in the inset. The decay labeled I is for the fluorescence of 1,3DCF and the decay labeled II is the instrument response function.

quantum yields measured for 1,3DCF in acetonitrile and F-4CA in toluene were taken as upper limits.

In the case of 3OHF in toluene, a nonexponential decay was also observed that was fitted to the sum of two exponentials with similar pre-exponential factors ($A_1 = 0.64$, $A_2 \approx 0.36$). However, the fluorescence decay of 3OHF in acetonitrile fits well to a monoexponential fit. As for F-4CA in toluene, the biexponential decay observed for 3OHF in acetonitrile was attributed to the possible formation of dimers or aggregates of 3OHF.

3.4 Time-Resolved Absorption Spectra of the Triplet Excited States

Laser flash photolysis was used to measure the transient absorption spectra of the triplet state for fluorenone and its derivatives in acetonitrile and toluene. The triplet states of these compounds absorbed in three main regions (Figure 3.6). The first occurred in the 300-350 nm region, a second in the 400-500 nm region and a third in the 550-700 nm region. Triplet decays were measured at the absorption maxima in the 400-500 nm region (Table 3.3). The decay of the triplet was monitored in the different wavelength regions and the same transient kinetics were observed (the inset of Figure 3.6 shows the decay at one
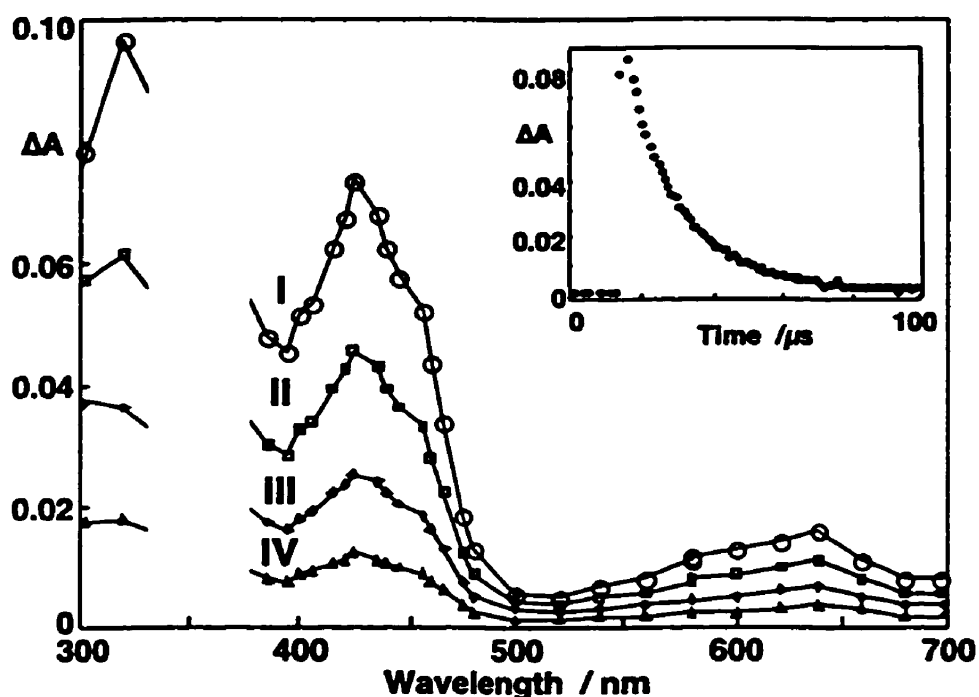
Figure 3.6 Transient absorption spectra of fluorenone in acetonitrile at several delays after the laser pulse: 7 (I), 17 (II), 34 (III), and 43 µs (IV). The inset shows the decay of the triplet excited state monitored at 425 nm. Transient absorption data was not collected in the region of the laser excitation wavelength (355 ± 15 nm).

wavelength). The transient absorption spectra were also monitored at different delays after the laser pulse, and no spectral shifts were observed. These similarities suggest that only one transient species was present upon excitation. In some cases, a second-order contribution attributed to triplet-triplet annihilation was observed for the decay of the fluorenone derivatives. This process occurs when two excited triplet states of the same molecule interact leading to their deactivation to the ground state. The contribution of triplet-triplet annihilation was reduced by decreasing the laser power used for excitation.

Table 3.3 Triplet-triplet absorption maxima and triplet lifetimes for the fluorenones in acetonitrile and toluene.[a]

Compounds	Acetonitrile		Toluene	
	λ_{max} / nm	τ_T / μs	λ_{max} / nm	τ_T / μs
FL	430	23	430	7
2,7DFF	435	28	450	18
2,7DCF	460	19	460	21
1,3DCF	460	8	460	19
2,7DBF	470	8	470	22
2OHF	450	16	455	3
3OHF	400	2	380	23
4OHF	425	16	490	24
4MF	440	19	445	18
F-2CA	450	12	b	b
F-4CA	420	8	440	9

(a) All maximum determinations are an average of at least two determinations. Errors for λ_{max} are ± 5 nm. (b) Not available due to low solubility.

This reduction in laser power lowers the population of triplets generated, and decreases the probability of this process. The triplet lifetimes of the fluorenones were typically longer than 5 μs. The triplet lifetimes were very sensitive to residual amounts of oxygen present in solution and varied somewhat between different experiments. As a result, the lifetimes listed (Table 3.3) are representative of values measured from experiments in which the least amount of oxygen was present. Transient absorption signals were observed for all fluorenone derivatives except for F-2CA in toluene, which had limited solubility in this solvent.

3.5 Laser Induced Optoacoustics

Optoacoustic measurements were used to determine the intersystem crossing quantum yields of the fluorenones. However, these measurements are possible provided that the triplet lifetimes of the molecules are longer than the response time of the transducer. This assures that the energy stored by the molecules in their triplet states has not been released as heat before the measurements can be made. Under our experimental conditions, the time after which the acoustic wave was generated from laser excitation, referred to as the acoustic transient time (τ_a), was calculated to be *ca.* 300-340 ns by

Equation 3.1

$$\tau_a = \frac{R}{v_a}$$

employing Equation 3.1, where R is the radius of the laser beam (0.4 mm) and v_a is the speed of sound in the solvent used (1.17×10^3 m s^{-1} and 1.30×10^3 m s^{-1} for toluene and acetonitrile,[65] respectively). The heat generated for times shorter than the acoustic transient time is called prompt heat. This prompt heat will contribute to the total amplitude of the

signal observed for the triplet states of the fluorenones. For example, in the case of 3OHF in acetonitrile, where the triplet lifetime was short (*ca.* 2 μs), *ca.* 15% of the signal amplitude measured for the acoustic wave was due to prompt heat, and not due to the energy that was stored in the triplet state. However, in the case of fluorenone in toluene, where the triplet lifetime was longer (*ca.* 7 μs), the contribution of prompt heat for the observed acoustic wave decreased to *ca.* 5%. Therefore, the negative $\phi_{isc}E_T$ values observed for 3OHF in acetonitrile and 2OHF in toluene may be a result of the error introduced into the amplitude of the acoustic wave from the prompt heat generated after laser excitation. Nevertheless, the contributions of prompt heat to the total amplitude of the acoustic values for all the fluorenones were within the error limits calculated for the $\phi_{isc}E_T$ values (Table 3.4).

The values of $\phi_{isc}E_T$ were determined using the energy balance equation (Equation 2.7) that include the value α that is obtained from linear plots of the amplitude of the transducer signal with respect to the laser energy for a standard and the unknown (Figure 3.7). The product $\phi_{isc}E_T$ was used to compare the differences and similarities in the intersystem crossing quantum yields for the fluorenone derivatives because the individual triplet energies for the derivatives are not known. As a result, we used the triplet energy for the parent fluorenone for the calculation of the product $\phi_{isc}E_T$, so that a reasonable comparison for the intersystem crossing quantum yields could be made. The signals for each of the derivatives in each of the solvents were compared to a standard, *ortho*-hydroxybenzophenone[65] that is known to release all its absorbed energy as heat. For these experiments, the laser energy at 355 nm was attenuated by directing the laser beam through an aqueous potassium dichromate solution. By varying the concentration of the potassium dichromate solution, we were able to observe a linear relationship between the amplitude of the photoacoustic signal measured and the relative laser energy employed. If the linear
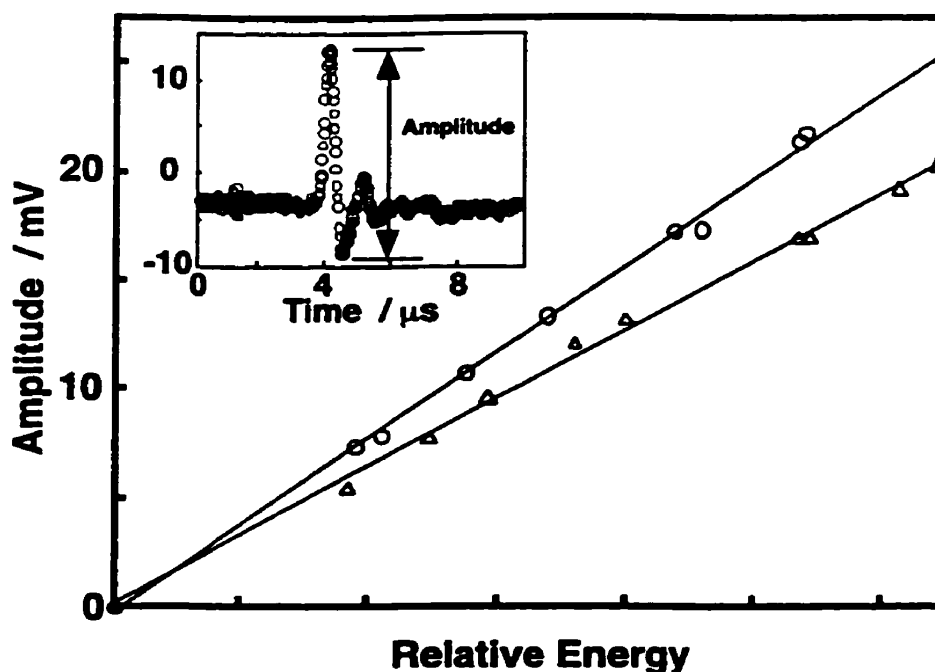
Figure 3.7 Dependence of the photoacoustic signal for the standard *ortho*-hydroxybenzophenone (upper trace) and 4MF in toluene (lower trace) with the relative energy of the laser pulse. The inset shows a typical waveform and the arrow indicates where the amplitude was measured.

plots deviated considerably from the origin, or a change in the waveform was observed within one set of experiments, the data were considered unreliable and were not used to determine the $\phi_{isc}E_T$ values.

The $\phi_{isc}E_T$ values were affected by the substitution pattern and the solvent polarity. The precision of these values decreased as the values became smaller since this product is related to the difference in slopes between the standard and the compound of interest. Therefore, any value below 5 kcal mol^{-1} could not be reported with confidence because the errors in the measurements were of the same magnitude. Considering this error value, and a E_T of *ca.* 50 kcal mol^{-1}, a lower limit of *ca.* 0.1 for the fluorenone ϕ_{isc} values was set and

Table 3.4 Product of the intersystem crossing quantum yield and triplet energy (kcal/mol)
for fluorenone derivatives in acetonitrile and toluene.[a]

Compounds	Acetonitrile	Toluene
FL	17 ± 3 (4)	36± 1 (2)
2,7DFF	4 ± 2 (3)	0 ± 2 (2)
2,7DCF	7 ± 2 (5)	11 ± 1 (3)
1,3DCF	47 ± 3 (3)	43 ± 2 (2)
2,7DBF	32 ± 4 (5)	28 ± 2 (2)
2OHF	2 ± 2 (4)	-7 ± 5 (3)
3OHF	-1 ± 2 (4)	29 ± 6 (3)
4OHF	3 ± 3 (3)	13 ± 1 (3)
4MF	-2 ± 3 (4)	16 ± 8 (5)
F-2CA	23 ± 1 (3)	b
F-4CA	21 ± 3 (4)	36 ± 3 (3)

(a) All measurements are an average of at least two determinations. For experiments
performed twice, the errors were calculated as average deviations, while other errors
correspond to standard deviations. The numbers in parenthesis correspond to the number
of independent experiments performed. (b) not soluble.

only values above this limit were considered reliable measurements. The triplet energies of

fluorenone have been measured from its phosphorescence spectra at low temperatures (77

K). In methylcyclohexane-isopentane $(5:1)$[67] and ethanol[18] the triplet energies were

determined to be 53.3 and 50.4 kcal mol^{-1}, respectively. We were unable to detect any low

temperature phosphorescence with our experimental set-up. The inability to detect

phosphorescence for fluorenone has been reported by others,[8] and is probably due to the

low phosphorescence quantum yield of this compound. Using the values reported for

fluorenone in polar and nonpolar solvents, the ϕ_{isc} values for fluorenone were calculated to

be 0.34 ± 0.06 in acetonitrile and 0.68 ± 0.02 in toluene (Table 3.5). These values

compare well with previous studies that reported ϕ_{isc} values of 0.46 ± 0.04 and 0.48 in

acetonitrile and 0.88 ± 0.08 in toluene.[8,9] The differences observed between the ϕ_{isc} values

reported earlier and those we measured are probably a reflection of the different techniques

used to determine these values. Again, it should also be noted that the ϕ_{isc} values we

recovered from the product of $\phi_{isc}E_T$, determined from the experimental measurements,

were calculated assuming the triplet energy for all the derivatives was equal to that reported

for fluorenone in toluene and acetonitrile. Until the triplet energies for the other fluorenone

derivatives are determined experimentally, this is the best assumption we can make. From

our ϕ_{isc} values for the fluorenones (Table 3.5), we were able to calculate the internal

conversion quantum yields (ϕ_{ic}) using Equation 3.2. In addition, the fluorescence (k_F),

intersystem crossing (k_{isc}) and internal conversion (k_{ic}) rate constants were calculated (Table

3.6 and Table 3.7) from the relationship shown in Equation 3.3, where τ_s is the observed

singlet lifetime of the respective fluorenones that is commonly referred to as the

fluorescence lifetime of the molecule.

Equation 3.2

$$\phi_{ic} = 1 - \phi_F - \phi_{isc}$$

Equation 3.3

$$k_j = \frac{\phi_j}{\tau_s}$$

Table 3.5 Intersystem crossing and internal conversion quantum yields for fluorenone derivatives in acetonitrile and toluene.[a]

Compounds	Acetonitrile		Toluene	
	ϕ_{isc}	ϕ_{ic}	ϕ_{isc}	ϕ_{ic}
FL	0.34 ± 0.06	0.63 ± 0.06	0.68 ± 0.02	0.31 ± 0.02
2,7DFF	< 0.1	> 0.9	< 0.1	> 0.9
2,7DCF	0.14 ± 0.04	0.84 ± 0.04	0.21 ± 0.02	0.73 ± 0.02
1,3DCF	0.93 ± 0.26	0.07 ± 0.02	0.81 ± 0.40	0.19 ± 0.40
2,7DBF	0.64 ± 0.08	0.35 ± 0.08	0.53 ± 0.04	0.46 ± 0.04
2OHF	< 0.1	> 0.9	< 0.1	> 0.9
3OHF	< 0.1	> 0.9	0.54 ± 0.11	0.45 ± 0.09
4OHF	< 0.1	> 0.9	0.24 ± 0.02	0.71 ± 0.02
4MF	< 0.1	> 0.9	0.30 ± 0.15	0.63 ± 0.15
F-2CA	0.46 ± 0.02	0.51 ± 0.02	b	b
F-4CA	0.42 ± 0.06	0.57 ± 0.06	0.68 ± 0.06	0.32 ± 0.06
2FF [c]	0.16	0.83	0.72	0.26
2MF [c]	0.05	0.95	0.16	0.83
F-2NO$_2$ [d]	–	–	1.0	0
F-2NH$_2$ [d]	–	–	0.02	0.98

(a) The errors shown represent the propagation of uncertainty calculated from the errors obtained in the $\phi_{isc}E_T$ values. (b) not soluble. (c) from reference 10. (d) from reference 12.

Table 3.6 Fluorescence, intersystem crossing and internal conversion rate constants for fluorenone derivatives in acetonitrile.[a]

Compound	Acetonitrile		
	k_F / 10^6 s^{-1}	k_{isc} / 10^6 s^{-1}	k_{ic} / 10^6 s^{-1}
FL	1.6 ± 0.2	21 ± 4	38 ± 5
2,7DFF	0.8 ± 0.2	< 23	$> 2.0 \times 10^2$
2,7DCF	2.8 ± 0.5	16 ± 5	99 ± 15
1,3DCF	< 2.4[b]	$(8.5 \pm 2.5) \times 10^2$[b]	> 64[b]
2,7DBF	3.3 ± 0.4	$(2.4 \pm 0.3) \times 10^2$	$(1.3 \pm 0.3) \times 10^2$
2OHF	c	c	c
3OHF	2.4 ± 0.3	< 7.4	> 67
4OHF	4.0 ± 0.4	< 14	$> 1.3 \times 10^2$
4MF	4.8 ± 0.3	< 17	$> 1.5 \times 10^2$
F-2CA	3.5 ± 0.4	51 ± 5	56 ± 5
F-4CA	1.7 ± 0.1	50 ± 7	68 ± 7
2FF[d]	1.4	15	77
2MF[d]	1.7	30	6.8×10^2

(a) The errors shown represent the propagation of uncertainty calculated from the errors obtained in the quantum yield and lifetime measurements. (b) shortest lifetime was employed for the calculation. (c) lifetime was not available. (d) from reference 10.

Table 3.7 Fluorescence, intersystem crossing and internal conversion rate constants for fluorenone derivatives in toluene.[a]

Compound	Toluene		
	$k_F / 10^6 \, s^{-1}$	$k_{isc} / 10^6 \, s^{-1}$	$k_{ic} / 10^6 \, s^{-1}$
FL	2.7 ± 0.4	$(1.9 \pm 0.3) \times 10^2$	86 ± 3
2,7DFF	1.6 ± 0.1	< 9.7	> 87
2,7DCF	4.3 ± 0.4	15 ± 2	53 ± 2
1,3DCF	c	c	c
2,7DBF	5.7 ± 0.7	$(3.1 \pm 0.4) \times 10^2$	$(2.7 \pm 0.6) \times 10^2$
2OHF	2.3 ± 0.3	< 23	$> 2.1 \times 10^2$
3OHF	d	d	d
4OHF	5.8 ± 0.8	29 ± 3	85 ± 6
4MF	6.6 ± 0.4	30 ± 1	62 ± 15
F-2CA	c	c	c
F-4CA	> 2.8 [b]	$> 6.8 \times 10^2$ [b]	$> 3.2 \times 10^2$ [b]
2FF [e]	2.0	67	24
2MF [e]	2.2	31	1.9×10^2
F-2NO$_2$ [f]	0	$> 2.0 \times 10^3$	0
F-2NH$_2$ [f]	1.3	25	1.2×10^2

(a) The errors shown represent the propagation of uncertainty calculated from the errors obtained in the quantum yield and lifetime measurements. (b) shortest lifetime was employed for the calculation. (c) lifetime was not available. (d) nonexponential decay was observed. (e) from reference 10. (f) from reference 12.

3.6 Discussion

The photophysics of fluorenone is very sensitive to solvent polarity, substitution and substitution patterns.[8-24] This sensitivity arises from the low-lying singlet and triplet energy levels that are close in energy and have either n,π^*, or π,π^* electronic configurations. The electronic configurations of the lowest energy levels in fluorenone vary depending on the polarity of the solvent (Figure 3.8). In polar solvents, the lowest
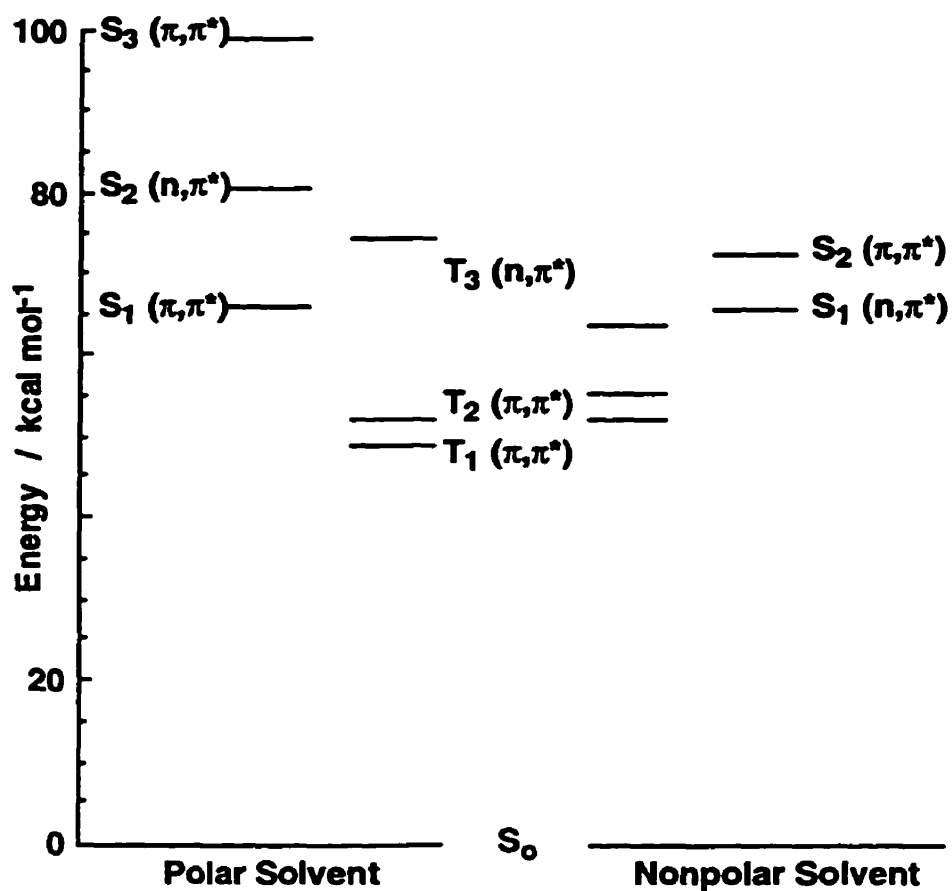
Figure 3.8 Energy level diagram for fluorenone in polar and nonpolar solvents (Adapted from reference 19).

singlet and triplet energy levels of fluorenone have π,π^* electronic configurations, whereas

in nonpolar solvents the lowest singlet state has a n,π^* electronic configuration.[19]

Accompanying the ordering of the electronic configurations of the singlet and triplet states

are the relative differences in energy between the singlet and triplet states. For example, in

polar solvents the energy of the T_3 state is higher than the S_1 state. However, in nonpolar

solvents the n,π^* states are stabilized and as a result the T_3 state is lower than the S_1 state.

It is the changes in the ordering of the electronic levels, and the relative differences in

energy between them that is responsible for the complex photophysics that has been

observed for fluorenone in solvents of varying polarities.[8-10,13,14,16-20,22]

In addition to solvent effects, the dependence of the photophysics of fluorenone

with substitution has also been reported.[11,12,15,21,23] The dependence with substitution

varies with the electronic nature of the substituent. For molecules with n,π^*

configurations, the dipole moment of the excited state is lower than the dipole moment of

the ground state. In contrast, molecules with π,π^* configurations have dipole moments

which are higher than the dipole moments of the respective ground state. In the excited

state, the presence of an electron-donating substituent on an aromatic molecule with a π,π^*

configuration lowers the energy of that electronic state. Upon excitation an electron from a

π orbital is excited to a π^* orbital, which results in the an electron deficient π system. This

electron deficient π orbital is stabilized by electron-donating substituents that delocalizes

electron density through resonance into the π system of the aromatic molecule. In contrast,

a n,π^* transition is stabilized by the presence of electron-withdrawing groups since upon

excitation an electron rich π orbital is formed. In addition, the position and number of the

substituents has also been shown to affect the photophysics of fluorenone. This former

aspect of substitution details the relative effect that the location of the substituent has on the

photophysical properties of fluorenone, whereas the latter addresses the role of additive

effects of multiple substituents on the fluorenone photophysics.

Many of the changes that are observed in the photophysics for fluorenone can be discussed in terms of the relative positioning of the lowest singlet excited state with that of the T_3 state of fluorenone. As mentioned, the T_3 state of fluorenone has a n,π^* configuration that is stabilized by nonpolar solvents and electron-withdrawing substituents. Therefore, the magnitude of the T_3 stabilization with respect to the S_1 governs much of the photophysics observed for fluorenone. For example, in nonpolar solvents the energy difference between these states in fluorenone is relatively small and efficient intersystem crossing is observed, whereas in polar solvents, the energy of the T_3 level is raised relative to the S_1, and the energy gap increases causing the efficiency of the intersystem crossing process to decrease.

The presence of heavy atoms on a molecule enhances spin-orbit coupling, and leads to an increase in the intersystem crossing rate constant. This heavy-atom effect, as the name implies, depends on the mass of the atom. For example, a larger effect would be expected for a molecule containing a bromine atom than that of a molecule with a chlorine. In our study, a comparison of the intersystem rate constants for three dihalogenated substituents was performed. The three fluorenone derivatives were 2,7DFF, 2,7DCF, and 2,7DBF. The rate constants for the intersystem crossing for 2,7DCF and 2,7DBF in both acetonitrile and toluene followed the expected trend. With an increase in the size of the halogen, an increase in the intersystem crossing rate constant was observed. However, the differences in the intersystem crossing rate constants for 2,7DFF and 2,7DCF were not as well correlated with the heavy-atom effect because the internal conversion process for 2,7DFF played a much larger role in the photophysics than for 2,7DCF.

In the case of the halogenated fluorenones, an additional comparison was made between 2,7DCF and another dichloro derivative, 1,3DCF, to examine the effect that the positioning of the halogens has on the photophysics of these two structural isomers. Similar effects have also been observed for a number of aminofluorenones.[21,23] In acetonitrile, the radiative rate constant for 3-diaminofluorenone was an order of magnitude

faster than 4-diaminofluorenone. In both toluene and acetonitrile, we observed a much higher intersystem crossing rate constant for 1,3DCF than 2,7DCF. This suggests that the proximity of the heavy atoms to the carbonyl moiety in 1,3DCF is important in enhancing the intersystem crossing process. In fact, the intersystem crossing rate constant for 1,3DCF is even greater than 2,7DBF for which a larger heavy-atom effect is expected.

Differences in the photophysics between the parent fluorenone and the halogenated fluorenones were also observed. For the halogenated fluorenones, increases in the internal conversion and intersystem crossing rate constants influenced the changes observed in the intersystem crossing quantum yields. For example, in the case of 2,7DFF in both acetonitrile and toluene, the increase in the internal conversion rate constant was more pronounced than the enhancement of the intersystem crossing rate constant, and as a result the quantum yield for intersystem crossing was lower for 2,7DFF than observed for the parent fluorenone. In addition to the electron-withdrawing fluoro substituents, not even the nonpolar solvent in toluene was sufficient enough to stabilize the T_3 state of 2,7DFF to bring this n,π^* state closer in energy to the S_1 in order to enhance the intersystem crossing process. To a lesser extent, a similar effect was also observed for 2,7DCF. In contrast, for 2,7DBF in acetonitrile, the heavy-atom effect predominates, and the intersystem crossing quantum yield was higher than fluorenone. To explain further the photophysics of these derivatives, the fluorescence, internal conversion, and intersystem crossing rate constants are all competing processes. The efficiency of these processes are defined from their quantum yields. With the sum of the quantum yields equaling unity, if the quantum yield for one process decreases, then the quantum yields for one, or both of the other two processes will increase. The extent of this increase will depend on the rate constants for each process. A larger rate constant will contribute to a larger quantum yield when comparing processes for the same molecule. These exchanges between the deactivation pathways were observed in the case of 2,7DCF when compared with the parent fluorenone.

In the case of 1,3DCF, we were not able to determine any of the rate constants in toluene due to the low fluorescence quantum yield that also precluded the determination of τ_s. However, a significant decrease of the fluorescence quantum yield for 1,3DCF was observed in acetonitrile. Furthermore, similar values for the internal conversion and intersystem crossing quantum yields for 1,3DCF were observed in acetonitrile and toluene. The similarities in the quantum yields, regardless of solvent, and the low fluorescence quantum yield in acetonitrile suggested that in toluene both the intersystem crossing and internal conversion rate constants increased with respect to fluorenone. This implies that the T_3 state, which is already better stabilized in toluene, was also lowered with respect to the S_1, and involved in the intersystem crossing process.

For 2,7DFF, the value for the fluorescence rate constant was smaller than fluorenone in both solvents, whereas the internal conversion rate constant increased significantly in acetonitrile. The latter observation suggests that substitution in the 2- and 7-positions of fluorenone enhances the internal conversion deactivation pathway at the expense of fluorescence and intersystem crossing. The changes in the rate constants for 2,7DFF when compared to fluorenone were more pronounced than observed for 2FF,[10] demonstrating that the substituent effects are additive. In the case of 2,7DFF, the intersystem crossing rate constant was smaller in toluene than in acetonitrile, whereas for 2FF the trend was reversed. This observation suggested that the additional fluorine led to an increase in the energy gap between S_1 and T_3. This is counterintuitive since in the presence of an additional electron-withdrawing substituent, the T_3 state should be more stabilized than for 2FF and even more than the parent fluorenone. However, the T_3 state also appears to be unimportant for the intersystem crossing of 2,7DCF and 2,7DBF in toluene since the values for the intersystem crossing rate constants were similar to those observed in acetonitrile, whereas in the parent fluorenone and 2FF both the intersystem crossing rate constants increased in toluene when compared with acetonitrile. Therefore,

the additional halogen must increase the probability of the internal conversion process at the expense of the intersystem crossing process, and only by the way of the heavy-atom effect can these halogenated compounds intersystem cross efficiently to the triplet state. It is interesting to note that only for 2,7DBF in acetonitrile, 2FF in toluene, and 1,3DCF in both solvents are the intersystem crossing quantum yields larger than for fluorenone in the respective solvents. As discussed earlier, the latter was attributed to the proximity of the halogens to the carbonyl moiety.

In a report by Biczók et al.,[12] they compared a variety of fluorenone derivatives in toluene with the substituents in the 2-position. These authors observed that fluorenones substituted with electron-withdrawing substituents (i.e., nitro, methyl ester) had intersystem crossing rate constants that were two orders of magnitude greater when compared with fluorenones substituted with electron-donating substituents (i.e., methoxy, amino). In contrast, the internal conversion rate constants were larger for the fluorenones substituted with electron-donating groups when compared to fluorenones substituted with electron-withdrawing substituents. In toluene, we observed a similar trend for 2OHF when compared with fluorenone. The rate constant for intersystem crossing decreased by an order of magnitude for 2OHF when compared with fluorenone. In the same manner as described above, the internal conversion rate constant increased by over two orders of magnitude for 2OHF when compared with the parent fluorenone.

The comparison of the photophysics of hydroxyfluorenones substituted at different positions was not very useful because in several cases only upper limits for the intersystem crossing quantum yields were obtained because the excited singlet lifetimes could not be measured, or the decays were biexponential. Only for 4OHF in both acetonitrile and toluene was a monoexponential fluorescence decay measured. The intersystem crossing rate constant for 4OHF in acetonitrile decreased slightly when compared with fluorenone. However, in toluene the rate constant for intersystem crossing for 4OHF decreased by *ca.* six fold when compared with the parent fluorenone. This observation suggests that the T_3

state does not participate in the intersystem crossing process since in toluene we would expect a lowering of the T_3 state of 4OHF that would favor intersystem crossing. Since the decrease in the intersystem crossing rate constant was lower for 4OHF in toluene when compared to fluorenone, the intersystem crossing rate constant for 4OHF in acetonitrile should be the same order of magnitude, or less than was observed when compared with fluorenone. Therefore, the T_3 state does not participate in the intersystem crossing process. In addition, the hydroxy group of 4OHF in toluene should help to destabilize n,π^* state in T_3, thereby increasing the S_1-T_3 energy gap when compared with fluorenone.

The effect of substituents that are not heavy atoms, and occupy the same position on the fluorenone moiety were compared with 4OHF, 4MF, and F-4CA. The hydroxy and methoxy substituents are electron-donating, whereas the carboxy acid substituent is electron-withdrawing. The photophysics for the electron-donating derivatives were very similar to one another. In acetonitrile, the photophysics was dominated by the substantial increases in the internal conversion rate constants. In toluene, the internal conversion rate constants were smaller than in acetonitrile such that intersystem crossing was a competitive process. However, the intersystem crossing rate constant in toluene was much smaller than for the parent fluorenone, which suggested that the S_1-T_3 energy gap was larger for electron-donating substituents when compared to fluorenone. This is consistent with the generalization that a n,π^* configuration, as in the case of T_3, is destabilized in the presence of electron-donating substituents. When our data was compared with those reported previously for 2MF, the intersystem crossing rate constants in both solvents[10] were similar to those in 4MF, again indicating that the T_3 level was not involved in the intersystem crossing process. However, the internal conversion rate constants were much higher for 2MF. This increase could be due to the proximity of the electron-donating substituent to the carbonyl moiety. Increased rates of internal conversion have also been observed for the 3- and 4-aminofluorenones,[21,23] and 1-aryl-fluorenones,[15] where charge -transfer mechanisms have been used to describe the enhanced rates of internal conversion when

compared with the parent fluorenone. We did not observe any results that would suggest a charge-transfer mechanism for the photophysics of the fluorenones investigated.

F-4CA and F-2CA have electron-withdrawing substituents that stabilize excited states with n,π^* configuration. As a consequence, the intersystem crossing rate constant increased for F-4CA in toluene since the S_1-T_3 energy gap will decrease due to the stabilization of the T_3 state when compared with that of fluorenone. In addition, the rate constant for internal conversion was *ca.* four times higher than that observed for fluorenone. These increases in the intersystem crossing rate constants for F-4CA are similar to those observed for 2,7DBF when compared with fluorenone. F-2CA behaved in a similar fashion as F-4CA in acetonitrile, and no significant increase of the internal conversion rate constant was observed when compared to fluorenone.

We have shown with additional examples that the photophysical properties of fluorenone are very dependent on the polarity of the solvent, and the nature and position of the substituents on the fluorenone moiety. In most cases, the photophysics of fluorenone with respect to solvent and substituent effects can be rationalized in terms of the stability of the n,π^* T_3 state with respect to the lowest singlet state. However, generalizations should be made with caution since compensating effects do occur, especially as the size of the substituent increases. For the first time, a detailed investigation on a series of halogenated fluorenones was performed. Intersystem crossing rate constants were shown to be consistent with the heavy-atom effect, and the proximity of the halogens to the carbonyl moiety was shown to be important in enhancing this effect. In addition, these dihalogenated fluorenones were shown to have very different properties than observed for a monosubstituted fluorenone. These differences were assigned to compensating effects observed from increasing rates for internal conversion for the dihalogenated fluorenones. These compensating effects were also used to explain some of the photophysical properties observed for the hydroxy and carboxylic acid derivatives, which have been studied for the first time. As discussed, comparisons of the photophysics of the hydroxyfluorenones were

not very informative since in most cases only upper limits for the intersystem crossing quantum yields were obtained because the excited singlet lifetimes could not be measured or the decays were biexponential. For those that were measurable, these examples provided additional comparisons for the photophysics of fluorenone derivatives with electron-donating substituents to that of the parent fluorenone. The carboxylic acid fluorenone derivatives provided further examples of the effect of electron-withdrawing substituents on the photophysics of fluorenone. In addition, enhanced intersystem crossing quantum yields were observed for these derivatives in acetonitrile over that of the parent fluorenone.

The largest increase in the intersystem crossing quantum yield for a fluorenone derivative over that of the parent fluorenone was observed for 1,3DCF in acetonitrile. As a result, 1,3DCF was further employed in the study of probe mobility in the presence of CDs with the LFP system. Unfortunately, the larger intersystem crossing quantum yields observed in acetonitrile were still not sufficient for a detailed study of the dynamics of fluorenone derivatives in aqueous CD systems. As yet, no fluorenone derivatives have been observed to have measurable triplet absorption signals with suitable signal to noise ratios in aqueous solution. Nevertheless, this investigation into the photophysical properties of fluorenone derivatives has contributed to the general study on the complexity of fluorenone photophysics by demonstrating that several effects such as the nature and position of substituents and the properties of the microenvironment are responsible for the relative energies between different excited singlet and triplet states of these aromatic ketones.

4. FLUORENONE/XANTHONE BINDING TO CYCLODEXTRINS

4.1 Ground State Absorption

This chapter describes the complexation of fluorenone to cyclodextrin. In the case of xanthone, most of the characterization of the complexation to cyclodextrins has been previously described.[29-31,49,59] The picosecond experiments we performed on this system complement the previous work.

The ground state absorption spectra of fluorenone changed in the presence of β-CD. A small enhancement of the fluorenone absorbance was observed upon increasing the concentration of β-CD. This behavior suggested that fluorenone formed a complex with the CD cavity. However, these changes were too small to be used in the determination of
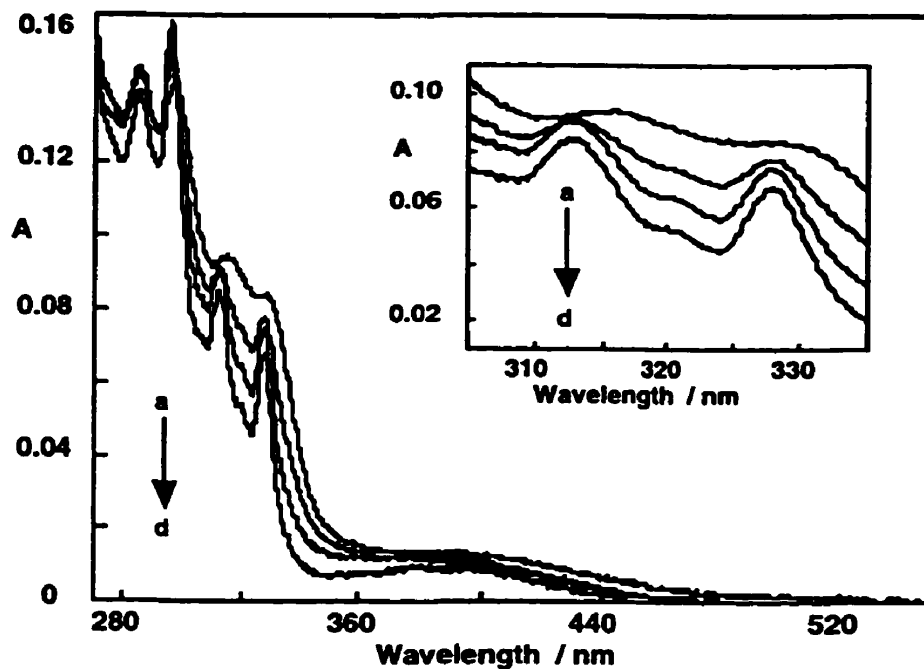
Figure 4.1 Corrected absorption spectra of fluorenone in the presence of α-CD at the following concentrations (mM): (a) 0, (b) 10, (c) 20 and (d) 30. The inset shows an enlargement of the spectra between 290 and 340 nm.

equilibrium constants for these ground state complexes. In contrast, in the presence of α-CD a significant sharpening of the absorption bands and a decrease in the absorption spectra was observed at concentrations of α-CD greater than 10 mM (Figure 4.1). This result also suggested the formation of a complex between fluorenone and α-CD. In addition, an isosbestic point was not detected, which indicates that more than one type of complex was formed (Figure 4.1).

The UV-Vis absorption spectrum of xanthone was also affected in the presence of CD. Previous reports have shown that increasing amounts of β-CD in the presence of xanthone causes a decrease in absorption intensity of xanthone.[29] From these changes in absorbance, the equilibrium constant for the complexation of xanthone to β-CD was determined to be 1500 M^{-1}.[29] The effect on the xanthone absorption spectra is smaller when α-CD is added. As a result, equilibrium constants could not be determined precisely from the absorption data.

4.2 Steady-State Fluorescence

The fluorescence quantum yield and emission maximum of fluorenone are dependent on solvent polarity.[8,9,11,13,14,16-20,22] In general, the fluorescence quantum yields are less than 0.04 (Section 3.2). In nonprotic solvents the fluorescence lifetimes and emission quantum yields of fluorenone increase with solvent polarity. However, in protic solvents the fluorescence quantum yields for fluorenone were much smaller due to hydrogen bonding with the solvent.[11,12,16-18,21-25] Interactions with the solvent, such as hydrogen bonding, provides an additional deactivation pathway that results in an increase in the internal conversion quantum yield for fluorenone and thus reduces the fluorescence quantum yield. The fluorescence quantum yield for fluorenone in ethanol was reported to be 1.5 × 10^{-3}.[25] We also observed a very weak emission in ethanol, but no emission was
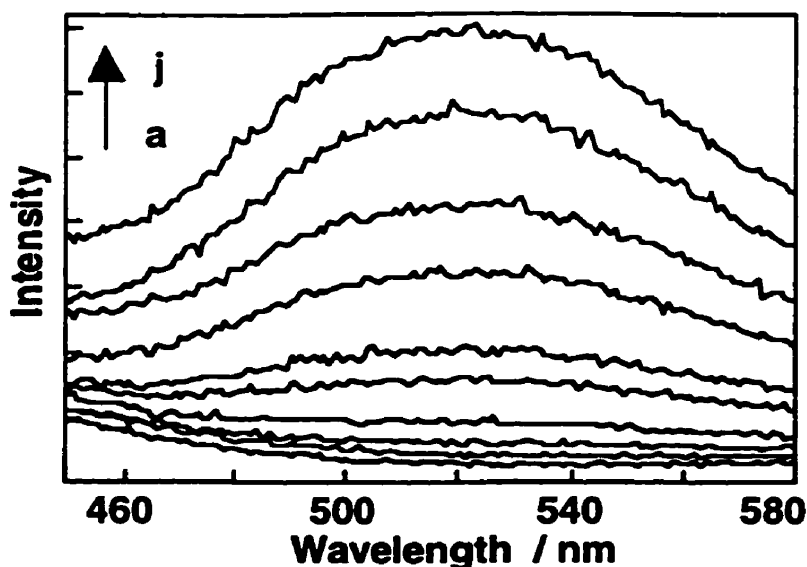
Figure 4.2 Corrected fluorescence spectra of fluorenone in the presence of different α-CD concentrations (mM): (a) 0, (b) 1, (c) 2, (d) 3, (e) 5, (f) 6, (g) 9, (h) 12, (I) 18, and (j) 30.

observed in water under the same experimental conditions. This result suggests that the fluorescence quantum yield for fluorenone in water is less than 1.5×10^{-3}.

In the presence of low concentrations of α-CD (< 5 mM), a very small increase in the fluorescence intensity was observed. However, in the presence of high concentrations of α-CD (≥ 5 mM), there was a significant increase in the fluorescence intensity. The maximum for the fluorescence of fluorenone at high α-CD concentrations was at ca. 525 nm (Figure 4.2). Based on this concentration dependence with the emission intensity, the increase was assigned to the formation of a 2:1 host-guest complex (see below). The addition of β-CD only led to a small enhancement in the emission intensity. This result suggests that fluorenone is fairly exposed to water when complexed to β-CD.

The equilibrium constants for the complexation of fluorenone to cyclodextrins were determined from changes in the fluorenone emission intensity. The changes in the fluorenone fluorescence intensities were plotted against the concentrations of α-CD. Equation 1.20 was used to fit the experimental data. This equation can be employed when

either a 1:1, or a 2:1 host-guest stoichiometry is assumed. Acceptable fits with Equation

1.20 assuming 1:1, or 2:1 host-guest stoichiometries were not obtained. This indicated that

multiple equilibria were present. The presence of multiple host-guest stoichiometries can

be verified with the use of Equation 1.21. Equation 1.21 is the double-reciprocal plot of

Equation 1.20, and is often referred to as a Benesi-Hildebrand plot.[52] When the inverse of

the changes in the emission intensities are plotted against the inverse of the CD

concentrations a linear plot will be observed if the host-guest stoichiometries are assumed

correctly. Fits to Equation 1.21 for the changes in fluorescence intensity for fluorenone in

the presence of α-CD were not linear (Figure 4.3), when either a 1:1, or 2:1 stoichiometry

was assumed. Hence, neither the sole formation of 1:1 nor 2:1 host-guest stoichiometry
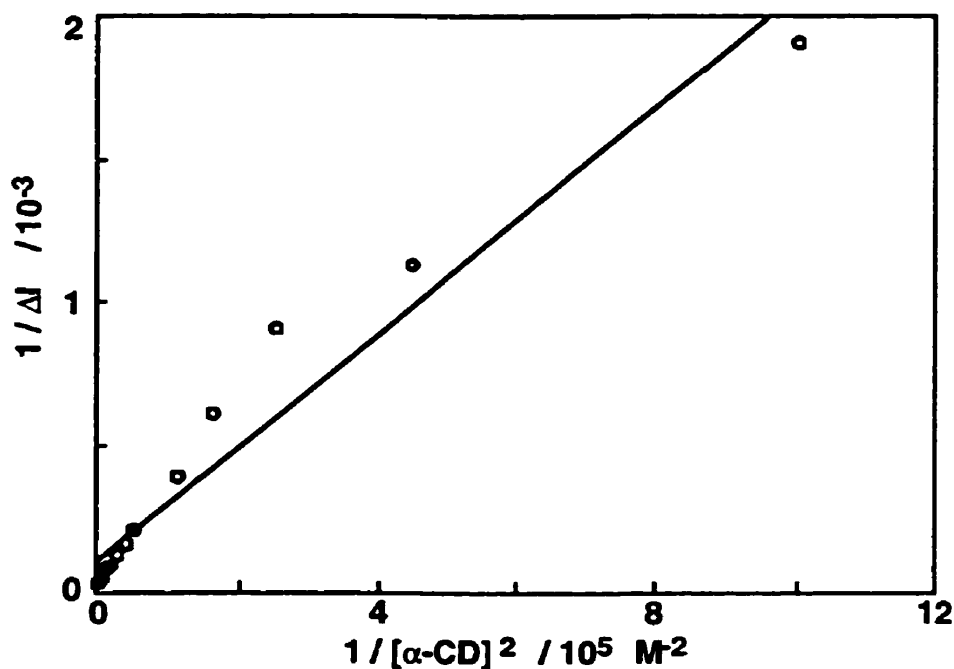
Figure 4.3 Double-reciprocal plot for the variation of the fluorenone fluorescence
intensity at 525 nm in the presence of different α-CD concentrations,
assuming a 2:1 host-guest stoichiometry.

was observed. In such a case, Equation 1.22 was employed to fit the experimental data. This equation assumes the presence of both 1:1 and 2:1 host-guest stoichiometries in solution. However, the fits to Equation 1.22 were still not optimal, so an additional assumption was made. It was observed that only a small difference in the fluorescence intensities of fluorenone in the presence of low concentrations of α-CD was observed when compared to fluorenone in water. This small difference in intensity suggests that the fluorescence quantum yields for fluorenone in water and for fluorenone present in a 1:1 complex are similar. This assumption was used to reduce Equation 1.22 to Equation 1.23. The fits were improved (Figure 4.4), but the errors for the recovered values of K_1 and K_2 were still large. To analyze these equilibrium constants further, several combinations for K_1 and K_2 were obtained when the value for one of the equilibrium constants was fixed in
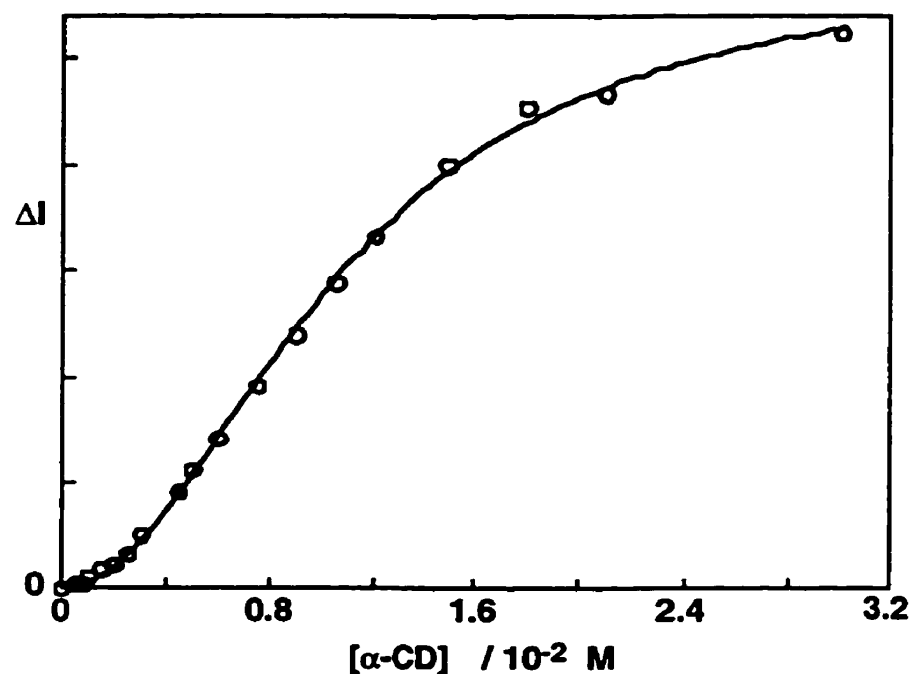
Figure 4.4 Nonlinear fit of the corrected fluorenone fluorescence intensities at 525 nm with various α-CD concentrations. The solid line corresponds to the fit obtained from using Equation 1.23.

Equation 1.23 and the other equilibrium constant was allowed to float. The individual equilibrium constants varied considerably with $K_1 = 1\text{-}50 \text{ M}^{-1}$ and $K_2 = 8700\text{-}200 \text{ M}^{-1}$. However, the product of K_1K_2 for these fits was $(9.3 \pm 0.6) \times 10^3 \text{ M}^{-2}$. The reasonably constant value recovered for K_1K_2 suggests that the individual equilibrium constants could not be precisely determined from the fluorescence data. Such a situation is often observed when multiple equilibria are present for the CD complexes and when the equilibrium constants themselves are of the same order of magnitude.

Fluorescence and ICD spectroscopy have been previously employed to characterize the complexes between xanthone and α-, β-, γ- and hydroxypropyl-β-CDs.[29,30] Binding is strongest with hydroxypropyl-β- $(1800 \pm 100 \text{ M}^{-1})$[30] followed by β- $(1100 \pm 200 \text{ M}^{-1})$[30], γ- $(220 \pm 30 \text{ M}^{-1})$[30] and α-CD $(50 \pm 8 \text{ M}^{-1})$[29]. These equilibrium constants are obtained from the fits to plots for the fluorescence, or ICD intensity changes with CD concentrations (Equation 1.20). For all complexes, a 1:1 host-guest stoichiometry is assumed. This stoichiometry is confirmed by linear double-reciprocal plots as described above.

4.3 Picosecond Fluorescence

Picosecond fluorescence experiments were only performed for fluorenone in the presence of high α-CD concentrations (≥ 20 mM). No appreciable fluorescence intensity was observed at lower α-CD concentrations (Section 4.2). In the presence of high α-CD concentrations, the fluorescence decay observed was fitted to a sum of two exponentials (Figure 4.5). As a background correction, an aqueous solution of α-CD was measured under the same experimental conditions. An appreciable amount of fluorescence was observed for the α-CD solution. For the fit to the biexponential decay of fluorenone in the presence of α-CD, the component with the largest preexponential term ($A_1 \approx 0.63$) had a lifetime of ca. 1.5 ns. This short-lived decay was assigned to fluorenone present in the 2:1
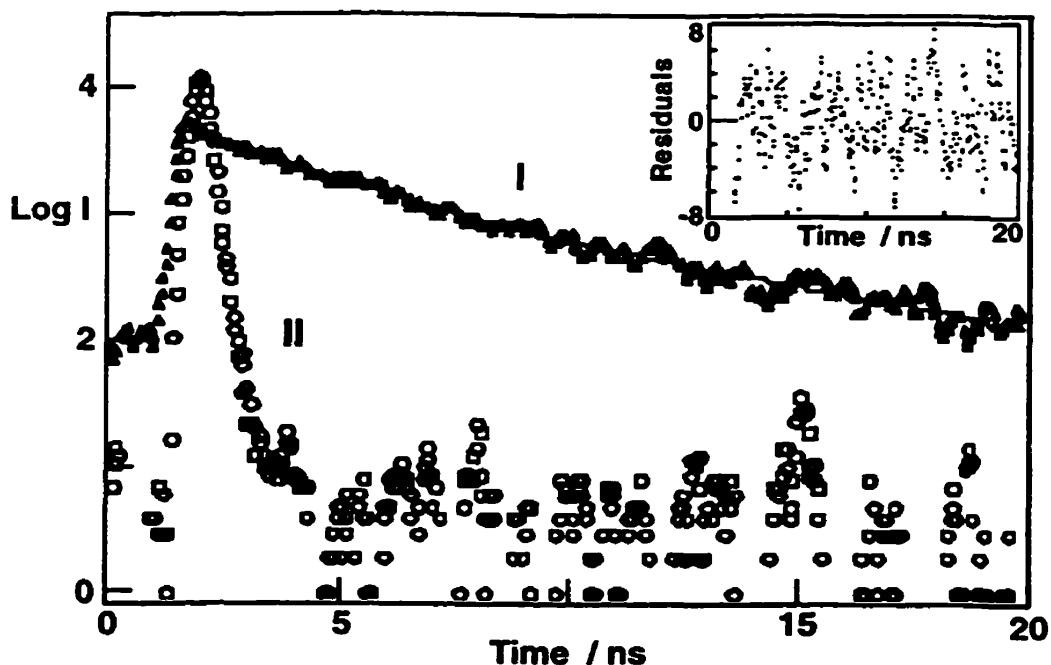
Figure 4.5 Time-resolved fluorescence decay of fluorenone in the presence of 30 mM α-CD fitted to the sum of two exponentials. The inset shows the residuals for the fit. Decay I is the fluorescence for fluorenone and decay II is the instrument response function.

host-guest complex. The second and longer-lived component (*ca.* 5 ns and $A_2 \approx 0.37$) was assigned to an artifact of the experiment since similar lifetimes were recovered from the fits for both this long-lived component and for the α-CD solution in the absence of fluorenone. This artifact could be due to an impurity present in α-CD, or related to the detection of background light. Nevertheless, this artifact was particularly noticeable since the fluorescence quantum yield of fluorenone in water is low.

Picosecond fluorescence experiments were also performed for the xanthone fluorescence in the presence of α- and β-CD. It has been previously reported that xanthone in water has a fluorescence lifetime that occurs in the subnanosecond time domain.[29] However, no accurate lifetime determinations were made.[29] With the use of the picosecond fluorescence system, the decay of xanthone in water was shown to be

monoexponential with a lifetime of 750 ± 50 ps (Figure 4.6, (A)). In the presence of 8 mM of β-CD, the fluorescence decay was multiexponential and was fitted to the sum of three exponentials with lifetimes of 50-80 ps, 600-800 ps, and 3-5 ns (Figure 4.6, (B)). The largest preexponential term (> 0.80) was associated with the 50-80 ps lifetime component, and it was assigned to the emission of xanthone in a 1:1 β-CD complex. The species with a lifetime of 600-800 ps and a preexponential of ca. 0.15 was assigned to the emission of xanthone in water since this lifetime was similar to that observed in pure water. Both of these species displayed time-resolved emission spectra with maxima between 390 and 400 nm that were characteristic of xanthone fluorescence. A long-lived component with a preexponential of < 0.05 was also observed. Similar to the case for fluorenone in the presence of α-CD , this emission had no defined spectrum and was assigned to an artifact of the experiment because it was observed when a solution containing only β-CD was measured. As discussed earlier, this emission could be due to an impurity present in β-CD, or related to the detection of background light. In addition, if the emission is due to an impurity in β-CD, it would be noticeable in the presence of xanthone since this ketone also has a low fluorescence quantum yield in water.

In the presence of 30 mM α-CD, the fluorescence decay of xanthone was adequately fitted to a monoexponential decay with a lifetime that was close to that observed for xanthone in water. This suggests that xanthone is not very well protected from the aqueous phase when it is complexed with α-CD, or analogous to fluorenone complexed to β-CD, the fluorescence quantum yields for the complexed xanthone and xanthone in water may be similar.
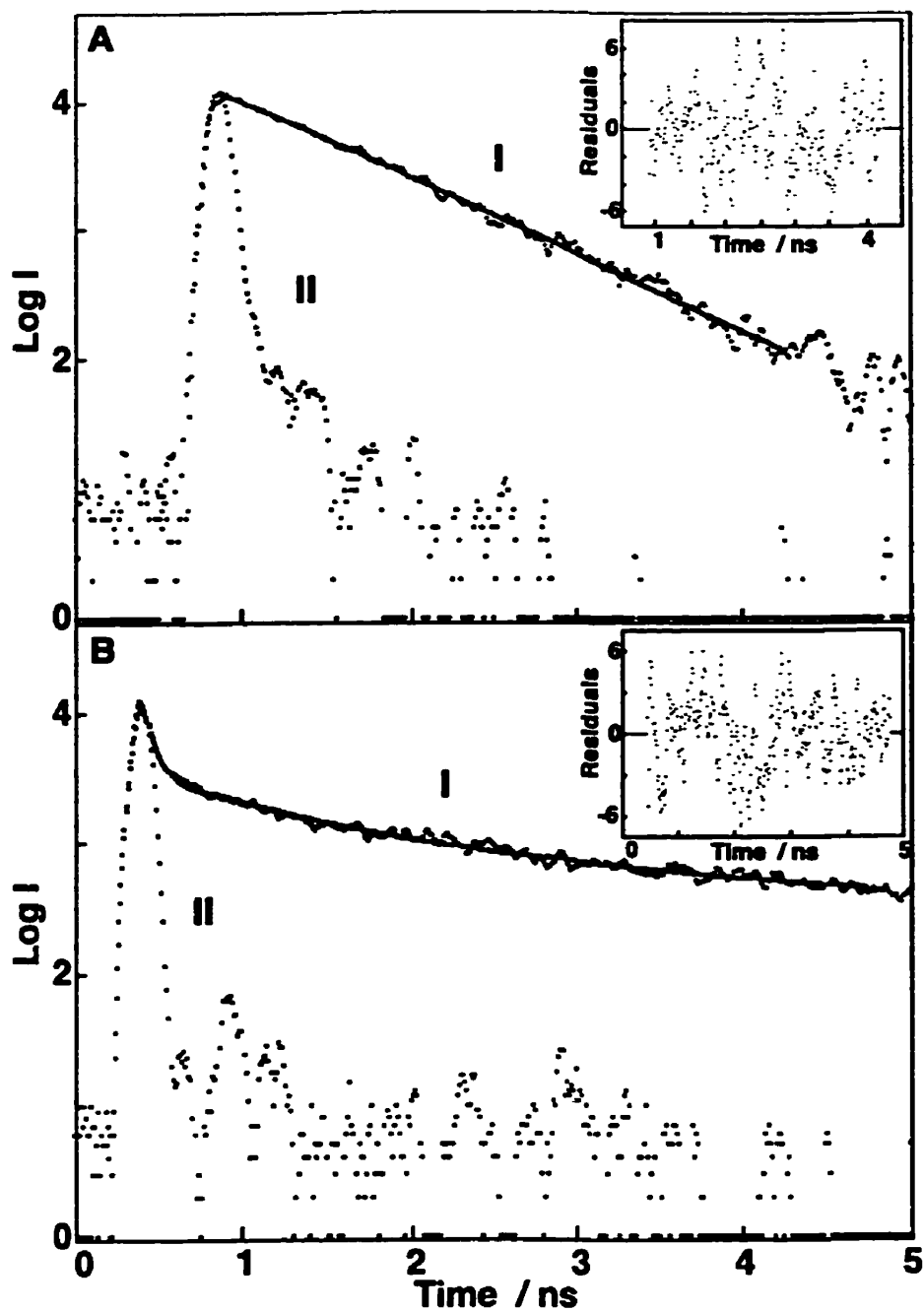
Figure 4.6 Time-resolved fluorescence decays of xanthone in the absence (A) and presence (B) of 8 mM β-CD fitted to one exponential (A) and the sum of three exponentials (B), respectively. The residuals for the fits are shown in the insets. The decays labeled I are the fluorescence of xanthone and the decays labeled II are the instrument response functions.

4.4 Induced Circular Dichroism

ICD has been used to determine equilibrium constants for xanthone complexed to

α-, β-, and γ-CD.[29] In addition, ICD has been used as a qualitative tool to provide

structural information on the association of these probes with CDs.[43,53,55-58,68-70] The

ICD spectra for fluorenone in the presence of α- and β-CD displayed opposite signals in the

spectral region investigated (Figure 4.7). In the case of α-CD, a small negative signal

followed by a small positive signal was observed. In the case of β-CD, only a positive

signal was observed. The change in the fluorenone ICD intensity with increasing β-CD

concentrations was fitted to Equation 1.20 assuming a 1:1 host-guest stoichiometry (Figure

4.8). The recovered equilibrium constant from the fit was 450 ± 50 M^{-1} from four

independent experiments. The stoichiometry for this complex was also confirmed from

linear double-reciprocal plots (inset of Figure 4.8). For α-CD, the change in the

fluorenone ICD intensity was monitored for two ICD bands; one at 296 nm and the other at

330 nm. The two bands were representative of two different host-guest stoichiometries for

the CD complexes. The changes in the ICD intensity observed at 296 and 330 nm were

fitted reasonably well to double-reciprocal plots (Equation 1.21) when 1:1 and 2:1

stoichiometries were assumed, respectively. However, due to the large errors in the

nonlinear fits the K_1 and K_2 values for the CD complexes with fluorenone were not

recovered with any precision.

ICD measurements for xanthone in the presence of α- and β-CD were also

performed and opposite signals in the long and short wavelength regions were observed

(Figure 4.9). In the case of β-CD, the values for the equilibrium constants using Equation

1.20 and assuming a 1:1 stoichiometry were 1000 ± 200 and 1200 ± 300 M^{-1} for

measurements made at 262 and 350 nm, respectively. These values agree well with those

determined previously.[29] The 1:1 stoichiometry of this complex was also confirmed from

linear double-reciprocal plots.
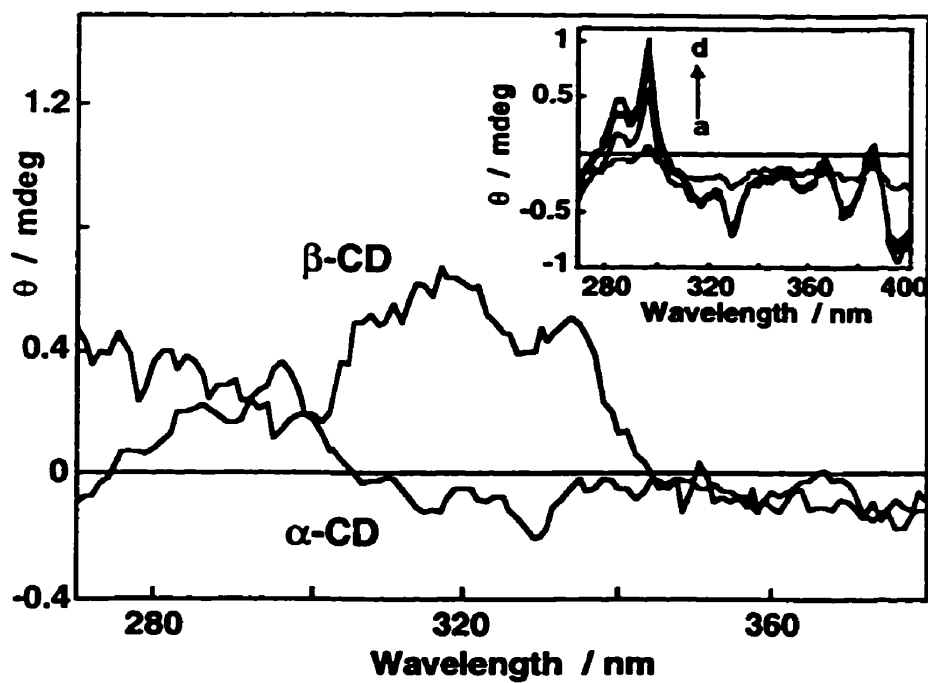
Figure 4.7 Fluorenone ICD spectra in the presence of 8 mM β-CD and 30 mM α-CD. The inset shows the ICD spectra of fluorenone in the presence of various concentrations of α-CD (mM): (a) 5, (b) 15, (c) 20, and (d) 30.
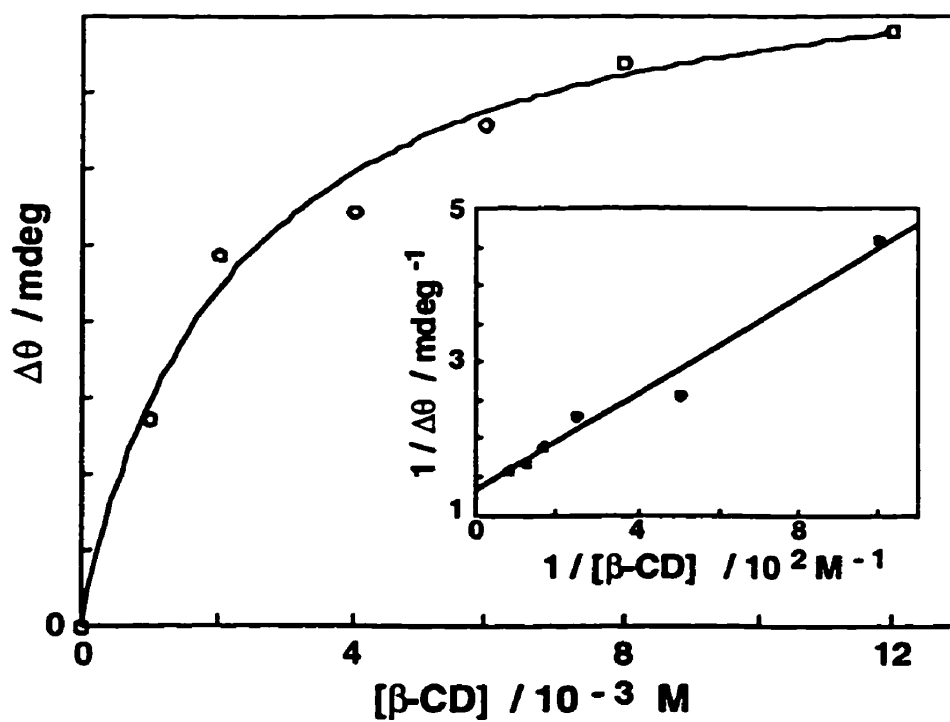
Figure 4.8 Nonlinear fit of the ICD signal at 320 nm for fluorenone in the presence of various β-CD concentrations. The solid line corresponds to the fit obtained from using Equation 1.20. The inset shows the double reciprocal plot for the same data.
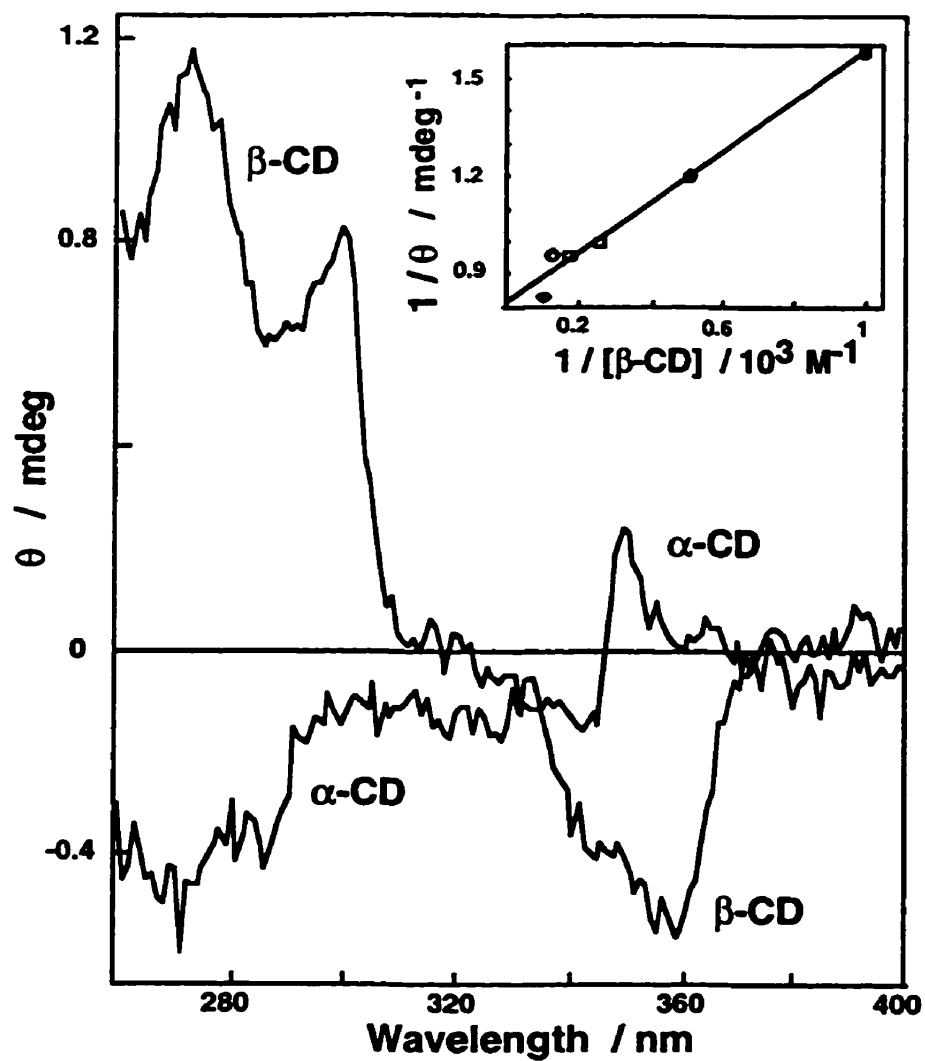
Figure 4.9 Xanthone ICD spectra in the presence of 8 mM β-CD and 30 mM α-CD. The inset shows the double reciprocal plot for the xanthone ICD signal at 262 nm at various β-CD concentrations.

4.5 Discussion

The equilibrium constants obtained from the changes in the absorption, steady-state fluorescence, and ICD intensities for guest molecules, such as xanthone and fluorenone, complexed with CDs provides detailed information on the efficiency of the formation of these complexes. ICD has also been shown to provide valuable information about the structural parameters associated with host-guest systems involving CDs.[43,53,55-58,68-70] From a collaboration with theoretical chemists (Dr. B. Mayer, University of Vienna, Vienna, Austria and Dr. G. Marconi, Istituto FRAE-CNR, Bolonga, Italy), we have gained additional support for our photophysical studies with calculations that describe the structures of the CD complexes with fluorenone and xanthone. In addition, picosecond fluorescence measurements have provided additional photophysical information to better describe the excited states of these host-guest systems.

Since the equilibrium constants obtained for these host-guest complexes are associated with the entry, and exit rate constants of these ground state complexes, a better understanding of the equilibria present in these host-guest assemblies will lead to a better understanding of the dynamics involved in such systems. Understanding the dynamics of these systems can provide valuable mechanistic information that can not be detailed entirely from equilibrium constants alone. From our studies on the ground state complexation, the picosecond fluorescence studies, and the calculations used for the structural determination of these ketones to CDs, it is hoped that we can better comprehend how dynamic processes evolve from host-guest associations.

4.5.1 The Complexation of Xanthone with CDs

Fluorescence and ICD spectroscopy have been previously employed to characterize the complexes of xanthone and α-, β- and γ-CDs.[29,30,49] The largest equilibrium constants for xanthone and CDs has been observed for β-CD (1100 ± 200 M⁻¹), followed by γ-, and α-CD,[29] suggesting that the best fit is with β-CD. For α-CD, the size of the cavity is too small, whereas for γ-CD, the cavity size is too large to complex xanthone efficiently. The same trend in equilibrium constants was observed for fluorenone complexed to α-, and β-CD. However, fluorenone also formed 2:1 host-guest complexes at higher α-CD concentrations.

The fluorescence decay for xanthone in the presence of β-CD was biexponential. This was expected since the fluorescence quantum yields for xanthone in water differed from that of xanthone in a 1:1 host-guest complex with β-CD. This assumption is made because a fluorescence quantum yield of a molecule is directly proportional to its singlet lifetime. Therefore, a decrease in the fluorescence quantum yield will affect the singlet lifetime accordingly. The biexponential decay was composed of a short-lived species with a lifetime of *ca.* 50-80 ps and a second component with a lifetime of *ca.* 600-800 ps. The longer-lived species was assigned to the decay of xanthone in water, for which a lifetime of *ca.* 750 ps was measured independently. The short-lived component was assigned to the decay of the 1:1 complex of xanthone to β-CD. These assignments were consistent with the decrease observed for the steady-state fluorescence intensity when xanthone was complexed to CDs.[29]

The behavior observed for the excited singlet decay for xanthone complexed to β-CD parallels that observed for the incorporation of xanthone in anionic and cationic micelles, where a substantial shortening of the lifetime from *ca.* 600 ps to that of *ca.* 67 ps was observed when this ketone was associated with the micellar environment.[71] The

photophysics of xanthone is similar to that observed for fluorenone (Section 3.6). As in fluorenone, the photophysics of xanthone is complex since the lowest singlet and triplet energy levels have different electronic configurations that are close in energy. Consequently, the photophysics of xanthone is very dependent on the polarity of its microenvironment. The intersystem crossing rate constant for xanthone has been shown to depend on the solvent polarity.[72] In alcohols and other organic solvents such as cyclohexane, the observed growth for the triplet state, which is directly related to the excited singlet decay, is shorter than 20 ps.[72] In the presence of water, we observed an increase in the singlet lifetime of xanthone that was over one order of magnitude larger when compared to the lifetimes reported in alcohols. These measurements demonstrate that the polarity of xanthone's microenvironment has a significant effect on its photophysics. Complexation of xanthone with β-CD reduced the excited singlet lifetime of xanthone from *ca.* 750 ps to *ca.* 65 ps, which is very similar to that observed for xanthone in the presence of micelles.[71] This suggests that the ketone is somewhat protected from water. However, this measured value was still longer than the lifetimes observed in alcohols, suggesting that the polarity sensed by the complexed xanthone was in the polarity range between alcohols and water.

The binding of xanthone to α-CD is much less efficient than for β-CD as shown by the lower equilibrium constant $(50 \pm 8 \text{ M}^{-1})$.[29] In the complex with α-CD, xanthone will be more exposed to the aqueous phase because the cavity size of α-CD is smaller than β-CD. A multiexponential decay was expected for the xanthone fluorescence in the presence of α-CD since the steady-state emission intensity of xanthone in water decreased in the presence of α-CD. However, a monoexponential decay with a lifetime close to that of xanthone in water was observed. To explain this observation, the fluorescence intensity of xanthone in water and in the presence of high concentrations of α-CD was measured. A decrease of *ca.* 20% in the fluorescence intensity upon complexation at the highest α-CD

concentration employed (30 mM) was observed. This decrease led to a ratio of lifetimes for xanthone in water to that complexed with α-CD of 1.25. This ratio may be too small to observe a difference in the fluorescence lifetimes for xanthone given the experimental errors associated with the time-resolved measurements. For this reason, the excited singlet lifetime for the complexed xanthone was suggested to be close to the lifetime of xanthone in water, and the decay was adequately fitted to a monoexponential function. This observation supports the assignment that xanthone is quite exposed to water when complexed with α-CD, whereas in the case of β-CD the shorter lifetime observed for xanthone when complexed to β-CD would be expected, since the guest is better protected from water.

These assignments on the photophysics of xanthone complexed with CDs were also supported by the calculated structures (Figure 4.10) obtained for the host-guest systems from a collaboration with theoretical chemists. In the case of xanthone complexed with α-CD (Figure 4.10 (A)), xanthone is not tightly bound to the interior of the CD cavity, and the molecule is mostly exposed to the aqueous phase. This exposure of xanthone to water could account for the small decrease observed in the steady-state fluorescence intensity upon the addition of α-CD. It also supports the monoexponential decay observed for the excited singlet lifetime of xanthone when complexed to α-CD from the picosecond fluorescence measurements. A similar structure is also observed when xanthone is complexed with β-CD (Figure 4.10 (B)). Once again the xanthone guest is not deeply included into the β-CD cavity and the ketone is still fairly exposed to the aqueous phase. However, the picosecond fluorescence results have shown that the inclusion of xanthone into the β-CD cavity must be greater than α-CD for xanthone to experience an appreciable difference in its microenvironment, as shown from the observed biexponential decay. This deeper inclusion has also been suggested from the larger equilibrium constants associated with β-CD than for α-CD complexation.
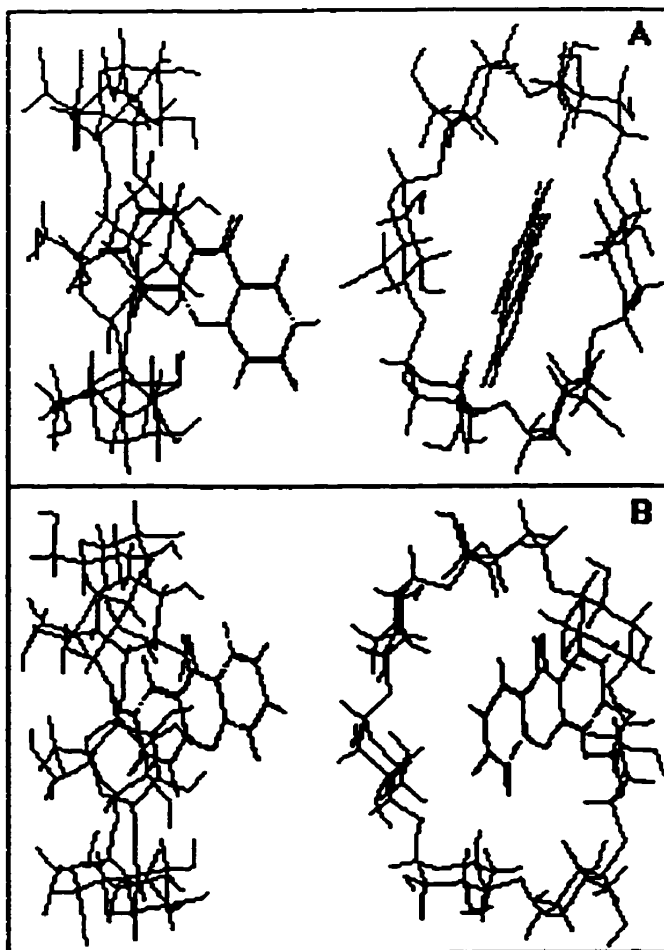
Figure 4.10 Calculated structures for the 1:1 complexes of xanthone with α-CD (A) and β-CD (B). (B. Mayer and G. Marconi, from reference 61)

4.5.2 The Complexation of Fluorenone to CDs

In the case of fluorenone, the equilibrium constant for the complexation with β-CD could only be determined from the ICD spectra since we only observed small changes in the absorption spectra, and only weak fluorescence for fluorenone in the presence of β-CD. Previously reported ICD and fluorescence studies verify that fluorenone does form

complexes with β-CD.[25,73] The fluorescence quantum yield of fluorenone in β-CD has

been reported (2.4×10^{-3}).[73] In addition, the reported fluorescence quantum yields for

fluorenone in hydroxylic solvents are of the same order of magnitude, and quite low ((1.5 -

2.5) $\times 10^{-3}$ for ethanol to 1-octanol, respectively).[73] Therefore, the lack of fluorescence

observed in our experiments, and those published earlier suggests that fluorenone is either

exposed to water, or its carbonyl group is hydrogen bonded to the hydroxyl groups of the

CD rim when complexed to β-CD. Although we were unable to measure the excited singlet

lifetime of fluorenone in water, or in the presence of β-CD, a lifetime of 1.2 ns for

fluorenone in β-CD is reported.[25] The fluorescence lifetimes have also been reported for

fluorenone in ethanol, 1-pentanol and 1-octanol with respective values of 0.8, 1.1, and 1.2

ns.[25] These measurements suggest that fluorenone is experiencing a polarity similar to

alcohols, and may be somewhat exposed to water. From the ICD experiments, the

complexation of fluorenone with β-CD occurs with a 1:1 host-guest stoichiometry similar

to the case for xanthone. This observation was supported with linear double-reciprocal

plots for the changes in the ICD intensities with the change in β-CD concentrations. The

equilibrium constant for complexes of β-CD with xanthone is higher (1100 ± 200 M^{-1}) than

with fluorenone (450 ± 50 M^{-1}), indicating that complex of β-CD to xanthone is more

favorable than that of fluorenone. Similar to the structures calculated for xanthone,

fluorenone is also shown (Figure 4.11) to be quite exposed to the aqueous phase.

The complexation of fluorenone with α-CD is more complex than the behavior

observed for xanthone. At low α-CD concentrations, the absorption spectrum of

fluorenone only changes slightly. However, at higher concentrations ($\geq$ 10 mM) the

absorption bands of the fluorenone spectrum sharpen significantly. The absorption spectra

of fluorenone in water, or ethanol were observed to be quite broad, yet the absorption for

the same spectral region in acetonitrile, or toluene was sharp. The sharpening of the
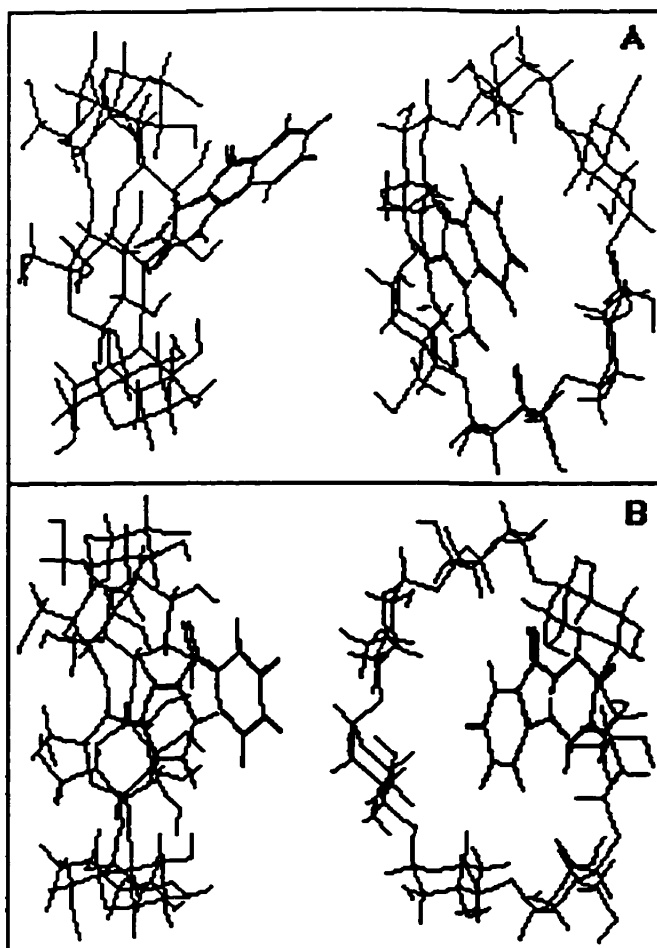
Figure 4.11 Calculated structures for the 1:1 complexes of fluorenone with α-CD (A) and β-CD (B). (B. Mayer and G. Marconi, from reference 61)

absorption bands observed at high α-CD concentrations indicates that fluorenone is fairly well protected from interactions with water molecules, and more specifically, hydrogen bonding with hydroxylic solvents. This result is consistent with the formation of a 2:1 host-guest complex of fluorenone with α-CD. In addition, the lack of an isosbestic point also suggests that other complexes, such as the 1:1 complex are present. Isosbestic points observed in absorption spectroscopy are often associated with the presence of an equilibrium formed between only two different species in solution.

From the fluorescence experiments, it was observed that at low α-CD

concentrations (< 10 mM) the fluorescence intensity was quite weak, but upon increasing

concentration of α-CD an increase in the emission intensity was observed. This lag in

fluorescence intensity increase upon the addition of α-CD is consistent with the formation

of a 2:1 complex. The fluorenone fluorescence maximum, as discussed earlier (Section

3.2), shifts from 490 nm in toluene to 510 nm in acetonitrile. In ethanol, the fluorescence

maximum shifts even further to longer wavelengths at 550 nm.[16] The emission maximum

for the complex of fluorenone with α-CD was observed at 525 nm, suggesting that the

polarity sensed by fluorenone is less than that for ethanol. This result is consistent with the

assignment that fluorenone is in a fairly nonpolar environment. In addition, the lifetime for

fluorenone at high α-CD concentrations was determined from picosecond fluorescence

experiments to be ca. 1.5 ns, which is similar to the lifetime reported for fluorenone in 1-

octanol (1.2 ns), but larger than that reported for fluorenone in ethanol (0.8 ns).[25] These

measurements suggest that the decay of fluorenone in hydroxylic solvents is accelerated in

the presence of stronger hydrogen bonding solvents. Therefore, the longer lifetime
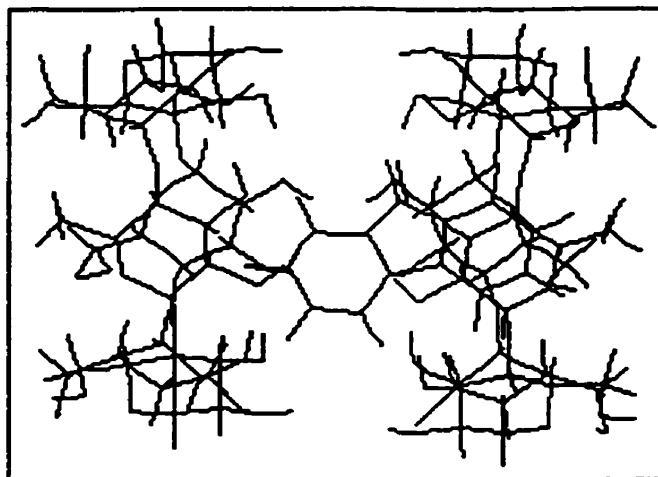
Figure 4.12 Calculated structure for the 2:1 complex of fluorenone with two α-CDs.
(B. Mayer and G. Marconi, from reference 61)

observed in the presence of α-CD indicates that fluorenone is not extensively hydrogen bonded in the 2:1 complex. In addition, the formation of a 2:1 complex is consistent with our lifetime measurements, where water molecules can not be positioned between the two CD units to participate in hydrogen bonds with the guest.

The presence of more than one complex between fluorenone and α-CD at high CD concentrations was also suggested from the dependence of the change in the fluorescence and ICD intensities with increasing CD concentrations. From the ICD measurements, double-reciprocal plots were linear but in two different spectral regions. One spectral region shows linear plots when a 1:1 complexation stoichiometry was assumed, whereas the other region is only linear when a 2:1 host-guest stoichiometry was assumed. From fluorescence measurements, the double-reciprocal plots were nonlinear when either a 1:1, or 2:1 complexation stoichiometry was assumed. For the latter, the formation of the 2:1 complex was efficient since the lower limit for the K_2 value is around 200 M^{-1}. The calculated structures for a 2:1 host-guest complex for fluorenone with two α-CDs (Figure 4.12) is also consistent with our suggestions that fluorenone is well protected from the ability to form hydrogen bonds with the water molecules that causes a decrease in the excited singlet lifetime of fluorenone.

It is noteworthy, that the formation of 2:1 host-guest complex of xanthone with α-CD was not observed from either photophysical studies, or calculations. However, fluorenone was observed to form higher ordered complexes with α-CD. This difference could be related to the observation that in the 1:1 host guest complexes with fluorenone the guest is more exposed to water than in the case of xanthone. As a result, this greater exposure may provide a more appropriate binding site to the second α-CD that is not afforded by xanthone.

4.5.3 Complexation Structure and Dynamics

The relationship between the structure and dynamics of host-guest systems has not been well characterized. Previous studies for the complexation dynamics of CD complexes have focused mainly on the arguments of guest size, and solvation properties to explain the rate constants for entry and exit.[43,46-48] While these reports successfully demonstrate the effect of size, and solvation on host-guest complexation with CDs, they do not detail the intricacies of host-guest structure, and its affect on the association and dissociation rate constants. In our studies, we examined the complexation of two aromatic ketones with CDs. Fluorenone and xanthone were chosen as probes because their photophysics is very dependent on the polarity of their environment. In addition, the structural differences between these two molecules are very small. This property allowed us to detail how small structural changes in the guest molecules can have a large impact on the observed photophysics, and insight into the effect of structure on the dynamics of these CD complexes.

The complexation dynamics of triplet xanthone with CDs has been well established.[29,30,49,59] Recently, the exit and entry rate constants have been reported for the triplet states of 1- and 2-naphthyl-1-ethanols (1- and 2-NpOH) with β-CD.[50] Comparing the entry and exit rate constants for these probes with β-CD we find that although the entry rate constants are within experimental error of each other, the exit rate constants are quite different. For the NpOHs, the exit rate constant for 2-NpOH from β-CD is ca. three times slower than the exit of the 1-NpOH. This difference in the exit rate constants was suggested to be a result of the differences in the structure of the host-guest complexes. It was proposed that the slower exit of 2-NpOH may be a reflection of a deeper inclusion into the CD cavity than the 1-NpOH that may only be interacting with the rim of the β-CD. The exit of triplet xanthone from β-CD is ca. 17 times faster than the exit of 1-NpOH from β-CD. It was suggested that the structure of the xanthone/CD complex

may also be responsible for the fast exit. However, based on the reported photophysical studies on the complexation of xanthone with β-CD, it is unlikely that a weaker interaction, or a significant difference in the location of xanthone in the β-CD complex could be responsible for the larger exit rate constants over that of the NpOHs. In fact, the ground state equilibrium constant of xanthone with β-CD is higher than that observed for the NpOHs.[30,50]

To detail the structure-dynamics relationship, we employed ICD, and picosecond fluorescence studies. It was shown that these two techniques are far more superior than absorption, and steady-state fluorescence methods for obtaining information on the complexation of probes with CDs. From the ICD, and picosecond fluorescence studies we observed very different photophysics for fluorenone, and xanthone when complexed with CDs. Namely, the observation that 2:1 host-guest complexes were observed for fluorenone with α-CD, but not for xanthone. It was suggested from theoretical calculations, that the reasoning lies with the deeper inclusion of xanthone into α-CD than fluorenone, which is more exposed to the aqueous phase, and more susceptible to binding with a second α-CD. This difference for the formation of higher ordered complexes will affect the dynamics of the guest from the CD. The exit rate constant of guest from a 2:1 host-guest complex is expected to be slower than that of a 1:1 host-guest complex. The difference in dynamics for higher ordered complexes was observed for the exit rate constant of 2-NpOH from a 2:2 host-guest complex with β-CD.[50] To better understand the reasons for the differences in complexation and dynamics of host-guest complexes with CDs more examples will have to be investigated. In addition, these investigations will have to include more detailed studies into the structure of these complexes. We have shown that ICD, time-resolved fluorescence studies and calculations of host-guest complexes provide useful tools for understanding the structural intricacies that are responsible for significant changes in the photophysics, and ultimately, the complexation dynamics of host-guest systems.

5. THE COMPLEXATION OF STYRENES AND THEIR RADICAL CATION DYNAMICS WITH CYCLODEXTRINS - RESULTS AND DISCUSSION

5.1 Structure and Derivatives

The two styrene derivatives that were chosen for this study are the 4-methoxystyrene, which is commonly called 4-vinylanisole (4-VA) and the β-methyl-4-methoxystyrene, which is also referred to as *trans*-anethole (t-Ane) (Scheme 5.1). These molecules are the precursors to the radical cations we have investigated.

5.2 Photogeneration of Radical Cations

The radical cations of styrenes are generated when the precursor styrenes are photoexcited with a laser.[34-37] From laser power dependence studies the formation of the radical cations occurs via a biphotonic mechanism whereby the first photon generates an excited state and the second photon causes the ejection of an electron from the excited state molecule (Scheme 5.1). In our investigations we generate the radical cations with the use of an Excimer laser at 308 nm.

5.3 Complexation of t-Ane and 4-VA to α- and β-Cyclodextrin

5.3.1 Ground state Absorption

The absorption spectra of both the styrenes are similar. Their absorption spectra are broad and the maxima are at approximately 260 nm. In the presence of α- and β-CD the

Scheme 5.1

4-VA   R = H
t-Ane   R = CH$_3$
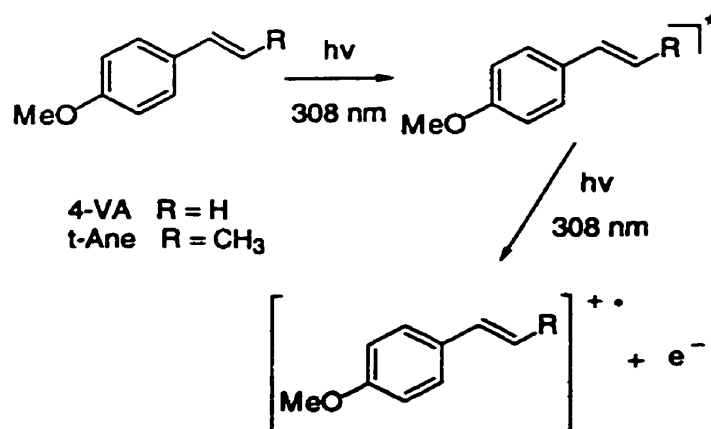
absorption spectra of the styrenes were not significantly different, although there was a slight increase in the total absorption in the region below ca. 350 nm that was due to absorption of the CDs. Since the changes in absorbance were small upon the addition of CD, the determination of equilibrium constants from this data was not considered reliable. In addition, if the increases observed were only due to the CD absorption then equilibrium constants can not be extrapolated from these absorbance differences.

5.3.2 Steady-State Fluorescence

4-VA and t-Ane were fluorescent. Both 4-VA and t-Ane in water had broad fluorescence spectra with similar maxima at ca. 323 nm. Upon the addition of α-, or β-CD to these styrenes the fluorescence intensity increased, but to different extents. 4-VA in the presence of α-CD exhibited a slight sharpening of the emission band and a very small shift of ca. 5 nm of the maximum to longer wavelengths. The fluorescence intensity increases by ca. six fold upon going from 0 to 30 mM α-CD (Figure 5.1).
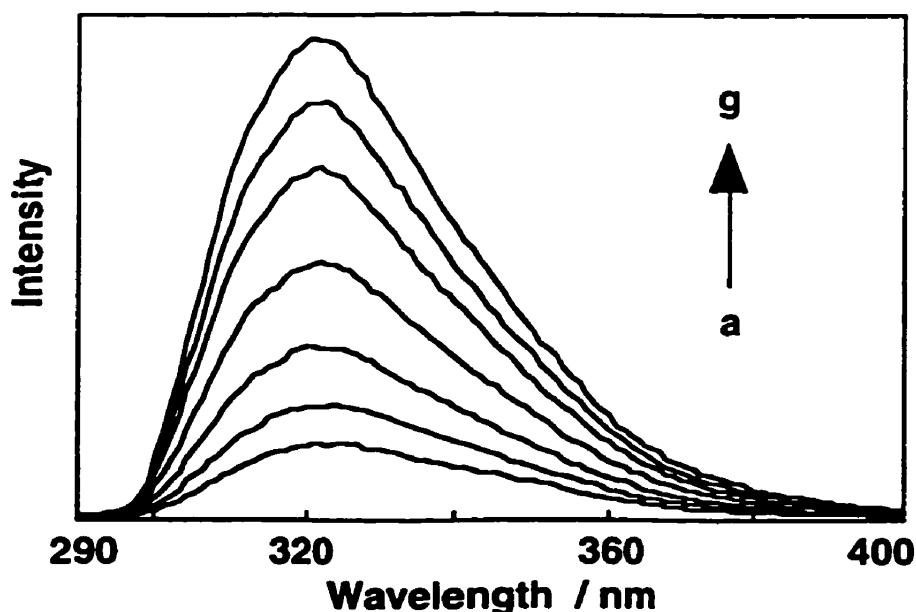
Figure 5.1 Corrected fluorescence spectra of 4-VA in the presence of different α-CD concentrations (mM): (a) 0, (b) 0.75, (c) 1.5, (d) 2.5, (e) 5, (f) 7.5, and (g) 30.

In the presence of β-CD, the fluorescence spectra of 4-VA also experiences a sharpening of the fluorescence band and a small shift of *ca.* 5 nm to longer wavelength. The fluorescence intensity of 4-VA increases by a factor of *ca.* three fold upon going from 0 to 10 mM β-CD (Figure 5.2). The fluorescence of t-Ane in the presence of α-CD also increased *ca.* two fold (Figure 5.3). In this case, there was a slight sharpening of the fluorescence band and a shift in the fluorescence maximum of *ca.* 5 nm to shorter wavelengths. For t-Ane, when β-CD was added there was very little change in the fluorescence intensity. The t-Ane fluorescence intensity was only *ca.* 10% higher in the presence of 10 mM β-CD and no apparent shift or sharpening of the spectrum was observed. This result indicates t-Ane may not be complexed very efficiently to β-CD, or that the quantum yields for fluorescence for t-Ane in the presence and absence of β-CD were very similar.
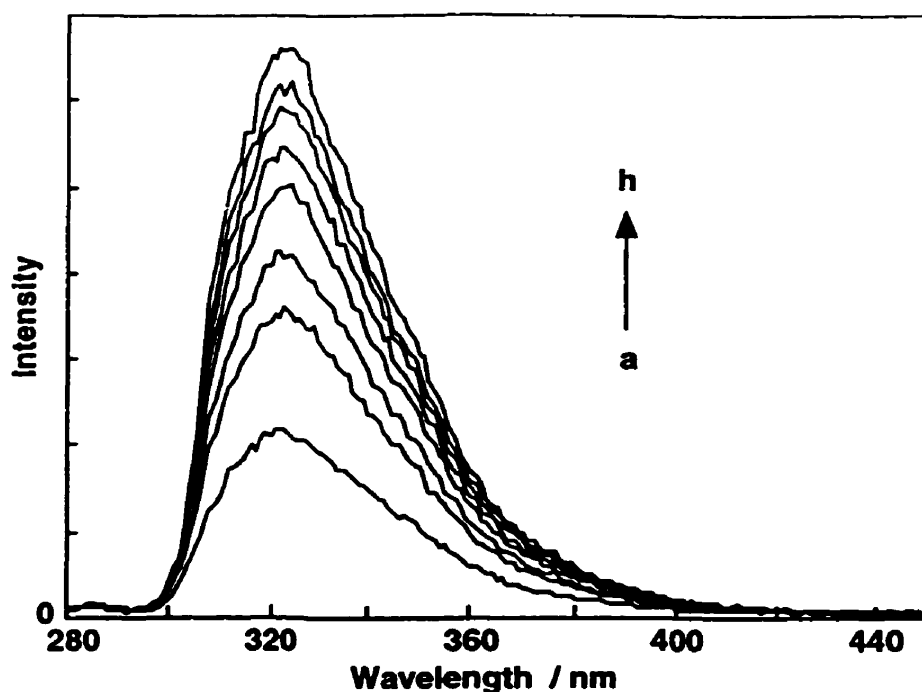
Figure 5.2 Corrected fluorescence spectra of 4-VA in the presence of different β-CD
concentrations (mM): (a) 0, (b) 0.5, (c) 1, (d) 2, (e) 3, (f) 4, (g) 6 and (h) 8.

From the fluorescence experiments, where the changes in the fluorescence intensity

were large upon the addition of CD, equilibrium constants were determined from nonlinear

fits using Equation 1.22, where both a 1:1 and a 2:1 complexation stoichiometries were

assumed (Figure 5.4). In the complexation studies for both 4-VA and t-Ane with α-CD,

the double reciprocal plots were not linear when either 1:1, or 2:1 host-guest

stoichiometries were assumed (Figure 5.5). This suggests that both 1:1 and 2:1 CD

complexes were present in solution. The recovered values for K_1 and K_2 were 110 ± 30 M^{-1} and 1500 ± 700 M^{-1} for 4-VA and 400 ± 30 M^{-1} and 1800 ± 700 M^{-1} for t-Ane,

respectively, using Equation 1.22. These values correspond to average of two experiments

and the errors quoted correspond to average deviations. The statistical errors obtained from

the fits of the experimental data to Equation 1.22 were of the same order of magnitude as
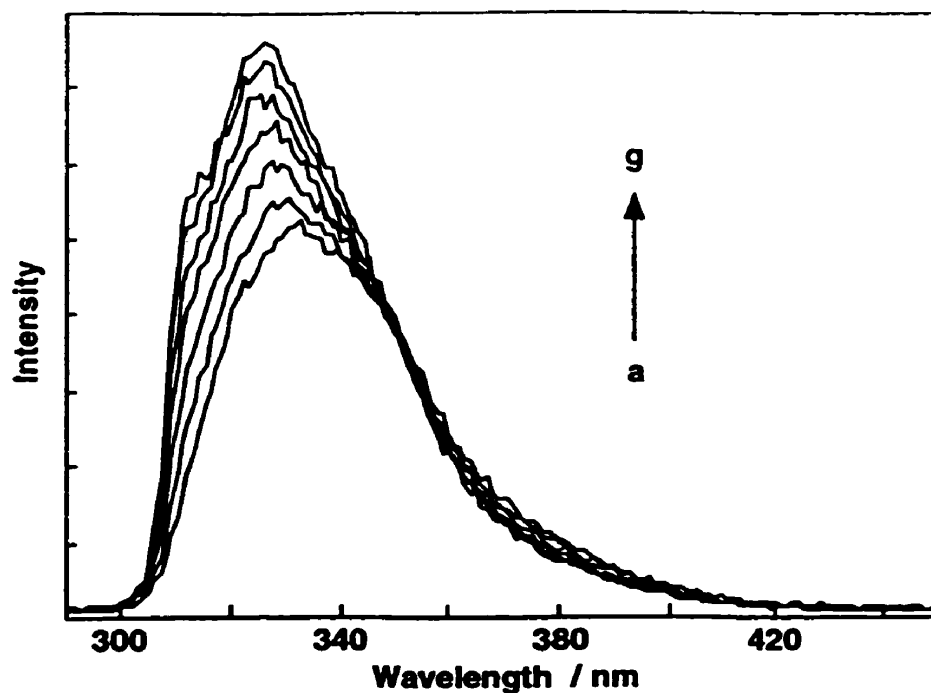
Figure 5.3 Corrected fluorescence spectra of t-Ane in the presence of different α-CD concentrations (mM): (a) 0, (b) 0.5, (c) 1, (d) 2, (e) 3, (f) 12, and (g) 30.

the average deviations. As shown, the errors in these recovered values were large. This is often the case when multiple equilibria are occurring for the CD complexes and when the equilibrium constants themselves are similar. In addition, both styrenes were excited at 260 nm where CD shows a small absorbance. This absorbance should lead to an inner filter effect that causes the styrene fluorescence intensity to be artificially lowered.[64] An attempt to correct for this effect was made, but due to the uncertainty of the CD absorption at 260 nm no improvement in the quality of the fits, or for the uncertainties of the recovered equilibrium constants was observed. In addition, the values for K_1 and K_2 did not change significantly after the correction was performed.
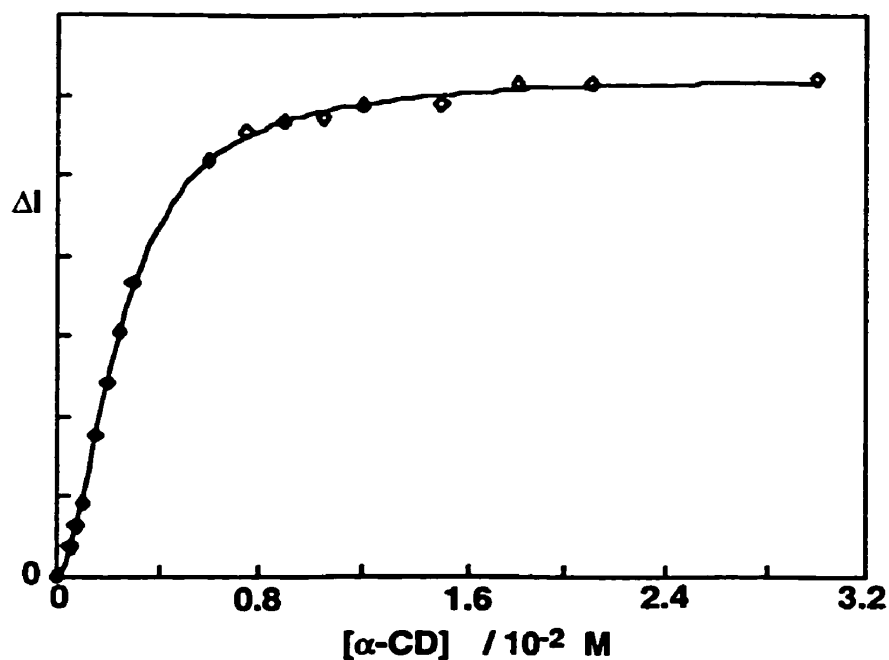
Figure 5.4 Nonlinear fit of the corrected 4-VA fluorescence intensity (323 nm) variation with the α-CD concentration. The solid line corresponds to the fit obtained from using Equation 1.22.

The changes in the fluorescence intensity for 4-VA in the presence of β-CD were fitted to Equation 1.20 for the determination of equilibrium constants assuming a 1:1 host-guest stoichiometry (Figure 5.6). Linear double-reciprocal plots support this assumption (inset of Figure 5.6). The recovered equilibrium constant for 4-VA using Equation 1.20 was $700 \pm 30\ M^{-1}$. As discussed previously, the changes in the fluorescence intensity for t-Ane in the presence of β-CD were too small for any reliable determination of equilibrium constants.
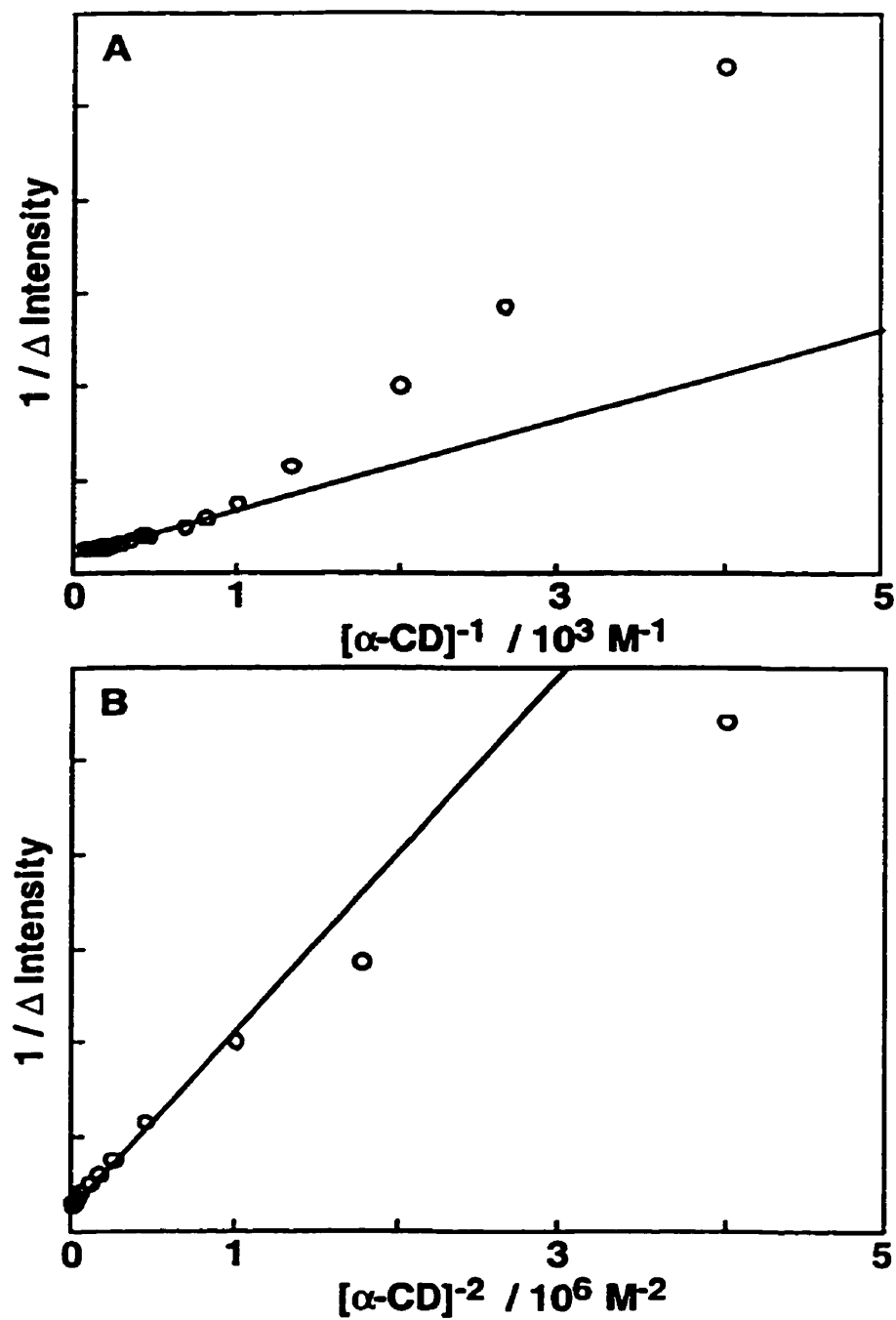
Figure 5.5 Double-reciprocal plots for the variation of the 4-VA fluorescence intensity at 323 nm in the presence of different α-CD concentrations for a 1:1 (A) and 2:1 (B) α-CD:4-VA stoichiometry.
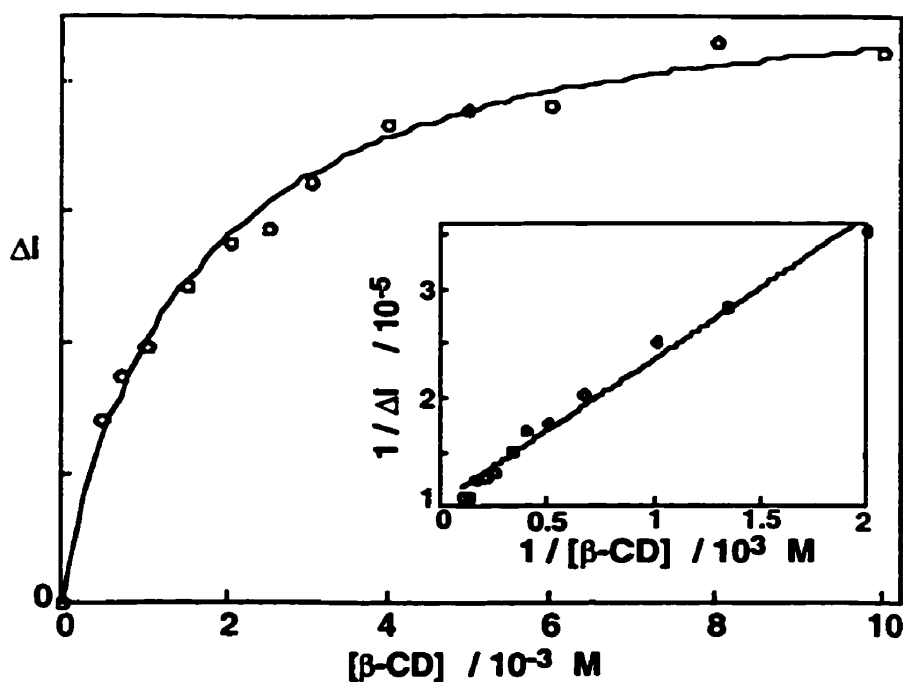
Figure 5.6 Nonlinear fit of the corrected 4-VA fluorescence intensity (324 nm)
variation with the β-CD concentration. The solid line corresponds to the fit
obtained from using Equation 1.20. The inset shows the double-reciprocal
plot for the same data.

5.3.3 Induced Circular Dichroism

ICD spectra were measured for t-Ane and 4-VA in the presence of α- and β-CD.

This method provided additional support for the complexation of these probes to CDs. 4-

VA in the presence of α- and β-CD did not show strong ICD signals in the spectral region

measured. A weak signal with a low signal to noise ratio was observed in the 300 nm

region. However, in the case of t-Ane strong ICD signals were detected for both α- and β-

CD (Figure 5.7). In the presence of β-CD a positive signal at *ca.* 308 nm and a negative

signal at *ca.* 304 nm were observed. The positive signal observed at *ca.* 307 nm in the

presence of α-CD was less intense; however, a negative signal observed at *ca.* 303 nm was

of comparable magnitude as that shown in the presence of β-CD. These results confirm that t-Ane forms complexes with both CDs.
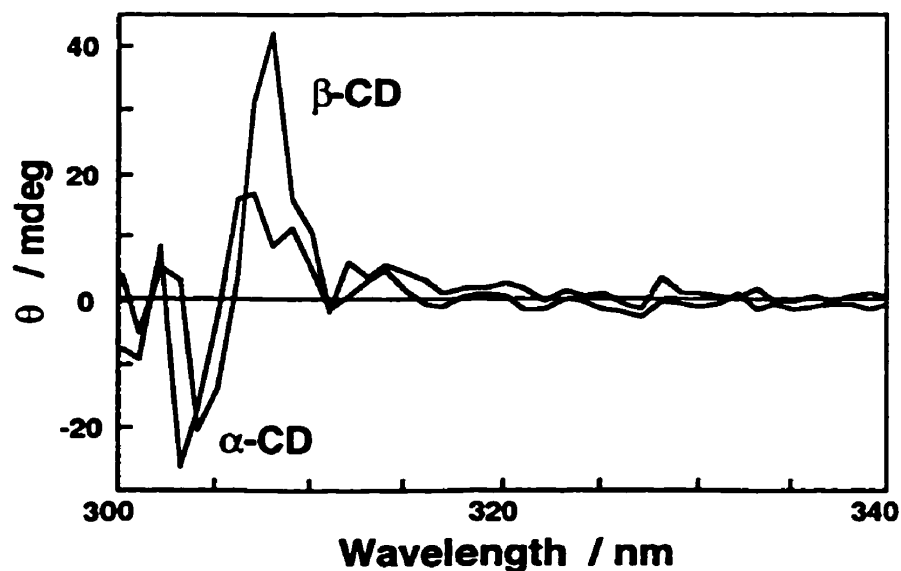
Figure 5.7 Corrected ICD spectra of t-Ane in the presence of 8 mM β-CD and 30 mM α-CD.

5.3.4 Time-Resolved Transient Absorption Spectra

The biphotonic ionization of the styrenes in aqueous solution leads to the formation of their radical cations and solvated electrons (Scheme 5.1). These radical cations show absorption in two regions, one between 320-390 nm and the other between 520-660 nm. The maxima for the absorption bands for the radical cations of 4-VA and t-Ane were observed at 360 and 380 nm, respectively. The transient absorption band at longer wavelengths for both radical cations had maxima at ca. 600 nm. These absorption spectra are similar to those previously reported in 4:1 water-acetonitrile mixtures.[34] Both of these
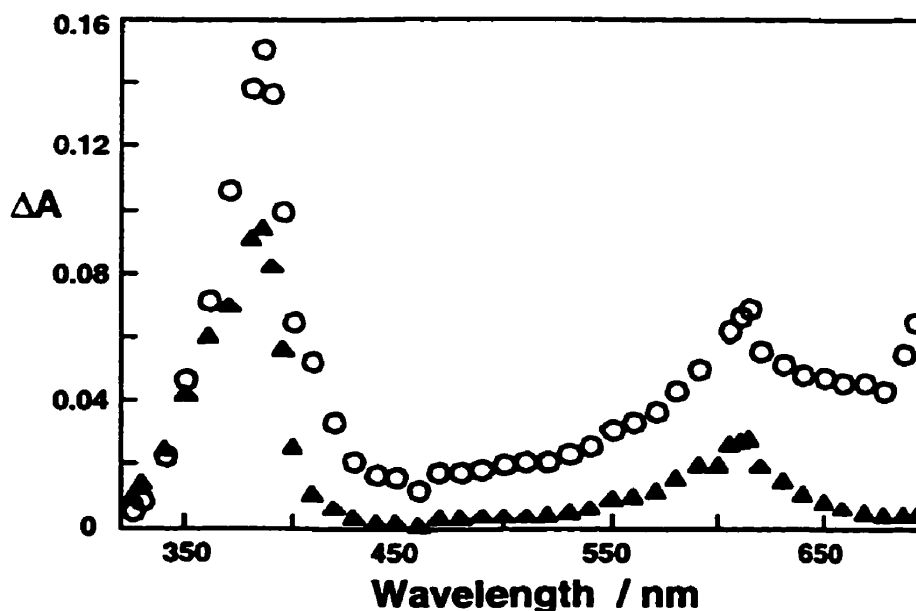
Figure 5.8 Transient absorption spectra for the photolysis of 4-VA in water at 85 ns (O) and 740 ns (▲) delays after the laser pulse.

bands were reported to be due to the same transient, since they decayed with the same transient lifetimes. Aerated solutions were used because the 4-VA and t-Ane radical cations are not significantly quenched by oxygen.[34] Upon the photogeneration of the radical cations with an Excimer laser at 308 nm, solvated electrons were formed that absorb somewhat throughout the whole spectrum with larger absorptions above 600 nm (Figure 5.8). The absorption of these solvated electrons was observed at short delays after the laser pulse, which corresponds to lifetimes in the nanosecond time domain. In aerated aqueous solutions the concentration of oxygen is low, at ca. 0.29 mM.[66] These concentrations are too low to act as efficient quenchers for the solvated electrons. Previous studies[34] were mainly carried out in water:acetonitrile mixtures, where the concentration of oxygen is higher. As a result, solvated electrons may be more efficiently quenched in water:acetonitrile mixtures than that of aqueous solutions. However, solvated electrons in

the presence of acetonitrile are known to form an equilibrium between stable monomer and dimer radical anions.[33] These radical anions have very broad and weak absorption in the transient regions investigated in previous studies and is most likely the reason for the lack of transient absorption due to solvated electrons. In our studies, the kinetics for the transient absorption of both styrenes in the 600 nm region displayed a double exponential decay. Of the two exponential decays, the longer-lived decay was assigned to the decay of the radical cations. The lifetimes for the radical cations of 4-VA and t-Ane were *ca.* 2 and *ca.* 20 μs, respectively. The fast decay in each of the kinetic traces was assigned to the decay of the solvated electron. This decay had lifetimes of *ca.* 230-250 ns. To avoid the detection of solvated electrons, the solutions were purged with nitrous oxide (N_2O). N_2O is known to efficiently trap solvated electrons with a rate constant of $(9.1\pm0.2) \times 10^9$ $M^{-1}s^{-1}$.[74] Solvated electrons were generated independently in the photolysis of $K_4Fe(CN)_6$ in nitrogen purged solutions.[75] The lifetime of the solvated electron when $K_4Fe(CN)_6$ was excited at 308 nm was 860 ns.

The transient absorption spectra for the radical cations of t-Ane and 4-VA did not change in the presence of α-, or β-CD. However, the lifetime of the 4-VA radical cation did increase from *ca.* 2 to 8 μs in the presence of α-CD but was unchanged in the presence of β-CD. The initial yield of radical cation formation (ΔA_{max}) is proportional to the ΔA value immediately after the laser pulse. The ΔA_{max} values for the 4-VA radical cation formation were somewhat higher in the presence of both CDs than in water. In the case of t-Ane, the radical cation lifetime in the presence of both CDs were the same as those observed in aqueous solution and similar ΔA_{max} values were measured in water and in the presence of both CDs.

.

5.3.5 Quenching Experiments

The mobility of an excited state molecule between a homogeneous phase and that of

a supramolecular system can be investigated with an indirect method known as the

quenching methodology.[45] This methodology is used to determine the association and

dissociation rate constants for probe molecules with α- and β-CD. In homogeneous

solution, the kinetics of probe molecules follows Equation 1.24, and linear quenching plots

are observed. In the presence of host molecules, the quenching plots are frequently no

longer linear, but level off with increasing quencher concentrations. The leveling off

occurs because the quenching efficiency of the quencher is reduced due to the protection

provided to the complexed probe by the host molecule. At high quencher concentrations,

the decay of the excited state in the aqueous phase will be very fast, and the exit of the

excited state from the host molecule will be rate limiting.

In the study of the complexation dynamics of radical cations with α- and β-CD, the

quenching methodology was employed to determine the entry and exit rate constants for

radical cations with CDs. The direct spectroscopic methodology[45] was not employed

because no significant changes were observed for the transient absorption spectra of the

styrene radical cations in the absence and presence of the CDs. Three different quenchers

were used to study the mobility of these radical cations. Iodide, in the form of

tetrabutylammonium iodide (TBAI), sodium azide (NaN_3), and sodium cyanide (NaCN)

were chosen as quenchers because these ions remain primarily in the aqueous phase and the

latter two and other halides, such as chloride and bromide, were previously shown to react

with styrene radical cations.[34] All the quenching experiments were performed in the

presence of N_2O so as to avoid interference from the absorption due to solvated electrons

and all decays for the radical cations followed a monoexponential function (Figure 5.9) for

all the quencher concentrations employed. Quenching plots, employing Equation 1.24,

were observed to be linear (Figure 5.10). A summary of the recovered quenching rate
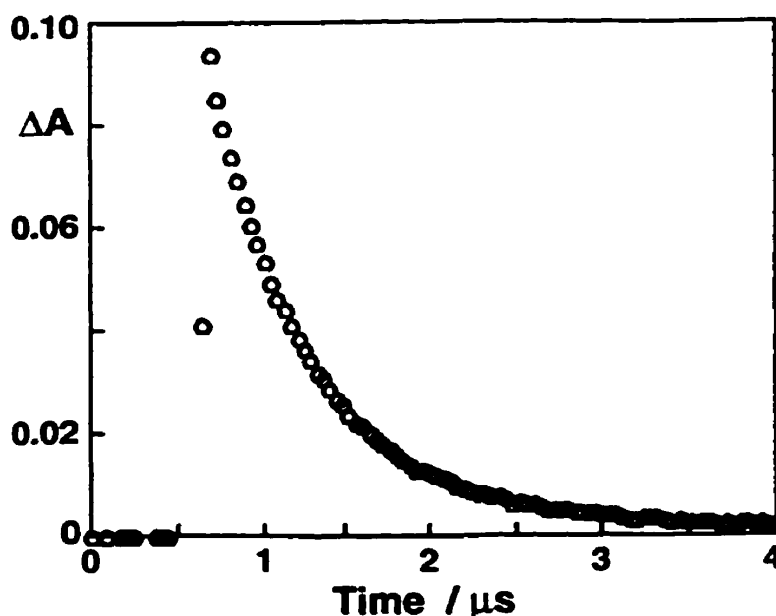
Figure 5.9 Decay of the radical cation of 4-VA in water purged with N$_2$O. The kinetic trace was monitored at 600 nm.

constants (k$_q$) for iodide and cyanide in the presence of various CD concentrations for the radical cations are tabulated (Table 5.1). When quenching experiments were carried out in the presence of CD a downward curvature was expected because a large fraction of the styrenes were complexed at high CD concentrations, and most of the radical cations should be generated within the CD cavities. However, for the radical cations in the presence of CDs only linear quenching plots were observed for all the quenchers employed in the presence of different CD concentrations. The decays were always monoexponential in the presence of CD. In the case of 4-VA, a decrease in the quenching rate constant was observed in the presence of 30 mM α-CD, whereas in the presence of 8 mM β-CD no decrease was observed. A more detailed investigation was performed on the effect of CD concentration on the quenching rate constant for t-Ane. The quenching rate constants for t-Ane in the presence of a variety of β-CD concentrations were within experimental error of the rate constants measured for t-Ane in aqueous solution. The same result was observed
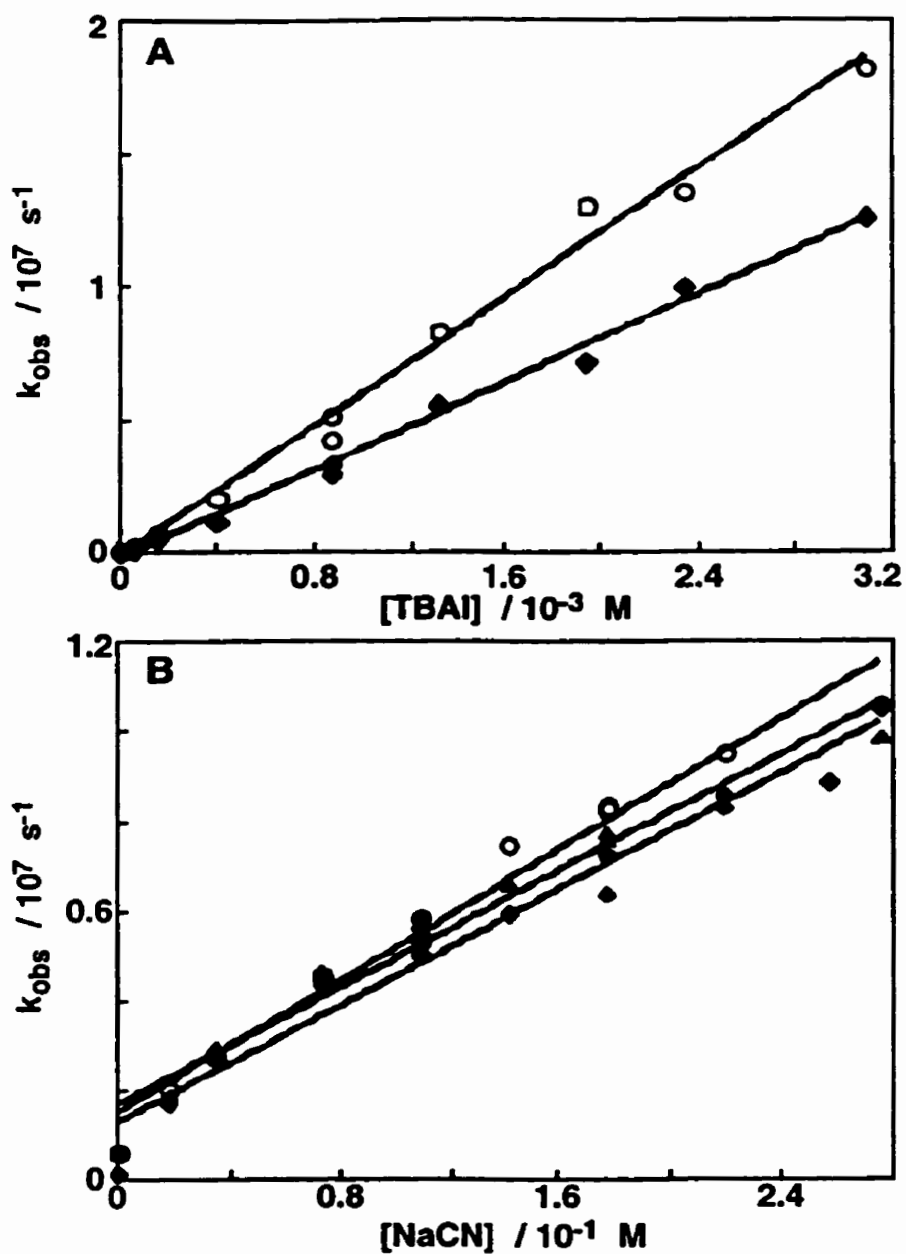
Figure 5.10 (a) Iodide quenching plots observed at 600 nm for t-Ane radical cation in the absence (O) and presence (♦) of 30 mM α-CD. (b) Cyanide quenching plots for the 4-VA radical cation in the absence (O) and presence (♦) of 30 mM α-CD and (▲) 10 mM β-CD.

Table 5.1   Quenching rate constants determined from the slope of the quenching plots
for the 4-VA and t-Ane radical cations by iodide and cyanide.[a]

Styrene	[CD] / mM	k_q / 10^9 $M^{-1}s^{-1}$	k_q / 10^9 $M^{-1}s^{-1}$
		I^-	CN^-
t-Ane	no CD	7.3 ± 1.1 (6)	–
	α-CD / 10	8.2 ± 0.6 (1)	–
	α-CD / 30	3.5 ± 0.6 (2)	–
	β-CD / 8	9.6 ± 0.4 (1)	–
4-VA	no CD	18.0 ± 2.0 (2)	3.6 ± 0.05 (2)
	α-CD / 5	–	4.0 ± 0.3 (1)
	α-CD / 30	14.0 ± 0.4 (3)	3.5 ± 0.3 (2)
	β-CD / 8	17.0 ± 0.3 (1)	–
	β-CD / 10	–	3.3 ± 0.2 (1)

(a) Errors correspond to standard deviations for experiments performed more than twice
and to average deviations for experiments performed twice. For experiments performed
once the errors correspond to the statistical deviations for the linear fit of the quenching
data. The numbers in parenthesis correspond to the number of independent experiments
performed.

for t-Ane in the presence of the low concentrations of α-CD, but a significant lowering of

the quenching rate constants were observed for the higher α-CD concentrations. In the

case of azide, the quenching rate constants for 4-VA and t-Ane in water were (1.06 ± 0.02)

$\times 10^{10}$ M^{-1} s^{-1} and $(6.10 \pm 0.05) \times 10^9$ M^{-1} s^{-1}, respectively, and were of the same order of

magnitude as observed for iodide. No change in the slope of the quenching plots with azide was observed for both styrenes in the presence of 30 mM α-CD when compared to the plots in water. The quenching of the 4-VA radical cation by cyanide was three orders of magnitude less efficient than the quenching by iodide and azide. Cyanide quenching was performed for the 4-VA radical cation in the presence of α- and β-CD, but no differences in the quenching rate constants were observed from those determined in aqueous solution. The quenching plots were not as linear (r = 0.983 - 0.986) as observed in the case of iodide, or azide because at the high cyanide concentrations used the magnitude of the radical cation signal decreased due to the absorption of laser light by the quencher. Therefore, as the signal to noise ratio decreased the precision in the lifetime measurements decreased. The quenching of t-Ane by cyanide was not studied because for this radical cation the quenching efficiency was smaller than that for 4-VA. As a result only an estimate of the quenching rate constant was obtained ($<< 5 \times 10^6$ M^{-1} s^{-1}).

The quenching of the t-Ane and 4-VA radical cations by TBAI was also studied in aqueous and α-CD solutions in the presence of alcohols. All decays followed a monoexponential function and the quenching plots were linear. For both 4-VA and t-Ane in aqueous solution, the quenching rate constants in the presence of the alcohols were the same as those observed in the absence of the alcohols (Table 5.2). For 4-VA in the presence of 30 mM α-CD and 1- and 2-butanol the same quenching rate constants were observed as in the absence of the alcohols. However, in the case of 1-pentanol a slight increase in the quenching rate constant was observed for 4-VA in the presence of 30 mM α-CD. In the case of t-Ane in the presence of 30 mM α-CD, the quenching rate constants in the presence of 1-butanol and 1-pentanol were slightly higher than was observed in the absence of the alcohols. Equilibrium constants for the complexation of the styrene precursors to CDs in the presence of alcohols were not determined since no alcohol effect was observed from the quenching studies. However, equilibrium constants for the complexation of xanthone to γ-CD have been shown to increase in the presence of

alcohols.[31] As discussed earlier, the exit rate constant of triplet xanthone from β- and γ-CD significantly decreases in the presence of alcohols by at least a factor of five than that in the absence of the alcohols.[31] It was suggested that preferential solvation of the alcohols at the rim of the CD cavities could create a barrier for the exit of the triplet xanthone from the CDs. As a result, a decrease in the dissociation rate constants would be observed.

Table 5.2 Quenching rate constants by iodide for t-Ane and 4-VA in aqueous and α-CD solutions in the presence of alcohols.

Alcohol	$k_q / 10^9 \, M^{-1}s^{-1}$			
	0 mM α-CD		30 mM α-CD	
(1% v/v)	4-VA	t-Ane	4-VA	t-Ane
No Alcohol[a]	18.0 ± 2.0 (2)	7.3 ± 1.1 (6)	14.0 ± 0.4 (3)	3.5 ± 0.6 (2)
1-Butanol[b]	17.6 ± 0.3	8.1 ± 0.2	14.3 ± 0.4	5.9 ± 0.2
2-Butanol[b]	17.7 ± 0.4	—	13.9 ± 0.2	—
1-Pentanol[b]	16.2 ± 0.3	8.3 ± 0.2	15.6 ± 0.2	6.0 ± 0.3

(a) Errors correspond to standard deviations for the experiments performed more than twice. The numbers in parenthesis corresponds to the number of independent experiments performed. (b) Errors correspond to the statistical deviations for the linear fit of the quenching data from one experiment.

5.3.6 Quantum Yield Experiments

One possible reason for the absence of a downward curvature in the quenching plots for the radical cations in the presence of CDs is that the radical cations generated within the CD cavity may be reacting with the CD immediately and can not exit from the CD into the aqueous phase. To test this hypothesis, the relative quantum yields for the

formation of the radical cations and the solvated electrons were determined for the radical cations in aqueous and CD solutions. For the determination of the radical cation to solvated electron ratio for the styrenes, the transient absorption of the styrenes were measured. The radical cations absorb in the ultraviolet and visible regions, however, the ultraviolet region also contains absorption due to photoproducts generated as a result of the photoionization process. Therefore, the absorptions of the radical cations were measured at 600 nm, where there was no contribution from photoproducts. The solvated electrons absorb throughout the ultraviolet and visible regions, including the 600 nm region, but the absorption is strongest at ca. 700 nm,[75] where there is no contribution from the absorbance of the radical cations. This was confirmed from transient absorption spectra measured in the presence of nitrous oxide. As mentioned earlier, nitrous oxide is known to efficiently trap solvated electrons.[74] The relative yield of radical cation formation was measured at 600 nm, where there were contributions from radical cations, and solvated electrons in the absorbance value observed. An internal standard was employed in order to separate the contributions for each species from the total absorbance at 600 nm. The internal standard used was the absorption of the solvated electrons at 700 nm. Independently, the transient absorption spectra for solvated electrons generated in the photolysis of $K_4Fe(CN)_6$ were measured (Figure 5.11 (A)). From these experiments, the ratio of the solvated electron absorption at 600 and 700 nm ($\Delta A_{600}/\Delta A_{700}$) was determined to be 0.637 ± 0.004 (three experiments). By employing the ratio for the solvated electron absorption at 600 and 700 nm and the measured absorbance for the solvated electron at 700 nm, the contribution of the solvated electron absorption at 600 nm was calculated for the transient absorption spectrum of a radical cation (Figure 5.11 (B)). Consequently, the absorbance at 600 nm for the solvated electron was subtracted from the total absorbance, which equals the absorbance due to the radical cation. From these two absorbance values the ratio of radical cation to solvated electron was determined.

Equation 5.1

$$\frac{\phi_{RC}}{\phi_e} = \frac{(\Delta A_{600} - 0.637 \Delta A_{700})}{\Delta A_{700}} \frac{\varepsilon_e(700)}{\varepsilon_{RC}(600)}$$

Included in this ratio is the dependence of the yields on the molar absorptivities for both species (Equation 5.1). This treatment was performed since only in the case of the t-Ane radical cation is the molar absorptivity known and reported to be $10,960 \ cm^{-1}$ in acetonitrile at 600 nm.[76] For the 4-VA radical cation the value for the molar absorptivity is not known. In water the molar absorptivity for solvated electrons has been reported to be $19,000 \ cm^{-1}$ at 720 nm.[75] In addition, the values for the molar absorptivities of the radical cations were not expected to change with the complexation to CDs since no shifts in the transient absorption spectra were observed in the presence of the CDs. For this reason, the ratio of ε values were assumed to be constant and thus the ratio of relative yields was proportional to the absorbances of the radical cations measured at 600 nm and the solvated electron absorbance at 700 nm.

The measured ratios for the quantum yields of radical cation to solvated electron formation in water were 0.66 ± 0.22 (six experiments) and 0.46 ± 0.11 (thirteen experiments) for the radical cations of t-Ane and 4-VA, respectively. The difference in these values is due to the different molar absorptivities of the radical cations at 600 nm. If the reported molar absorptivities for the t-Ane radical cation and the solvated electron are employed in Equation 5.1 then the ratio for the quantum yields of the t-Ane radical cation to solvated electron becomes ca. 1.1. This is in agreement with the assumption that upon the formation of one radical cation, one solvated electron is also formed. In each experiment, a smaller radical cation to solvated electron ratio was always observed for the radical cations generated in the presence of CD than in aqueous solution. However, the absolute values for the ratio of radical cation to solvated electron yield between experiments on different days varied considerably for the samples containing CDs. Therefore, the errors for the
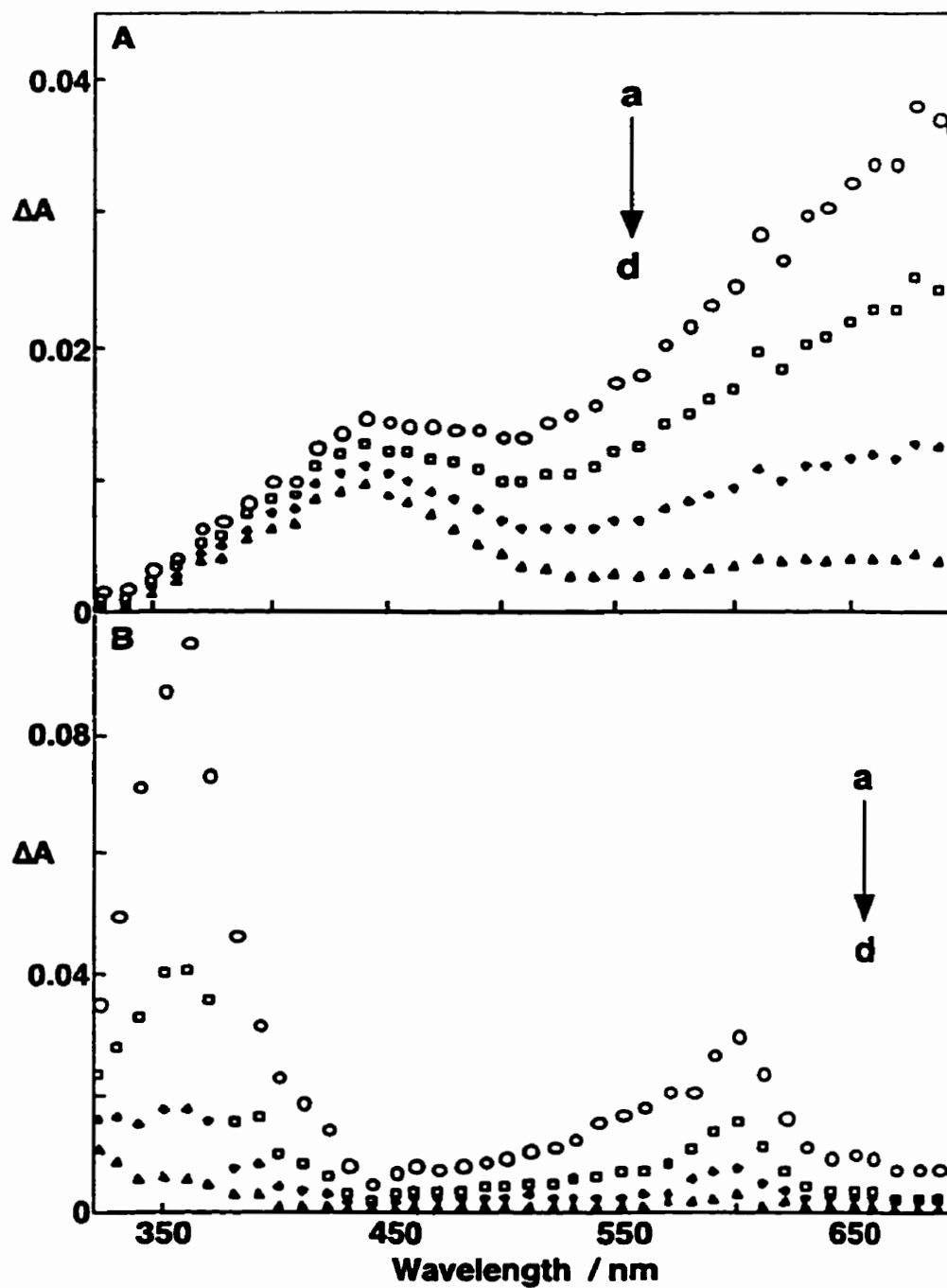
Figure 5.11 Transient absorption spectra for the photolysis of a $K_4Fe[CN]_6 \cdot 3H_2O$ deaerated aqueous solution ((A), with delays of 400 ns (a), 1.5 μs (b), 3.0 μs (c) and 4.5 μs (d) after the laser pulse) and an aerated solution of 4-VA in the presence of 30 mM α-CD ((B), with delays of 2 (a), 6 (b), 13 (c), and 18 μs (d) after the laser pulse).

averaged values are quite large. Nonetheless, it was apparent that the ratio did decrease for both styrene radical cations as the concentration of α-CD was increased (Table 5.3). The effect of β-CD on the ratios was not as large as observed in the case of α-CD.

Table 5.3 Ratio for the relative yield of radical cation and solvated electron formation in the absence and presence of α- and β-CD.[a]

[CD] / mM	ϕ_{RC} / ϕ_e	
	t-Ane	**4-VA**
No CD	0.66 ± 0.22 (6)	0.46 ± 0.11 (13)
α-CD / 0.5	0.55 ± 0.01 (2)	–
α-CD / 1	0.49 ± 0.07 (4)	0.40 ± 0.01 (2)
α-CD / 5	0.47 ± 0.12 (4)	0.33 ± 0.01 (2)
α-CD /10	0.42 ± 0.15 (4)	0.25 ± 0.08 (7)
α-CD /20	0.45 ± 0.12 (4)	0.26 ± 0.06 (4)
α-CD /30	0.35 ± 0.14 (6)	0.33 ± 0.15 (13)
β-CD /2	0.50 ± 0.02 (2)	0.61 ± 0.04 (2)
β-CD / 8	0.45 ± 0.14 (2)	0.52 ± 0.08 (2)

(a) Errors correspond to standard deviations for experiments performed more than twice and to average deviations for experiments performed twice. The numbers in parenthesis correspond to the number of independent experiments performed.

5.4 Discussion

In the study of the complexation of styrene derivatives to CDs two different aspects were examined. The first objective was to investigate the dynamics of the radical cations photogenerated from the precursor styrenes in the presence of CDs. The complexation dynamics of other probes with CDs were first studied using temperature-jump and ultrasonic relaxation methods.[43,46,47] From these studies, it was established that the exit and entry rate constants for molecules in their ground state are not reflected in their equilibrium constants. Furthermore, it has been established that the determination of entry, and exit rate constants for excited state molecules can not be extrapolated from ground state equilibrium constants.[30,49] Other studies investigating the dynamics of guest molecules within CDs have also been reported to achieve a better understanding into the dynamics of these host-guest systems.[45,48,50,60] This understanding of the dynamics associated with host-guest systems will make CDs more useful in such applications as catalysis, drug delivery, and chromatography.[39,40]

The second objective in this study was to establish whether, or not the presence of alcohols affects the complexation dynamics of radical cations with CDs. Recently, it was shown that the exit rate constant of triplet xanthone from β-and γ-CD significantly decreases in the presence of alcohols.[31] It was suggested that in the presence of alcohols, these co-solvents could be solvating preferentially the entrances of the CD cavities. As a result of this preferential solvation, a barrier for the exit of the triplet xanthone from the CDs to the aqueous phase could be created. Thus, a decrease in the dissociation rate constants would be expected. Studies into the effect of alcohols on the complexation dynamics of additional CD host-guest systems could have important implications for general applications of CDs in drug delivery, and separation technology. Alcohols are known to act as nucleophiles with radical cations.[34] Thus, if preferential solvation is

involved in the mechanism for the dissociation of guest molecules from CDs, then we should expect to observe an effect from the interaction of styrene radical cations with the alcohols as they exit the preferentially solvated CD cavities.

5.4.1 Ground State Complexation Efficiency

Before the dynamics of the styrene radical cation complexation can be investigated, the complexation efficiencies of the precursor styrenes with α- and β-CD have to be determined. Fluorescence spectroscopy was employed to determine the complexation efficiencies of the styrenes to the CDs. Increases in both the fluorescence of t-Ane and 4-VA were observed in the presence of α-CD, which indicates that the styrenes have formed complexes with the CD. Accompanied with the increase in intensity was a sharpening of the fluorescence band and small shift of the emission maximum to shorter wavelengths. These spectral changes are also indicative of CD complexation. In the presence of β-CD, 4-VA exhibited large increases in fluorescence intensity with a sharpening of the fluorescence band and a shift of the fluorescence maximum to shorter wavelengths. In the case of t-Ane, only very small changes in the fluorescence intensity were observed. This may suggest that complexation with β-CD is inefficient, but it may also indicate that the fluorescence quantum yield for t-Ane is similar in water and in the complex with β-CD.

Induced circular dichroism (ICD) was also employed to provide additional information on the complexation of the styrenes to both CDs. ICD was very helpful in supporting the assignment for the complexation of t-Ane to β-CD, since complexation for t-Ane and β-CD could not be confirmed from the fluorescence studies. ICD signals were observed for t-Ane in the presence of β-CD. This indicates that the achiral t-Ane molecules are interacting with the chiral environment of the CD cavity, which suggests the complexation of t-Ane to β-CD. ICD signals were also observed for t-Ane in the presence of α-CD.

From the fluorescence spectra obtained for the styrenes with α- and β-CD both the host-guest stoichiometries and the equilibrium constants for the different stoichiometries were determined. The host-guest stoichiometries were confirmed from the double reciprocal plots for the inverse of the change in fluorescence intensity against the inverse of the CD concentration. The double reciprocal plots for t-Ane and 4-VA in the presence of α-CD showed that both 1:1 and 2:1 host-guest stoichiometries were present. The formation of complexes with stoichiometries higher than 1:1 is not unusual and has been observed for a number of guest molecules.[42-44] The introduction of a second CD is often observed when the guest molecule is not completely included in the first CD. In effect the second CD caps the exposed portion of the guest molecule not included by the first CD. The formation of a 2:1 complex provides better protection of the guest molecule from the aqueous environment. This often leads to an increase in the fluorescence quantum yield and lifetime of the guest molecule. For example, guest molecules that do not fluoresce in an aqueous environment, such as fluorenone, show fluorescence when complexed to two molecules of α-CD (Section 4.2). In addition, in the complexation of pyrene to β-CD it was observed that the fluorescence lifetime of the 1:1 complex was similar to that measured in water, whereas a significant lengthening of the lifetime was measured for 2:1 complex.[77] The observation of higher order complexes in the case of the styrenes with α-CD suggests that in the 1:1 host-guest complex the styrene molecule is not completely included into the α-CD cavity and that part of the styrene molecule is exposed to the aqueous phase. Therefore, a 2:1 complex is formed that provides additional protection from the aqueous phase for the 1:1 host-guest complex with α-CD. In the case of β-CD, which has a larger cavity, a styrene molecule may include deeper into the cavity, and not provide enough of a surface for the binding of a second CD. The changes in the fluorescence intensities for the 1:1 complexes of the styrenes with β-CD were smaller than the fluorescence changes observed for the 2:1 complexes of the styrenes with α-CD. The absence of significant changes in the fluorescence intensities for styrene in the presence of β-CD shows that a 2:1

complex is not forming for this CD. However, the absence of large changes in the fluorescence intensities of the styrenes in the presence of β-CD may also indicate that the fluorescence quantum yields for the styrenes in water, and complexed in the 1:1 and 2:1 complexes with β-CD are similar. However, based on the fluorescence studies demonstrating the formation of 2:1 complexes of the styrenes with α-CD, it is unlikely, that similar fluorescence parameters would differ so significantly in the case for the emission of the styrenes in β-CD. In fact, the small changes in fluorescence for the styrenes in the presence of β-CD would suggest that the styrenes are somewhat exposed to water when complexed to this CD.

The equilibrium constants measured for the 2:1 complexes of both t-Ane and 4-VA with α-CD were higher than for the 1:1 complex to α-CD. Therefore, the fraction of styrene that was complexed to α-CD will be highest for the 2:1 complexes. From the equilibrium constants obtained from fluorescence studies, the fraction of styrenes bound in the different host-guest stoichiometries and in water were determined. For example, the fractions of 4-VA free in solution, involved in a 1:1 and 2:1 complex at 5 and 30 mM α-CD were 0.17, 0.10, 0.73 and 0.007, 0.022, 0.97, respectively. In the presence of β-CD, a 1:1 stoichiometry was observed for the complex with 4-VA. The fraction of 4-VA complexed to 2 and 10 mM β-CD was 0.58 and 0.88, respectively. In the case of t-Ane, only a small enhancement in fluorescence was observed in the presence of β-CD. One explanation for this could be that t-Ane was not forming complexes with β-CD. However, as discussed, circular dichroism demonstrates that t-Ane is interacting with the chiral environment of β-CD. The small enhancement in the fluorescence of t-Ane in the presence of β-CD may either be a result of the exposure of t-Ane to water and not deeply included in the β-CD cavity, or it may reflect similar fluorescence quantum yields for t-Ane in water and in a 1:1 complex with β-CD.

5.4.2 Radical Cation Lifetimes and Transient Absorption Spectra

The complexation of 4-VA to α-CD led to a increase in the lifetime of the radical cation. It has been shown on previous accounts that the radical cation of 4-VA are efficiently quenched by the precursor styrene of 4-VA. This self-quenching process results in a shortening of the radical cation lifetime in homogenous solution. The observed rate constant, assuming that no self-quenching occurs when 4-VA is complexed to CD, can be calculated using Equation 1.24, where $k_o \approx 1.25 \times 10^5 \, s^{-1}$ (the lifetime in the presence of CD), $k_q = 1.1 \times 10^9 \, M^{-1} \, s^{-1}$ in acetonitrile[34], and the [4-VA] $\approx 60 \, \mu M$. The calculated rate constant $(1.9 \times 10^5 \, s^{-1})$ is comparable to the experimentally observed rate constant $(5 \times 10^5 \, s^{-1})$. The effect that α-CD has on the radical cation lifetime can be explained by a sequestering of the 4-VA radical cation within the CD cavity from the aqueous phase. As a result, this leads to a reduction in the effective free styrene concentration in the aqueous phase, and to a smaller degree of self-quenching. In the presence of β-CD, no lengthening of the radical cation lifetime of the 4-VA was observed. From earlier discussions, this could be explained by the larger fraction of 4-VA bound in α-CD solutions when compared with the fraction bound in the presence of β-CD. As a result, a smaller fraction of 4-VA radical cation was sequestered by β-CD from the aqueous phase, and a larger effective free concentration of 4-VA would be available to the self-quenching process than was observed for 4-VA in α-CD. As a result, no reduction in the degree of self-quenching would be expected, and no increase in the radical cation lifetime would be observed. However, the fraction of 4-VA bound even at a 2 mM β-CD was greater than 50%. This suggests that there is an additional quenching mechanism responsible for the absence of an observed increase in the radical cation lifetime. One possibility is that the 1:1 host-guest complex of 4-VA and β-CD may be able to participate in the self-quenching process. This seems reasonable considering that from fluorescence studies it was suggested that the styrenes are not well protected from the aqueous phase in the presence of β-CD. In the case of t-Ane,

the reported self-quenching rate constant in acetonitrile ($< 1 \times 10^8$ M^{-1} s^{-1})[34] is much lower

than 4-VA in acetonitrile. As a result, self-quenching will be very inefficient at the t-Ane

concentrations (*ca.* 50 μM) employed in these experiments. Consequently, the

complexation of t-Ane to either CD did not affect the lifetime of the t-Ane radical cation.

The complexation of t-Ane and 4-VA to α- and β-CD did not lead to any spectral

changes in the transient absorption spectra of the respective radical cations. A change in

transient absorption spectra of the radical cations complexed to the CDs in comparison with

the radical cations in water would be expected if the complexed radical cations have

different molar absorptivities than the radical cations in water. As discussed earlier

(Section 1.3.1), the excited triplet state of xanthone is observed to have a spectral shift of

ca. 20 nm in its transient absorption spectra at short times after the laser pulse. This shift

was assigned to the relocation of xanthone from the less polar CD cavity to the more polar

aqueous phase,[29] and a result of the changes in the molar absorptivities for the different

microenvironments.

5.4.3 Radical Cation Quantum Yields

CDs are composed of glucose units and for this reason they contain alcohol

functionalities that are located at both entrances of the CD cavity. One would expect that

the radical cations would be more reactive towards the CDs than the solvent because

alcohols are better nucleophiles than water. Although the reactivity of both radical cations

towards methanol measured in acetonitrile/water mixtures is low ($<3 \times 10^4$ M^{-1} s^{-1})[34], one

can not rule out that the effective concentration at the rim of the CD is high enough for a

reaction to occur between the radical cations and the CD. As discussed, in the presence of

CDs the lifetimes of the radical cations were either unchanged, or lengthened suggesting

that the radical cations in the aqueous phase do not react to a significant extent with the

CDs. However, these lifetime measurements do not necessarily reflect the reactivity of the

radical cations when complexed to the CD cavity if such a reaction occurs during the laser pulse (*ca.* 15 ns). The absorption of solvated electrons was used as an internal standard to estimate the amount of radical cations that reacted with the CD cavities during the laser pulse. The photoionization of the styrenes leads to the formation of a radical cation and an electron. As a result, the ratio of the absorbances for the radical cations and solvated electrons at 600 nm in aqueous solution are present in a 1:1 concentration ratio of these two transients. As discussed earlier, this assumption is supported for the case of t-Ane, where the molar absorptivities for the radical cation and solvated electron are known and a ratio of *ca.* 1.1 was determined by incorporating the ε values mentioned above (Section 5.3.6) into Equation 5.1. From N_2O experiments, there was no absorption observed for the radical cations at 700 nm. Independently, the ratio of the absorption of solvated electrons at 600 and 700 nm was determined. Employing this ratio to the absorption of solvated electrons measured at 700 nm, the absorption due to solvated electrons at 600 nm in the presence of the styrene radical cations was determined, and the ratio for the relative yield of radical cation to the yield of solvated electron was calculated. Although the errors for the average of the ratios measured are high, in the presence of α-CD it was observed that the relative yield for the radical cation formation decreased with respect to the solvated electron yield. This result suggests that some of the radical cations are reacting with the CD during the laser pulse. This suggestion can only be made if one assumes that the yield of solvated electron is constant in the absence or presence of CDs. If solvated electrons were being trapped by the CD cavities, and the radical cations were not reacting with the CDs then one would observe an increase in the ratio of the quantum yields. In addition, if the solvated electron were reacting with the CDs, a decrease in the transient lifetime of the solvated electron at 700 nm would be observed in the presence of CDs. In either case, no experimental evidence was found to suggest that the yield of solvated electron or lifetime differed in the presence or absence of CDs.

.

In addition to the decrease in the ratio for radical cation formation to that of solvated electron in the presence of CD, a decrease of this ratio was observed to enhance as the α-CD concentration was increased. This suggests that the decrease in the ratios are directly related to the fraction of styrene complexed to α-CD. As discussed earlier, at α-CD concentrations greater than 4 mM, more than 75% of 4-VA was bound to α-CD either as a 1:1, or a 2:1 complex. At least 85% of bound 4-VA was in the form of a 2:1 complex at this CD concentration. As a result, a larger decrease in the ratio for the 4-VA radical cation to solvated electron would be expected at the higher concentrations of α-CD than observed at the lower concentrations of α-CD, if the radical cations were reacting with the CD. The effect of CD concentration on the decrease in the ratio of quantum yields was much less significant with increasing concentrations of β-CD. This may stem from the observation that the fraction of 4-VA complexed to β-CD was smaller than the fraction complexed to α-CD, as observed from the equilibrium constants determined from fluorescence experiments. In addition, the absence of 2:1 complex formation for 4-VA may also be responsible for the smaller decrease in the ratios upon increasing concentrations of β-CD. With an additional CD present in the 2:1 complexes of 4-VA with α-CD, it would be expected that the probability of a radical cation reacting with the CD cavity would increase by two fold. This possibility is not available for the complexes of 4-VA formed with β-CD.

It is difficult to quantify from these ratio measurements the percentage of the radical cations that react with the CDs because the errors in the ratios are large. However, a conservative estimate is that significantly less than 50% of the radical cations react with the CD during the laser pulse. This estimate is in agreement with the ΔA_{max} values measured at 600 nm. In the presence of CDs, the ΔA_{max} values did not change significantly (within 15%). However, we have shown that at α-CD concentrations greater than 4 mM, more than 75% of 4-VA was bound to α-CD. For this reason, if all the radical cations formed within the CD cavities reacted with the CD before exit into the aqueous phase then a much

more substantial decrease of the relative yield of the radical cations and of the ΔA_{max} values would have been observed. This is particularly true in the case of 4-VA in the presence of 30 mM α-CD where more than 99% of the styrene molecules are complexed, for which 98% of the bound 4-VA is in the form of a 2:1 complex. In this case if the reaction of the radical cation and the CD was occurring during the laser pulse then no signal for the radical cation should have been observed. This is clearly not the case. The same argument can be made for t-Ane because the equilibrium constants of this styrene with α-CD are higher than for 4-VA, which means the fraction of radical cation bound to the CDs will be larger. Transient absorption signals were also observed in the microsecond time domain for the radical cations in the presence of β-CD; therefore, as in all cases, only a small percentage (<< 50%) of the radical cations react with the CDs before exciting into the aqueous phase. The exit of the radical cation from the CD cavity into the aqueous phase is expected, since this relocation is probably driven by the formation of a charged guest. More specifically, the positively charged radical cation can not be efficiently solvated by the interior of the CD cavity. Therefore, as the radical cation explores the volume of the CD cavity it will get close to the rim of the CD cavity and as soon as it encounters water molecules and a more hydrophilic environment, the radical cation will exit into the aqueous phase.

5.4.4 Radical Cation Quenching Studies

The dynamics of the styrene radical cations complexed to CDs could not be determined using direct spectroscopic studies because the transient absorption spectra for the radical cations in water were the same as in the presence of the CDs. For this reason, quenching studies were performed with anions that primarily reside in the aqueous phase. Previously, anionic quenchers have been used in quenching studies with CDs.[50,60,78] In this study, iodide in the form of tetrabutylammonium iodide, as well as azide and cyanide in the form of their sodium salts were chosen as quenchers. The quenching rate constants

for t-Ane and 4-VA radical cations by these quenchers have not been previously reported in pure water. However, azide, cyanide, chloride and bromide were previously employed as nucleophiles to quench these radical cations in neat acetonitrile and 4:1 water:acetonitrile.[34] The quenching rate constants for the radical cations by iodide (Table 5.1) and azide in water were equal to, or slightly higher than the diffusional rate constant in this solvent (6.5×10^9 M^{-1} s^{-1} at 20 °C).[66] The quenching rate constant for cyanide (Table 5.1) was much less efficient, and not diffusion-controlled. However, the diffusional rate constant in water may be higher considering that additional Coulombic interactions may enhance the rate of diffusion of the anionic quenchers to the positively charged radical cations.

For the quenching methodology to become applicable, it is necessary that the quenching mechanism involves contact between the guest (radical cation) and the quencher. In these studies, all of these anions are nucleophiles and can react with the styrene radical cations through nucleophilic addition. However, electron transfer should also be considered when the quenching rate constants are higher than the diffusional limit. The reason for such a precaution is that a quenching rate constant can only be higher than the diffusional rate constant in a specific solvent if there is an additional quenching process that is of the same order of magnitude, or larger than the diffusion-controlled rate constant. These larger rate constants will only be observed if the quenching process can occur at a distance larger than that of an encounter complex. Electron transfer is such a process. It has been established that the reaction of styrene radical cations in acetonitrile with azide[79] and olefins[38] can involve electron transfer. Furthermore, in our studies electron transfer can also be involved in the quenching mechanism if the standard potential for the quencher is lower than the standard potential of the styrene radical cations. Such a case would involve a favorable, or exergonic electron transfer from the quencher to the radical cation. An example of such a reaction is the quenching of the radical cation of 4-VA by iodide. The potential (E^o) for this redox reaction (Scheme 5.2) can be calculated by subtracting the

Scheme 5.2

$$\underline{E^\bullet \ / \ V}$$

$$4\text{-VA}^{+\bullet} \ + \ e^- \ \rightleftharpoons \ 4\text{-VA} \qquad E^\bullet_1 = \ < 1.49$$

$$1/2 \ I_2 \ + \ e^- \ \rightleftharpoons \ I^- \qquad E^\bullet_2 = 1.2$$

$$4\text{-VA}^{+\bullet} \ + \ I^- \ \rightleftharpoons \ 4\text{-VA} \ + \ 1/2 \ I_2$$

$$E^\bullet \ = \ E^\bullet_1 \ - \ E^\bullet_2 \ = \ < 0.29$$
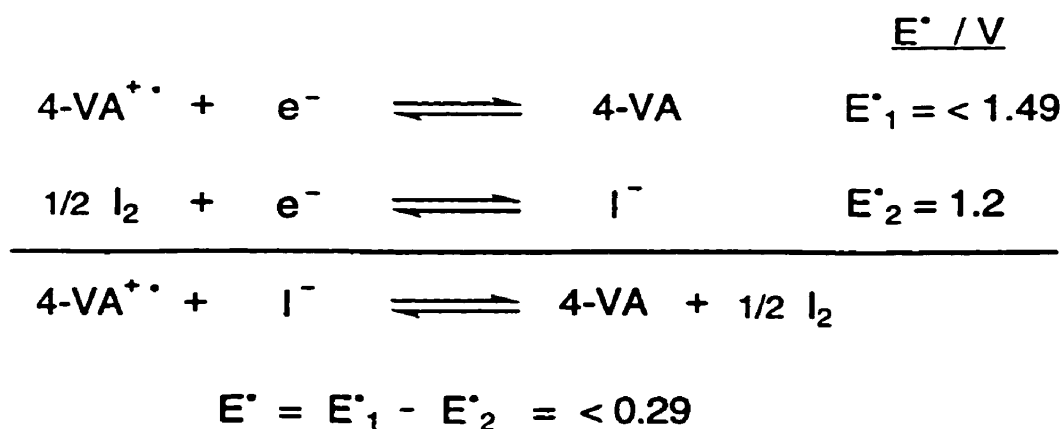
oxidation potential of the iodide (E_2°) from the reduction potential of the radical cation (E_1°). In acetonitrile, the half-wave standard potentials versus the saturated calomel electrode (SCE) for the t-Ane and 4-VA radical cations are 1.39 and 1.49 V, respectively.[38] In water, the standard reduction potentials for the styrene radical cations will decrease because the radical cations are stabilized in water. Hence, the standard potentials reported in acetonitrile can be considered as the upper limits for the standard potentials in water. The standard potential versus the SCE for iodide, azide and cyanide in acetonitrile are 0.9, 1.2, and 1.3 V, respectively.[80] In water, the standard potentials versus the SCE for the quenchers increase to 1.2, 1.6, and 1.7 V for iodide, azide and cyanide, respectively.[80] From these standard potentials, the net potential for the redox reaction can be determined. In our example, the standard potential of the 4-VA radical cation in water versus the SCE is given as < 1.49 V. Under the same conditions, the standard potential for iodide is given as 1.2 V.[80] In this redox reaction (Scheme 5.2), the reduction is occurring with the radical cation of the 4-VA accepting an electron to return to the neutral styrene precursor. The oxidation occurs as the iodide gives up an electron to the radical cation and as a result becomes neutral iodine. For the oxidation, the sign of the standard potential is reversed before the potentials of each half reaction are added. The net result is a positive standard

potential of < 0.29 V. Equation 5.2 describes the relationship between the free energy

change (ΔG°) of a chemical reaction to the potential difference (E°) between the two half

Equation 5.2

$$\Delta G^\circ = -nFE^\circ$$

reactions. Consequently, we observe a net positive potential for a redox reaction, which is

indicative of a exergonic reaction with a $\Delta G^\circ \geq$ -28 kJ mol^{-1}. This demonstrates that the

quenching of the radical cation of 4-VA by electron transfer could be favorable for the case

of iodide. However, if the potential for the reduction of the 4-VA radical cation in water is

lower than estimated, then the reaction will be less exergonic, and will even become

endergonic if the reduction potential for the radical cation is smaller than 1.2 V.

If long-range electron transfer is a part of the quenching mechanism for the radical

cations by the quenchers employed then the quenching methodology breaks down in its

assumption that there must be an encounter complex formed between the quencher and the

radical cation. If this long-range process is present then at high quencher concentrations a

quenching plot with a downward curvature will not be observed since the exit of the guest

from the CD cavity will not be the rate-determining step in the quenching mechanism.

Under the assumptions of the quenching methodology, the quenching efficiency is defined

as the ability of the quencher to form an encounter complex with the guest molecule. If the

quenching mechanism involves long-range electron transfer then quenching can occur at a

distance before the guest exits the cavity. In such a case, it would be impossible to

differentiate between the quenching mechanism resulting from the formation of an

encounter complex with the exit of the radical cation from the CD cavity, and quenching by

long-range electron transfer of the radical cation complexed to the CD.

Cyanide was used as a quencher to eliminate the possibility of long-range electron

transfer. From calculations using the standard potential for cyanide as a quencher in the

redox reaction with either of the radical cations, it is shown that electron transfer with this anion is an endergonic process that makes this quenching process less favorable than anionic quenchers with lower standard potentials. More importantly, the quenching efficiency of the radical cations by cyanide was ca. three orders of magnitude smaller than that of iodide and azide. The quenching of the radical cations by anionic quenchers parallels the kinetics of bimolecular quenching mechanisms (Section 1.2.2.4), where the observed quenching rate constant is described by Equation 1.19. For the quenching reaction, if we assume that the lifetime of an encounter complex (k_{-diff}) for the radical cation and the cyanide ion is ca. 100 ps (ca. $1 \times 10^{10} \, s^{-1}$), a k_{diff} of ca. $1 \times 10^{10} \, M^{-1} \, s^{-1}$, and a $k_q(obs)$ of ca. $1 \times 10^{7} \, M^{-1} \, s^{-1}$, the quenching rate constant (k_q) will be ca. $1 \times 10^{7} \, s^{-1}$, which translates into a lifetime of ca. 100 ns. This demonstrates that even if the free energy for the redox reaction were exergonic, quenching by long-range electron transfer will not be present since the quenching rate constant for the reaction is of the magnitude that an encounter complex will be formed. Consequently, long-range electron transfer was eliminated as a possible mode of quenching for the radical cations by the anionic quenchers employed.

As discussed earlier, when the quenching methodology is employed to determine the entry and exit rate constants of a guest with CDs, the complexed guest molecule is protected from the quencher in the bulk phase. At high quencher concentrations, a quenching plot with a downward curvature is generally expected because the rate limiting step corresponds to the exit of the guest from the CD cavity, and the quenching efficiency of the complexed guest.[45] No curvature was observed for the quenching plots of both radical cations in the presence of CDs. There are two possible explanations for this behavior. Either the exit of the radical cation is fast, or the quencher has access to the radical cation within the CD cavity. It is important to note that linear plots were observed in the presence of α-CD for experimental conditions, where most of the styrenes are complexed with two CDs. In a recent study of the complexation dynamics of 2-naphthyl-

1-ethanol (2-NpOH) with β-CD, where complexes with 1:1 and 2:2 stoichiometries were formed, it was observed that the ratio for the quenching efficiency of the excited triplet state of 2-NpOH by Mn^{2+} in water to that of 2-NpOH in a 1:1 complex was between six and ten.[50] This suggested that the protection provided by β-CD was approximately an order of magnitude better than in the homogeneous aqueous solution. Assuming the ratio of the quenching efficiencies for 2-NpOH with β-CD in a 1:1 host-guest complex by Mn^{2+} is similar to that of cyanide for a 1:1 host-guest complex, we would expect a similar ratio in the quenching efficiencies for the radical cations in the presence of α-CD. This was not the case. To further exemplify that the quenching of the radical cations by cyanide occurs in the aqueous phase, in the case of the 2:2 complexes of 2-NpOH with β-CD, a significantly larger ratio for the quenching efficiencies was observed at ca. 500 when compared to 2-NpOH in water.[50] Therefore, if we were to assume a comparable decrease of the quenching efficiency by Mn^{2+} for a 2:2 host-guest complex with the quenching efficiency by cyanide for a 2:1 complex, then the ratio of quenching efficiencies for the radical cations in the presence of α-CD would be expected to be significantly smaller than observed in water. Since no reduction in the quenching efficiencies by cyanide of any magnitude was observed for the radical cations complexed to α-CD, the linear quenching plots indicate that the radical cations being quenched reside in the aqueous phase.

The quenching of the radical cations in the aqueous phase can either be due to the fast exit of the radical cations from the CD cavities, or to a fast reaction of the radical cations with the CDs. The latter possibility was excluded, since the decrease in the relative radical cation to electron yields were small compared to the fraction of styrene bound to the CD cavities. Hence, the linear quenching plots are due to the fast exit of the radical cations from the CD cavities, and the exit lifetime has to be smaller than the time resolution of the equipment (≤ 20 ns). In the case of cyanide, one may argue that the quenching plots at the high concentrations of quencher may show some curvature. To investigate this possibility, an attempt was made to fit the experimental data to Equation 1.25. In doing so, the value

for k_{p+} was fixed, and the values for $k_q(eff)$ were varied. From these fits, values for the exit rate constant (k_p) were recovered. From the best fits of the experimental data, the exit rate constant was estimated to be $> 1 \times 10^7 \, s^{-1}$ that corresponds to a radical cation lifetime within the CD complexes of less than 100 ns. As discussed earlier, this fast exit is probably driven by the fact that a charged guest molecule is formed in the photoionization process of the styrene.

The fast exit observed for the radical cations from α- and β-CD could have been expected for the 1:1 complexes since the fluorescence experiments indicated that the styrenes were somewhat exposed to the aqueous phase. However, it is surprising that even for the 2:1 complexes with α-CD the exit of the radical cation was fast especially since the dissociation of a 2:2 complex between β-CD and 2-naphthyl-1-ethanol was estimated to occur in the millisecond time-domain.[50] One possibility for the fast exit of the styrene radical cations is that they exit through the CD entrance that is not involved in the complexation of the second CD. A second possibility is that the formation of a charged guest leads to a very fast dissociation of the two CDs. This latter explanation would mean that the dynamics of CD complexes with higher stoichiometries spans more than four orders of magnitude. To differentiate between these two possibilities one would have to ensure that the complex involving two CD molecules has the narrower entrances exposed to the aqueous phase and that the charged guest is too large to exit through the narrower opening.

It is noteworthy, that for t-Ane in the presence of high α-CD concentrations the quenching rate constant decreased by a factor of ca. two. Linear quenching plots with smaller slopes than observed for measurements in aqueous solution are the first indication that the dynamics of complexation is competing with the quenching process. This can be seen from the derivative of Equation 1.25 with respect to [Q] to give Equation 5.3. Since the rate constant for the decay of the radical cations in water is much smaller than the

Equation 5.3

$$\frac{dk_{obs}}{d[Q]} = k_q(eff) + \frac{k_{qo}k_{p-}k_{p+}[H]}{(k_{p+}[H] + k_o + k_{qo}[Q])^2}$$

product of the entry rate constant and the CD concentration (i.e., $k_o \ll k_{p+}[H]$), and the quencher concentration is small for the initial slope (i.e., $[Q] \rightarrow 0$), Equation 5.3 becomes Equation 5.4. From this expression, we can see that the initial slope obtained from linear

Equation 5.4

$$slope = k_q(eff) + \frac{k_{qo}k_{p-}}{k_{p+}[H]}$$

quenching plots in the presence of different concentrations of CD can be useful in determining the effective quenching rate constants for the radical cations complexed with CDs. More importantly, it demonstrates that the observed decrease in quenching rate constant for 4-VA at high α-CD concentrations is most likely an indication that complexation dynamics are competing with the quenching process. Furthermore, since the lower quenching efficiency was only observed at the high α-CD concentrations, this suggests that the exit from the 2:1 complex is responsible for the observed decrease in the quenching rate constants. The smaller effect observed for 4-VA could be due to a decrease in steric hindrance associated with the absence of the β-methyl substituent when compared with t-Ane. However, a more detailed study would have to be performed for t-Ane at various CD concentrations before a quantitative assessment could be made on the decreases observed for the quenching plots of t-Ane at high concentrations of α-CD.

5.4.5 The Effect of Alcohols

As outlined earlier, the second objective in this study was to establish whether, or not the presence of alcohols affects the complexation dynamics of radical cations with CDs. It has been shown that the exit rate constant of triplet xanthone from β-and γ-CD significantly decreases in the presence of alcohols.[31] It has been suggested that the alcohols may be preferentially solvating the entrances of the CD cavities. If this was the case for the dynamics of radical cations with CDs, we would also expect to see a decrease in the exit rate constants.

The addition of alcohols did not affect the quenching behavior for the 4-VA radical cations in the presence of the CDs. The small increase observed in the quenching rate constants for t-Ane in the presence of α-CD could be explained by a slight inhibition of the formation of the 2:1 CD complexes with t-Ane, which would lead to easier access for the quencher to the guest molecule. Unfortunately, the results in the presence of alcohols are inconclusive because the exit of the radical cation is fast. Even if there is an alcohol effect, given the time-resolution of our kinetic measurements, a decrease in the exit rate constant may not be detectable. The dissociation rate constants observed for xanthone complexed to β- and γ-CD was decreased by at least a factor of five in the presence of alcohols. Assuming a similar effect with the radical cations we might expect to see an increase in the radical cation lifetime exiting the CD from *ca.* 20 ns to that of *ca.* 100 ns, and as a result a detectable transient for this exit may be observable. However, this is not the case. This is surprising, considering that 2:1 complexes of the radical cations with α-CD are present when compared to the 1:1 host-guest complexes reported for xanthone with β- and γ-CD. The higher order stoichiometries should lead to slower exit rate constants of the radical cations and hence increase the probability of an alcohol effect, yet as observed from the quenching studies there is no concrete evidence to support this hypothesis.

5.4.6 The Dynamics of Charged Guests

We have shown that the exit of charged guests from CDs is very fast. These studies demonstrate that there is a large driving force for the exit of radical cations from CDs. This has been observed for xanthone, which exhibits a large change in its dipole moment upon excitation.[29] In order to better understand the dynamics of these systems, host-guest assemblies that will impede the exit of the guest, and consequently lower the dissociation rate constant of the guest from the host molecule will have to be employed. Either the guest or host could be synthetically altered such that the exit of the guest from the host molecule will be sterically hindered. Another way of achieving a better understanding of the fast dynamics associated with these systems would be to employ time-resolved instrumentation capable of measuring transient events on shorter time scales.

5.4.7 Applications in Drug Protection

As mentioned earlier, CDs have been employed in drug delivery systems. These CD systems have also been investigated for their ability to protect drugs from photodecomposition. In this respect, the incorporation of drugs into CDs may lead to a decrease in the quantum yield of photodecomposition of the drugs, or to a change in the degradation mechanism and production of less toxic by-products. The photodegradation of some drugs, such as ketoprofen and suprofen[81-83], have been shown to form ionic intermediates. Since reactive intermediates of these drugs may be responsible for some of the undesirable side effects, it is necessary to understand how efficiently CDs bind to these species. We have demonstrated that the residence time of these charged guests in CDs is very short even in the case of 2:1 host-guest complexes. This observation has a direct impact on the usefulness of CDs as protective molecules for drugs which photodegrade and can lead to phototoxic effects. If an intermediate of the encapsulated drug is a charged

species, then the degradation process may not be inhibited by the presence of CDs since the residence time of our charged guests was very short. In this respect, CDs will only be useful in protecting drugs from photodegradation if the photochemistry of the drug molecule is altered by the complexation to CD, so that no charged intermediates are formed.

5.4.8 Concluding Remarks

In this investigation, we have shown from the fluorescence experiments that both t-Ane and 4-VA form complexes with both α- and β-CD. In the case of α-CD, it was observed that both complexes with 1:1 and 2:1 stoichiometries were present, whereas for β-CD only 1:1 complexes were formed. Quantum yield studies have shown that the reaction of the radical cations with the CDs was a minor decay pathway for these intermediates. Quenching studies have demonstrated that the exit of the radical cations of t-Ane and 4-VA complexed to CD, even in the presence of alcohols, was faster than 20 ns. In addition, complexes with 2:1 host-guest stoichiometries were also unsuccessful in reducing the dissociation rate constant of these charged species. These results suggest that charged guest molecules formed within the CD cavities have a very short residence time within these complexes.

6. CONCLUSIONS

We investigated in greater detail, several aspects of the complexation dynamics of guest molecules with CDs. CDs have been the focus of many studies as host systems for their potential application in such areas as catalysis, chromatography, drug delivery systems, and as biomimics for enzyme-substrate binding.[39,40] To achieve success in these areas of application, a better understanding of the relationship between structure and dynamics for these host-guest systems is required. We have shown with the use of a variety of photophysical techniques and in collaboration with theoretical calculations that the complexation dynamics for guests with CDs are very dependent on the structure of the guest molecule.

Our initial studies began with a detailed analysis of the photophysics of fluorenone. This probe molecule was chosen since the photophysics of this aromatic ketone was known to be similar to xanthone. A detailed photophysical characterization for several fluorenone derivatives in different solvent polarities was performed to obtain a better understanding of the role of substituents and solvent on several photophysical parameters. These photophysical studies were performed with the use of steady-state fluorescence, UV-Vis absorption, and laser-induced optoacoustic spectroscopies. In addition, time-resolved techniques that included single photon counting fluorescence and triplet-triplet absorption spectroscopies were implemented to further characterize the photophysics of these molecules. From these investigations, we have demonstrated that several compensating effects are responsible for the observed photophysics. This combination of effects derived from the nature and position of substituents, and the properties of the microenvironment are responsible for the inherent photophysics of these molecules.

The complexation of fluorenone and xanthone to CDs was investigated to obtain more information of how the structure of the guest molecule can affect the complexation dynamics of host-guest systems. Induced circular dichroism and picosecond fluorescence

spectroscopy were employed to detail the structural differences observed for the CD complexes of these two ketones. We found that the slight difference in the chemical structure of these ketones has a large impact on the photophysics within CD complexes. Furthermore, these studies were complemented with theoretical calculations that provided additional insight into the aspects responsible for the observed photophysics. For the 1:1 host-guest complexes of xanthone and fluorenone with β-CD, a higher complexation efficiency was observed for xanthone with β-CD than for fluorenone with β-CD, which suggests that the complexation of xanthone is favored over that of fluorenone. The calculations for the 1:1 complexes of these aromatic ketones also suggested that xanthone forms a deeper inclusion complex than fluorenone. In addition, picosecond fluorescence results demonstrated that the inclusion of xanthone into the β-CD cavity must be greater than fluorenone since xanthone experienced an appreciable difference in its microenvironment, as indicated from its biexponential fluorescence decay. This protection afforded by the complex of β-CD to xanthone was not observed in the case for fluorenone. This result suggested that fluorenone was not as well protected from the aqueous environment in its complex with β-CD than in the case for xanthone.

Steady-state and picosecond fluorescence measurements were performed for fluorenone in the presence of high concentrations of α-CD. Under these experimental conditions, fluorenone was observed to form a 2:1 complex with α-CD. However, in the case of xanthone no higher ordered complexes were observed. These observations were also supported by theoretical calculations. These differences in the photophysics for xanthone and fluorenone with α-CD are a result of the inherent structural differences between these ketones.

We have shown that ICD, and time-resolved fluorescence studies in combination with theoretical calculations of these host-guest complexes provide useful tools for understanding the structural intricacies that are responsible for significant changes in the photophysics of these systems. As a result, we have demonstrated that structure is

important to the photophysical characterization of CD host-guest systems. To this end, these types of studies will be invaluable to the understanding of dynamics within supramolecular systems.

To further expand our knowledge on the structure-dynamics relationship that exits for CD complexes, we investigated the complexation dynamics of charged probes with CDs. Two styrene derivatives, t-Ane and 4-VA, were chosen as precursors for the radical cations investigated in these studies. From steady-state fluorescence measurements, these styrene molecules were observed to form 1:1 and 2:1 complexes with α-CD. Quenching studies have demonstrated that the exit of the radical cations of t-Ane and 4-VA complexed to CD, even in the presence of alcohols, was faster than 20 ns. In addition, the exit of the radical cations was favored over the reaction of these reactive intermediates with CDs, which was demonstrated from quantum yield experiments for these systems. Even complexes with 2:1 host-guest stoichiometries were unsuccessful in reducing the dissociation rate constant of these charged species.

From these studies we have established that a structure-dynamics relationship does exist for these host-guest complexes. With the use of a variety of photophysical techniques and in a collaboration with theoretical calculations, we have illustrated how the photophysics of probe molecules can be used to explore host-guest complexation. Minor changes in structure have significant effects on the photophysics and binding efficiencies of these probes with CDs. Ultimately, these structural differences are responsible for the dynamics associated with these systems. From these investigations on the complexation of guest molecules with CDs, we have obtained a better understanding of the structure-dynamics relationship that exists for these host-guest complexes. This information will not only enhance the applicability of CDs in areas of practical importance, but more importantly, this comprehension will aid in our understanding of the structure-dynamics relationship that exists between more complex supramolecular systems.

7. REFERENCES

(1) Klessinger, M.; Michl, J. *Excited States and Photochemistry of Organic Molecules*; VCH Publishers, Inc.: New York, New York, 1995

(2) Brealey, G. J.; Kasha, M. *J. Am. Chem. Soc.* **1955**, *77*, 4462-4468.

(3) Turro, N. J. *Modern Molecular Photochemistry*; University Science Books: Mill Valley, California, 1991

(4) El-Sayed, M. A. *J. Chem. Phys.* **1963**, *38*, 2834-2838.

(5) Gilbert, A.; Baggott, J. *Essentials of Molecular Photochemistry*; Blackwell Scientific Publications: Oxford, 1991

(6) Wigner, E.; Wittmer, E. E. *Z. Physik.* **1928**, *51*, 859.

(7) Stern, O.; Volmer, M. *Z. Physik.* **1919**, *20*, 183.

(8) Andrews, L. J.; Deroulede, A.; Linschitz, H. *J. Phys. Chem.* **1978**, *82*, 2304-2309.

(9) Biczók, L.; Bérces, T. *J. Phys. Chem.* **1988**, *92*, 3842-3845.

(10) Biczók, L.; Bérces, T.; Márta, F. *J. Phys. Chem.* **1993**, *97*, 8895-8899.

(11) Biczók, L.; Bérces, T.; Linschitz, H. *J. Am. Chem. Soc.* **1997**, *119*, 11071-11077.

(12) Biczók, L.; Bérces, T.; Inoue, H. *J. Phys. Chem. A* **1999**, *103*, 3837-3842.

(13) Caldwell, R. A. *Tetrahedron Lett.* **1969**, 2121-2125.

(14) Caldwell, R. A.; Gajewski, R. P. *J. Am. Chem. Soc.* **1971**, *93*, 532-534.

(15) Demeter, A.; Timári, G.; Kotschy, A.; Bérces, T. *Tetrahedron Lett.* **1997**, *38*, 5219-5222.

(16) Fujii, T.; Sano, M.; Mishima, S.; Hiratsuka, H. *Bull. Chem. Soc. Jpn.* **1996**, *69*, 1833-1839.

(17) Guttenplan, J. B.; Cohen, S. G. *Tetrahedron Lett.* **1969**, 2125-2128.

(18) Huggenberger, V.; Labhart, H. *Helv. Chim. Acta* **1978**, *61*, 250-257.

(19) Kobayashi, T.; Nagakura, S. *Chem. Phys. Lett.* **1976**, *43*, 429-434.

(20) Kuboyama, A. *Bull. Chem. Soc. Jpn.* **1964**, *37*, 1540-1544.

(21) Moog, R. S.; Burozski, N. A.; Desai, M. M.; Good, W. R.; Silvers, C. D.; Thompson, P. A.; Simon, J. D. *J. Phys. Chem.* **1991**, *95*, 8466-8473.

(22) Singer, L. A. *Tetrahedron Lett.* **1969**, 923-926.

(23) Yatsuhashi, T.; Nakajima, Y.; Shimada, T.; Inoue, H. *J. Phys. Chem. A* **1998**, *102*, 3018-3024.

(24) Yoshihara, K.; Kearns, D. R. *J. Chem. Phys.* **1966**, *45*, 1991-1999.

(25) Biczók, L.; Jicsinszky, L.; Linschitz, H. *J. Incl. Phenom. Molec. Recog. Chem.* **1994**, *18*, 237-245.

(26) Thompson, P. A.; Broudy, A. E.; Simon, J. D. *J. Am. Chem. Soc.* **1993**, *115*, 1925-1929.

(27) Allen, N. S.; Hardy, S. J.; Jacobine, A.; Glaser, D. M.; Catalina, F. *Eur. Polym. J.* **1989**, *25*, 1219-1225.

(28) Scaiano, J. C. *J. Am. Chem. Soc.* **1980**, *102*, 7747-7753.

(29) Barra, M.; Bohne, C.; Scaiano, J. C. *J. Am. Chem. Soc.* **1990**, *112*, 8075-8079.

(30) Liao, Y.; Frank, J.; Holzwarth, J. F.; Bohne, C. *J. Chem. Soc., Chem. Commun.* **1995**, 199-200.

(31) Liao, Y.; Bohne, C. *J. Phys. Chem.* **1996**, *100*, 734-743.

(32) Abuin, E. B.; Scaiano, J. C. *J. Am. Chem. Soc.* **1984**, *106*, 6274-6283.

(33) Johnston, L. J.; Schepp, N. P. *Adv. Electron Transfer Chem.* **1996**, *5*, 41-102.

(34) Johnston, L. J.; Schepp, N. P. *J. Am. Chem. Soc.* **1993**, *115*, 6564-6571.

(35) Johnston, L. J.; Schepp, N. P. *Pure Appl. Chem.* **1995**, *67*, 71-78.

(36) Schepp, N. P.; Johnston, L. J. *J. Am. Chem. Soc.* **1994**, *116*, 6895-6903.

(37) Schepp, N. P.; Johnston, L. J. *J. Am. Chem. Soc.* **1994**, *116*, 10330-10331.

(38) Schepp, N. P.; Johnston, L. J. *J. Am. Chem. Soc.* **1996**, *118*, 2872-2881.

(39) Szejtli, J. *Chem. Rev.* **1998**, *98*, 1743-1753.

(40) Szejtli, J.; Osa, T. *Cyclodextrins*; Elsevier Science Ltd.: New York, 1996; Vol. 3.

(41) Paulaitis, M. E.; Garde, S.; Ashbaugh, H. S. *J. Colloid Interface Sci.* **1996**, *1*, 376-383.

(42) Rekharsky, M. V.; Inoue, Y. *Chem. Rev.* **1998**, *98*, 1875-1917.

(43) Connors, K. A. *Chem. Rev.* **1997**, *97*, 1325-1357.

(44) Bortolus, P.; Monti, S. *Adv. Photochem.* **1996**, *21*, 1-133.

(45) Kleinman, M. H.; Bohne, C. In *Organic Photochemistry: Molecular and Supramolecular Photochemistry*; V. Ramamurthy and K. S. Schanze, Ed.; Marcel Dekker, Inc.: New York, 1997; Vol. 1; 391-466.

(46) Cramer, F.; Saenger, W.; Spatz, H.-C. *J. Am. Chem. Soc.* **1967**, *89*, 14-20.

(47) Rohrbach, R. P.; Rodriguez, L. J.; Eyring, E. M.; Wojcik, J. F. *J. Phys. Chem.* **1977**, *81*, 944-948.

(48) Turro, N. J.; Okubo, T.; Chung, C.-J. *J. Am. Chem. Soc.* **1982**, *104*, 1789-1794.

(49) Liao, Y.; Frank, J.; Holzwarth, J. F.; Bohne, C. *J. Chem. Soc., Chem. Commun.* **1995**, 2435-2436.

(50) Barros, T. C.; Stefaniak, K.; Holzwarth, J. F.; Bohne, C. *J. Phys. Chem. A* **1998**, *102*, 5639-5651.

(51) Connors, K. A. *Binding Constants - The Measurement of Molecular Complex Stability*; John Wiley & Sons: New York, 1987

(52) Benesi, H. A.; Hildebrand, J. H. *J. Am. Chem. Soc.* **1949**, *71*, 2703-2707.

(53) Kodaka, M. *J. Am. Chem. Soc.* **1993**, *115*, 3702-3705.

(54) Kodaka, M.; Fukaya, T. *Bull. Chem. Soc. Jpn.* **1989**, *62*, 1154-1157.

(55) Kodaka, M. *J. Phys. Chem.* **1991**, *95*, 2110-2112.

(56) Kodaka, M. *J. Phys. Chem. A* **1998**, *102*, 8101-8103.

(57) Harata, K.; Uedaira, H. *Bull. Chem. Soc. Jpn.* **1975**, *48*, 375-378.

(58) Marconi, G.; Monti, S.; Mayer, B.; Köhler, G. *J. Phys. Chem.* **1995**, *99*, 3943-3950.

(59) Barra, M. *Supramolec. Chem.* **1997**, *8*, 263-266.

(60) Turro, N. J.; Bolt, J. D.; Kuroda, Y.; Tabushi, I. *Photochem. Photobiol.* **1982**, *35*, 69-72.

(61) Murphy, R. S.; Barros, T. C.; Barnes, J.; Mayer, B.; Marconi, G.; Bohne, C. *J. Phys. Chem. A* **1999**, *103*, 137-146.

(62) Janata, E. *Rev. Sci. Instrum.* **1986**, *57*, 273-275.

(63) Eaton, D. F. In *Handbook of Organic Photochemistry*; J. C. Scaiano, Ed.; CRC Press: Boca Raton, Florida, **1989**; Vol. I; 231-239.

(64) Street Jr., K. W.; Acree Jr., W. E. *Analyst* **1986**, *111*, 1197-1201.

(65) Braslavsky, S. E.; Heibel, G. E. *Chem. Rev.* **1992**, *92*, 1381-1410.

(66) Murov, S. L.; Carmichael, I.; Hug, G. L. *Handbook of Photochemistry*; 2nd ed.; Marcel Dekker, Inc.: New York, **1993**

(67) Herkstroeter, W. G.; Lamola, A. A.; Hammond, G. S. *J. Am. Chem. Soc.* **1964**, *86*, 4537-4540.

(68) Grabner, G.; Monti, S.; Marconi, G.; Mayer, B.; Klein, C.; Köhler, G. *J. Phys. Chem.* **1996**, *100*, 20068-20075.

(69) Marconi, G.; Mayer, B. *Pure Appl. Chem.* **1997**, *69*, 779-783.

(70) Yoshida, N.; Yamaguchi, H.; Iwao, T.; Higashi, M. *J. Chem. Soc. Perkin Trans. 2* **1999**, 379-386.

(71) Mohtat, N.; Cozens, F. L.; Scaiano, J. C. *J. Phys. Chem. B* **1998**, *102*, 7557-7562.

(72) Cavaleri, J. J.; Prater, K.; Bowman, R. M. *Chem. Phys. Lett.* **1996**, *259*, 495-502.

(73) Yamaguchi, H.; Ninomiya, K.; Ogata, M. *Chem. Phys. Lett.* **1980**, *75*, 593-595.

(74) Janata, E.; Schuler, R. H. *J. Phys. Chem.* **1982**, *86*, 2078-2084.

(75) Buxton, G. V.; Greenstock, C. L.; Helman, W. P.; Ross, A. B. *J. Phys. Chem. Ref. Data* **1988**, *17*, 513-886.

(76) Brancaleon, L.; Brousmiche, D.; Johnston, L. J. *Can. J. Chem.* **1999**, *77*, 787-791.

(77) Xu, W.; Demas, J. N.; DeGraff, B. A.; Whaley, M. *J. Phys. Chem.* **1993**, *97*, 6546-6554.

(78) Hashimoto, S.; Thomas, J. K. *J. Am. Chem. Soc.* **1985**, *107*, 4655-4662.

(79) Workentin, M. S.; Schepp, N. P.; Johnston, L. J.; Wayner, D. D. M. *J. Am. Chem. Soc.* **1994**, *116*, 1141-1142.

(80) Wayner, D. D. M. In *Handbook of Organic Photochemistry*; J. C. Scaiano, Ed.; CRC Press: Boca Raton, Florida, 1989; Vol. II; 363-368.

(81) Sortino, S.; De Guidi, G.; Marconi, G.; Monti, S. *Photochem. Photobiol.* **1998**, *67*, 603-611.

(82) Monti, S.; Sortino, S.; De Guidi, G.; Marconi, G. *J. Chem. Soc., Faraday Trans.* **1997**, *93*, 2269-2275.

(83) Martinez, L. J.; Scaiano, J. C. *J. Am. Chem. Soc.* **1997**, *119*, 11066-11070.